

**AN *IN VITRO* STUDY OF AEROSOLIZED SURFACTANT CARRIER  
DEPOSITION AND DISPERSION ON AIRWAY SURFACE MODELS**

by

Amy L. Marcinkowski

BS, Boston University, 2004

Submitted to the Graduate Faculty of  
School of Engineering in partial fulfillment  
of the requirements for the degree of  
Master of Science

University of Pittsburgh

2006

UNIVERSITY OF PITTSBURGH

SCHOOL OF ENGINEERING

This thesis was presented

by

Amy L. Marcinkowski

It was defended on

July 11<sup>th</sup>, 2006

and approved by

William Federspiel, Ph.D., Professor,  
Department of Chemical Engineering, Surgery, and Bioengineering, University of Pittsburgh

Stephen Garoff, Ph.D., Professor,  
Department of Physics, Carnegie Mellon University

Joseph Pilewski, M.D., Associate Professor,  
Department of Medicine, University of Pittsburgh

Bruce Pitt, Ph.D., Chairman and Professor,  
Department of Environmental and Occupational Health, University of Pittsburgh

Robert Tilton, Ph.D., Professor,  
Department of Chemical and Biomedical Engineering, Carnegie Mellon University

Thesis Advisor: Timothy Corcoran, Ph.D., Research Assistant Professor,  
Department of Medicine and Bioengineering, University of Pittsburgh

Copyright © by Amy L. Marcinkowski

2006

**AN *IN VITRO* STUDY OF AEROSOLIZED SURFACTANT CARRIER DEPOSITION  
AND DISPERSION ON AIRWAY SURFACE MODELS**

Amy L. Marcinkowski, M.S.

University of Pittsburgh, 2006

Inhaled antibiotics are frequently used for treating infections associated with cystic fibrosis (CF) and are under development for other uses including hospital-acquired pneumonias. However, the long-term efficacy of inhaled anti-infectives depends largely on the uniformity of pulmonary drug deposition, which is variable in diseased lungs. In surfactant replacement therapy (SRT), premature infants who lack adequate levels of surfactant receive a bolus of exogenous surfactant through an endotracheal tube. The success of this therapy is due to the pulmonary dispersion of surfactant from convective flows generated by surface tension gradients along the airway surface. Based on this same mechanism, aerosolized surfactant drug carriers have been proposed as a potential means of augmenting drug distribution in diseased lungs. However, little experimental evidence exists to support this. The goal of this study was to assess the potential for aerosolized surfactant drug carriers to improve the dispersion of medications in the lungs following aerosol deposition. This study included the design of an aerosol delivery system that produced an aerosol of respirable size that was delivered onto two realistic *in vitro* models of the airway surface. The first model incorporated porcine gastric mucin (PGM) and the second utilized human bronchial epithelial (HBE) cell cultures, including CF and non-CF cells. Differences in the dispersion of various surfactants (cationic, anionic, and non-ionic) vs. saline (control) were quantified using fluorescence microscopy and different sized fluorescent tags acting as drug analogs. The tags spanned a size range from the molecular level to a 1.0 micron polystyrene sphere. On the PGM model, surfactants enhanced dispersion by 2-20 fold vs. saline with fairly uniform dispersion for all sized tags. When sufficiently hydrated, the HBE cell cultures, both CF and non-CF, also demonstrated significant surfactant spreading compared to saline, with similar areas and patterns for all sized tags. This study demonstrates the potential for aerosolized surfactant carriers to improve the uniformity of pulmonary drug distribution

following deposition. Further studies are required to demonstrate their efficacy in these in vitro models and for in vivo drug applications.

## TABLE OF CONTENTS

<b>LIST OF TABLES .....</b>	<b>VIII</b>
<b>LIST OF FIGURES .....</b>	<b>IX</b>
<b>ACKNOWLEDGEMENTS .....</b>	<b>XIV</b>
<b>1.0 INTRODUCTION.....</b>	<b>1</b>
<b>2.0 BACKGROUND .....</b>	<b>3</b>
<b>2.1 AIRWAY PHYSIOLOGY .....</b>	<b>3</b>
<b>2.1.1 Airway Epithelium.....</b>	<b>3</b>
<b>2.1.2 Airway Surface Liquid Layer (ASL).....</b>	<b>5</b>
<b>2.2 CYSTIC FIBROSIS.....</b>	<b>6</b>
<b>2.2.1 Pathogenesis.....</b>	<b>6</b>
<b>2.2.2 ASL Volume Regulation.....</b>	<b>8</b>
<b>2.2.3 In Vitro Study.....</b>	<b>8</b>
<b>2.3 AEROSOL DELIVERY .....</b>	<b>9</b>
<b>2.3.1 Aerosol Delivery to the Diseased Lung .....</b>	<b>12</b>
<b>2.3.2 Aerosol Antibiotics.....</b>	<b>13</b>
<b>2.4 DRUG DISTRIBUTION FOLLOWING DEPOSITION.....</b>	<b>15</b>
<b>2.4.1 Diffusion.....</b>	<b>15</b>
<b>2.4.2 Surface Tension Driven Flows .....</b>	<b>16</b>
2.4.2.1 Surface tension.....	16
2.4.2.2 Marangoni flow.....	16
<b>2.4.3 Pulmonary Surfactant .....</b>	<b>18</b>
2.4.3.1 Alveolar.....	18
2.4.3.2 Airway Surfactant .....	19
2.4.3.3 Other Considerations .....	20

<b>2.5</b>	<b>PREVIOUS WORK.....</b>	<b>21</b>
2.5.1	Surfactant Bolus: Surfactant Replacement Therapy .....	21
2.5.2	Surfactant Bolus: Drug Delivery Vehicle .....	23
<b>3.0</b>	<b>SPECIFIC AIMS.....</b>	<b>25</b>
<b>4.0</b>	<b>METHODS .....</b>	<b>26</b>
4.1.1	Aerosol Delivery System.....	26
4.1.2	Surfactants.....	27
4.1.3	Microscopy.....	28
4.1.4	Mucus Model Surface .....	29
4.1.5	Epithelial Cell Culture Model.....	29
4.1.5.1	Cell culture preparation.....	29
4.1.5.2	Calu3 Model.....	31
4.1.5.3	HBE Model (CF and non-CF).....	32
4.1.5.4	Liposome delivery to HBEs.....	33
4.1.6	Image Analysis .....	33
<b>5.0</b>	<b>RESULTS .....</b>	<b>34</b>
5.1	PRELIMINARY MUCUS EXPERIMENTS .....	34
5.2	AEROSOL SIZING .....	36
5.3	AEROSOL DELIVERY.....	42
5.3.1	Mucus Model Surface .....	42
5.3.2	Calu3 Model .....	47
5.3.3	HBE Model – Group 1.....	49
5.3.4	HBE Model – Group 2.....	54
5.3.5	Drug Formulation .....	63
5.4	QUANTITATIVE ANALYSIS .....	67
<b>6.0</b>	<b>DISCUSSION .....</b>	<b>77</b>
6.1	MUCUS MODEL.....	77
6.2	CELL CULTURE MODEL .....	80
6.3	CONCLUSIONS .....	83
	<b>BIBLIOGRAPHY .....</b>	<b>84</b>

## LIST OF TABLES

Table 1: Selected cells of the airway epithelium [2].....	4
Table 2: Approximate surface tension values along the surface of the airway lumen from the trachea to alveoli [54-56].....	19
Table 3: Current FDA approved exogenous surfactant formulations for treating RDS and the corresponding measured minimum surface tensions [74-77]. .....	22
Table 4: The minimum surface tensions and concentrations used for saline (control) and the surfactants selected for experimentation.....	28
Table 5: Cell lines used with corresponding disease state and group number (Group 1 – washed only 24 hours prior to experiment, Group 2 - cells hydrated with PBS immediately prior to experiment). .....	32
Table 6: Aerosol size measurements taken at the cannula tip of the aerosol delivery system expressed as the average MMD. ....	36
Table 7: MMD of saline and calfactant measured from three different medical nebulizers. ....	40
Table 8: Factor by which the average surfactant area exceeds the average saline area post aerosol deposition on the PGM. ....	45
Table 9: ANOVA p-values obtained for each individual cell line and the combined CF and non-CF cell lines. ....	68

## LIST OF FIGURES

Figure 1: Model of two epithelial cells joined by a gap junction with the above airway surface liquid (ASL).....	6
Figure 2: The balance of Na <sup>+</sup> absorption and Cl <sup>-</sup> secretion is maintained when a functional CFTR is present in normal airway epithelia. The lack of a functional CFTR channel (right) results in Na <sup>+</sup> hyper-absorption and decreased Cl <sup>-</sup> secretion via other pathways, resulting in ASL dehydration and volume depletion [7, 19].....	7
Figure 3: ASL depletion leading to delayed mucociliary clearance.....	8
Figure 4: Inertial impaction of an aerosol in a normal airway (left) and obstructed airway (right). .....	10
Figure 5: Radioscintigraphy images of aerosol drug deposition (left) and xenon gas ventilation (right) in the lungs.....	13
Figure 6: Forces experienced by molecules at a boundary surface. The resultant tangential force (right) represents the surface tension force.....	16
Figure 7: The “soap boat” is a simple example of the surface tension driven Marangoni flows (reprinted with permission, from the Annual Review of Fluid Mechanics, Volume 38 © 2006 by Annual Reviews www.annualreviews.org).....	17
Figure 8: Aerosol drug deposition upon the ASL using a surfactant carrier.....	18
Figure 9: Alveolus lined with surfactant monolayer at the air-liquid interface (reprinted with permission from [53]). .....	19
Figure 10: Aerosol delivery system. 100% Humidified air at 37°C was used to deliver aerosol to a porcine gastric mucus (PGM) or epithelial cell culture surface. A micropump nebulizer was used to produce an aerosol. The diameters of the tubing and connectors gradually decrease in size: 1- 22mm , 2 - 16, 12mm, 3 - 4mm, 4 - 3.5 mm, 5 - 3mm, 6 - 2mm. The aerosol exiting the end of tubing section 6 ranges from 1-4 microns in median diameter.....	26
Figure 11: A single 12mm transwell filter insert with cells seeded on a microporous membrane. The microporous membrane lies 1mm above the culture dish bottom and contains 0.4 micron pores to allow the passage of media from the lower compartment to the cells. Once confluent,	

the media on the apical surface is removed and the cells remain at an air-liquid interface with only the basolateral side in contact with media. .... 31

Figure 12: PGM with saline (left), tyloxapol (center) and tween20 (right) pipetted on surface, labeled with blue dye. .... 35

Figure 13: PGM phase separation. Phase separation line appears at concentrations of 20 mg/ml and above. No separation occurred for the 10mg/ml. .... 35

Figure 14: Volume histograms for saline (top), calfactant (middle) and tyloxapol (bottom). Measurements were performed using a laser diffraction instrument and the average MMD was calculated from 10 measurements. The histogram represents the relative volume of aerosol with in each size range. Half micron bins were used. .... 37

Figure 15: Volume histograms (continued) for SDS (top) and CTAB (bottom). Measurements were performed using a laser diffraction instrument and the average MMD was calculated from 5 measurements. The histogram represents the relative volume of aerosol with in each size range. Half micron bins were used. .... 38

Figure 16: Volume histograms for Ambisome dissolved in distilled water only (top) and Ambisome dissolved in Calfactant (bottom). Measurements were performed using a laser diffraction instrument and the average MMD was calculated from 10 measurements. The histogram represents the relative volume of aerosol with in each size range. Half micron bins were used. .... 39

Figure 17: Volume histograms of saline (pink) and calfactant (blue) generated by three medical nebulizers: Aerogen Pro (top), AeroTech II (middle), and AeroEclipse (bottom). The histograms represent the relative volume of aerosol within each size range. .... 41

Figure 18: Images captured post aerosol deposition on PGM surface. Saline (top row), calfactant (center row), tyloxapol (bottom row) were labeled with texas red dextran (left column), 0.1 (center column) and 1.0 micron PS spheres (right column). .... 43

Figure 19: Images captured post aerosol deposition on PGM surface. SDS (top row) and CTAB (bottom row) were labeled with texas red dextran (left column), 0.1 (center column) and 1.0 micron PS spheres (right column). .... 44

Figure 20: Images captured at 2 and 8 minutes post aerosol deposition on the PGM surface demonstrate retraction behavior of ionic surfactants. Saline (top row), SDS (center row) and CTAB (bottom row) are shown labeled with 0.1 micron PS spheres. .... 46

Figure 21: Images captured post aerosol deposition on the Calu3 cell cultures. Saline (left), calfactant (center), and tyloxapol (right) were labeled with texas red dextran. A droplet formed on the surface and little to no spreading of surfactants was observed. No further hydration protocol was used. .... 47

Figure 22: Images captured post aerosol deposition on the Calu3 cell cultures. Saline (left) and tyloxapol (right) were labeled with texas red dextran. In this case, a larger degree of spreading occurred when tyloxapol was dosed on the surface of the culture. Because no further hydration protocol was used, we believe this variability is associated with the hydration level. .... 48

Figure 23: Images captured post aerosol deposition on cystic fibrosis cell cultures, CF 101 (top row) and CF 103 (bottom row). Saline (left column) and tyloxapol (right column) were labeled with texas red dextran. A droplet formed on the surface and little to no spreading of surfactant was observed. These group 1 studies did not include the added hydration steps included in group 2 experiments. .... 49

Figure 24: Images captured post aerosol deposition on CF 105 cell cultures. Saline (left), calfactant (center), and tyloxapol (right) were labeled 0.1 micron PS spheres. Droplets formed on the surface and little to no spreading of surfactants was observed. These group 1 studies did not include the added hydration steps included in group 2 experiments. .... 50

Figure 25: Images captured post aerosol deposition onto HBE 439 cell cultures. Saline (left) and calfactant (right) were labeled with texas red dextran. A droplet formed on the surface and little to no spreading of surfactant was observed. These group 1 studies did not include the added hydration steps included in group 2 experiments. .... 51

Figure 26: Images captured post aerosol deposition on HBE 456 cell cultures. Saline (left column), calfactant (center column), and tyloxapol (right) were labeled with 0.1 micron PS spheres. These group 1 studies did not include the added hydration steps included in group 2 experiments. .... 52

Figure 27: Images captured post aerosol deposition on HBE 457 cell cultures. Saline (left column), calfactant (center column), and tyloxapol (right) were labeled with 0.1 micron PS spheres. These group 1 studies did not include the added hydration steps included in group 2 experiments. .... 53

Figure 28: Images captured post aerosol deposition onto CF 102 cell cultures (run 1). Saline (top row), calfactant (center row) and tyloxapol (bottom row) were labeled with texas red dextran (left column), 0.1 (center column) and 1.0 micron PS spheres (right column). These group 2 studies included additional hydration steps not performed in group 1. .... 55

Figure 29: Images captured post aerosol deposition onto CF 102 cell cultures (run 2). Saline (top row), calfactant (center row) and tyloxapol (bottom row) were labeled with texas red dextran (left column), 0.1 (center column) and 1.0 micron PS spheres (right column). These group 2 studies included additional hydration steps not performed in group 1. .... 56

Figure 30: Images captured post aerosol deposition onto CF 103 cell cultures. Saline (top row), calfactant (center row) and tyloxapol (bottom row) were labeled with texas red dextran (left column), 0.1 (center column) and 1.0 micron PS spheres (right column). These group 2 studies included additional hydration steps not performed in group 1. .... 57

Figure 31: Images captured post aerosol deposition onto CF 105 cell cultures. Saline (top row), calfactant (center row) and tyloxapol (bottom row) were labeled with texas red dextran (left column), 0.1 (center column) and 1.0 micron PS spheres (right column). These group 2 studies included additional hydration steps not performed in group 1. .... 58

Figure 32: Images captured post aerosol deposition onto HBE 456 cell cultures. Saline (top row), calfactant (center row) and tyloxapol (bottom row) were labeled with texas red dextran (left column), 0.1 (center column) and 1.0 micron PS spheres (right column). These group 2 studies included additional hydration steps not performed in group 1. .... 59

Figure 33: Images captured post aerosol deposition onto HBE 456 cell cultures (run 2). Saline (top row), calfactant (center row) and tyloxapol (bottom row) were labeled with texas red dextran (left column), 0.1 (center column) and 1.0 micron PS spheres (right column). These group 2 studies included additional hydration steps not performed in group 1. .... 60

Figure 34: Images captured post aerosol deposition onto HBE 457 cell cultures (run 1). Saline (top row), calfactant (center row) and tyloxapol (bottom row) were labeled with texas red dextran (left column), 0.1 (center column) and 1.0 micron PS spheres (right column). These group 2 studies included additional hydration steps not performed in group 1. .... 61

Figure 35: Images captured post aerosol deposition onto HBE 457 cell cultures (run 2). Saline (top row), calfactant (center row) and tyloxapol (bottom row) were labeled with texas red dextran (left column), 0.1 (center column) and 1.0 micron PS spheres (right column). These group 2 studies included additional hydration steps not performed in group 1. .... 62

Figure 36: Images captured post aerosol deposition onto HBE 456 cell cultures. Ambisome in sterile water (left column) and Ambisome in calfactant/sterile water (right) were labeled with 0.1 micron PS spheres to trace drug movement on the cultures. The Group 2 hydration protocol was utilized. .... 64

Figure 37: Images captured post aerosol deposition onto HBE 457 cell cultures. Ambisome in distilled water (left column) and Ambisome in calfactant/ water (right) were labeled with 0.1 micron PS spheres to trace drug movement on the cultures. The Group 2 hydration protocol was utilized. .... 65

Figure 38: Images captured post aerosol deposition onto CF 102 cell cultures. Ambisome in distilled water (left column) and Ambisome in calfactant/ water (right) were labeled with 0.1 micron spheres to trace drug movement on the cultures. The Group 2 hydration protocol was utilized. .... 66

Figure 39: Average area of saline (red) or surfactant (CTAB-blue, SDS-green, tyloxapol - yellow, calfactant - gray) distribution on PGM post aerosol deposition (n=5). Each solution was labeled with texas red dextran, 0.1 and 1.0 micron PS spheres. A t-test and ANOVA were performed to obtain the corresponding p-values. .... 68

Figure 40: Average area of saline/surfactant distribution on CF 102 cell cultures post aerosol deposition. Saline (red), tyloxapol (blue), and calfactant (green) were labeled with texas red dextran, 0.1 and 1.0 micron PS spheres. The Group 2 hydration protocol was used. A t-test and single factor ANOVA were used obtain the corresponding p-values..... 69

Figure 41: Average area of saline/surfactant distribution on CF 103 cell cultures post aerosol deposition. Saline (red), tyloxapol (blue), and calfactant (green) were labeled with texas red dextran, 0.1 and 1.0 micron PS spheres (n=1). The Group 2 hydration protocol was used. A single factor ANOVA was used..... 70

Figure 42: Average area of saline/surfactant distribution on CF 105 cell cultures post aerosol deposition. Saline (red), tyloxapol (blue), and calfactant (green) were labeled with texas red dextran, 0.1 and 1.0 micron PS spheres (n=1). The Group 2 hydration protocol was used. A single factor ANOVA was used..... 71

Figure 43: Average area of saline/surfactant distribution on HBE 456 cell cultures post aerosol deposition. Saline (red), tyloxapol (blue), and calfactant (green) were labeled with texas red dextran, 0.1 and 1.0 micron PS spheres (n=2). The Group 2 hydration protocol was used. A t-test and single factor ANOVA were used to obtain the corresponding p-values. .... 72

Figure 44: Average area of saline/surfactant distribution on HBE 457 cell cultures post aerosol deposition. Saline (red), tyloxapol (blue), and calfactant (green) were labeled with texas red dextran, 0.1 and 1.0 micron PS spheres (n varies for each case). The Group 2 hydration protocol was used. A t-test and single factor ANOVA were used to obtain the corresponding p-values. . 73

Figure 45: Average area of saline/surfactant distribution on all three CF cell lines combined, CF 102, CF 103, CF 105, post aerosol deposition. Saline (red), tyloxapol (blue), and calfactant (green) were labeled with texas red dextran, 0.1 and 1.0 micron PS spheres (n varies for each case). The Group 2 hydration protocol was used. A t-test and single factor ANOVA were used to obtain the corresponding p-values. .... 74

Figure 46: Average area of saline/surfactant distribution on HBE 456 and HBE 457 cell cultures combined, post aerosol deposition. Saline (red), tyloxapol (blue), and calfactant (green) were labeled with texas red dextran, 0.1 and 1.0 micron PS spheres (n varies for each case). The Group 2 hydration protocol was used. A t-test and single factor ANOVA were used to obtain the corresponding p-values. .... 75

Figure 47: Average area of Ambisome+dH2O (red) and Ambisome+calfactant+dH2O distribution on HBE 456 (left), HBE 457 (center), and CF 102 (right) cultures, post aerosol deposition (n=2). The tag selected was the 0.1 micron PS spheres. The Group 2 hydration protocol was used. A t-test was used to obtain the corresponding p-values..... 76

## ACKNOWLEDGEMENTS

Throughout the past two years several people have contributed to the completion of my graduate studies. I will forever be grateful for all the guidance and support that Dr. Tim Corcoran, my thesis advisor, has provided me over the past two years. I thank him not only for his hard work and dedication that contributed greatly to the success of my thesis project, but for all his advice and guidance. I truly learned what it means to be a bioengineer. I would also like to thank all the members of my committee, especially Dr. Stephen Garoff for all his hours of pondering this project idea. Thank you to Dr. Pilewski and all the members of his lab, especially Erin McKenna and Joe Latoche for teaching me everything I needed to know about cells. Thank you to the members of the Aerosol Lab, Kevin Mihelc, Matt Wolf, and Abhiram Bhashyam, for all your help. I would like to thank the members of the Center for Biological Imaging, especially Dr. Simon Watkins, Glenn Papworth, and Stuart Shand and all the administrative staff in the division of the Pulmonary, Allergy, and Critical Care.

Most importantly I would like to thank my family for all their love and support. My Mom, Dad, and brothers have supported me through everything I have achieved and I never could have made it through without them. And I owe a special thank you to all the great friends and relationships I made in Pittsburgh. You made my time in Pittsburgh such a memorable experience. I will truly miss you all.

## 1.0 INTRODUCTION

In many cases, inhaled aerosol drugs can deliver substantial doses of medication directly to the lungs, while minimizing the systemic concentrations that are often associated with side effects such as nephrotoxicity. Antibiotics are regularly administered through this route for the treatment of pulmonary infections associated with cystic fibrosis (CF). These infections are the leading cause of morbidity and mortality in this population. For an aerosol anti-infective to fully eradicate an infection, it must be delivered in sufficient dose to all portions of the lung. The airway obstructions associated with CF lead to altered ventilation patterns and may cause inhaled drugs to deposit non-uniformly. Some lung regions may receive high local doses of medication while others go untreated. Infections may be suppressed by aerosol antibiotics, but are rarely eradicated due to the reservoirs of infection that are never effectively treated by the therapy.

One approach to improving the non-uniformities of aerosol delivery is to augment the distribution of drug beyond aerosol transport itself. Exogenous surfactants are widely administered to premature babies who lack sufficient amounts of endogenous pulmonary surfactant to sustain proper lung function. A surfactant bolus is usually delivered through an endotracheal tube and is transported through the lungs by gravity and surface tension gradients that generate convective flows, called Marangoni flows. The success of this treatment has led to the proposed use of surfactants in the delivery of aerosol medications; however little experimental evidence has been produced to support this. Most aerosol medications are dissolved in saline, with a relatively high known surface tension. Aerosol medications dissolved in surfactants (significantly lower surface tensions) or surfactant components may distribute more uniformly over the airway surfaces after deposition, because of convective flows caused by surface tension gradients. Aerosolized surfactant drug carriers have the potential to improve the uniformity of drug distribution in the lungs and to increase antibiotic drug concentrations in lung areas affected by altered ventilation, increasing the probability of eradicating infection. This

would also have the potential to improve the overall efficacy of many aerosol medications used to deliver drugs to the airways for lung conditions such as asthma, chronic bronchitis, and pneumonia.

The purpose of the present study was to evaluate the potential for surfactant driven flows within the lungs following aerosol deposition of a surfactant carrier liquid. A novel aerosol delivery system was developed to quantify distribution following aerosol deposition onto in vitro models of the airway surface. The range in dispersion following aerosol deposition of several surfactant carrier liquids vs. saline was quantified and the future role of surfactant carriers in the delivery of aerosol medications is discussed.

## **2.0 BACKGROUND**

### **2.1 AIRWAY PHYSIOLOGY**

The primary function of the lungs is to exchange oxygen and carbon dioxide between an organism and the external environment. Inspired air passes through either the nose or the mouth into the pharynx, and then the larynx, which contains the vocal folds. The trachea connects these upper airways to the large central airways of the lung. The airways of the lungs form an asymmetrical branching system that begins at the trachea and bifurcates successively into tubes of decreasing diameter and increasing number from the central airways towards the peripheral lung. The first bifurcation occurs at the base of the trachea forming the carina and the left and right mainstem bronchi. These bronchi further bifurcate into the bronchioles, terminal bronchioles, respiratory bronchioles, eventually terminating at the gas exchange units, the alveoli. The airways beyond the larynx are divided into two zones: 1) the conducting zone, which extends from the trachea to the bronchioles, that leads inspired air to the gas exchange region; and 2) the respiratory zone, extending from the respiratory bronchioles on down to the alveoli, that is the region of the lung where gas exchange occurs [1].

#### **2.1.1 Airway Epithelium**

A continuous layer of epithelial cells lines the luminal surface of the airways. Tight gap junctions between these cells may allow for limited passage of materials across the epithelium, which is otherwise relatively much less permeable than the respiratory surfaces of the alveoli. Several cells types that perform a variety of functions are found along the airway epithelium (see Table 1).

**Table 1: Selected cells of the airway epithelium [2].**

<b>Cell Type</b>	<b>Function</b>
Ciliated columnar	Mucus movement
Mucous (goblet)	Mucus secretion
Serous	Periciliary fluid; mucus secretion
Clara (non-ciliated epithelial)	Xenophobic metabolism; surfactant stem cell
Basal	Progenitor for ciliated epithelial and goblet cells
Lymphocytes	Immunoregulation

Ciliated columnar cells are usually 20 $\mu$ m in height, 10  $\mu$ m in width, with approximately 100-200 cilia/cell [3]. Cilia are tiny hair-like structures that line the apical surface of the airways from the trachea to the bronchioles. These cells are attached to the basal lamina and extend to the luminal surface. Mucous, clara, and serous cells are considered the major secretory cells in the airways because they contain membrane bound, fluid-filled secretory granules. Clara cells are non-ciliated columnar cells found mostly in the terminal and respiratory bronchioles replacing the mucous cells in the smaller airways. They secrete several proteins, including some surfactant proteins. Clara cells also secrete enzymes for detoxification of inhaled substances and may also act as stem cells for the epithelium [4]. Basal cells are found on the basement membrane between the ciliated epithelial and secretory cells. It has been suggested one of the basal cells' function is to anchor the columnar cells to the basement membrane [3]. Lymphocytes are also present in normal airways and sometimes form aggregates referred to as bronchial-associated lymphoid tissue (BALT). Increases in the number of lymphocytes in the airway lumen and airway wall have been associated with several disease states such as asthma, bronchitis, and pneumonia [3].

### 2.1.2 Airway Surface Liquid Layer (ASL)

When fully extended, cilia reach a height of approximately 7  $\mu\text{m}$  [5]. The cilia are surrounded by a watery layer called the periciliary liquid (PCL) (Figure 1). Above the PCL lies a viscoelastic mucus layer, composed of 95% water, 2% glycoproteins, 1% proteins, 1% lipids, and 1% inorganic salts [6]. Mucin composition has been estimated to range from 50-90% carbohydrate by weight. Although the mucus is often referred to as a “layer”, it is suggested that this may be a tangled network of mucins [7] linked by linear or branched disulfide bridges [8-10]. Mucins are heavily glycosylated proteins that represent a family of large (1 - 50 MDa) glycoproteins with a peptide backbone and oligosaccharide side chain that when dissolved form an entangled mucus hydrogel. They also have regions containing both neutral and acidic, branched and linear saccharides [11] and a net negative charge due to the presence of sialic acid residues [12]. The mucus network is unable to penetrate between the cilia because the pore size of the the gel (100nm) is less than the diameter of cilia (200nm) [13]. Mucins are secreted mostly from goblet cells and submucosal glands in the large airways and by clara cells and serous cells in the small airways. The mucus serves two functions: 1) to trap inhaled particles and bacteria to be removed from the airways, and 2) to act as a liquid reservoir for the PCL [5]. The PCL hydrates the cell layer below it and its low viscosity facilitates the ciliary beating that propels the mucus layer toward the mouth to be cleared from the airways. This action is a primary defense mechanism in the conduction zone known as mucociliary clearance.

Collectively the PCL and the mucus layer are known as the airway surface liquid (ASL). This model two-compartment system has been generally accepted; however its exact composition and structure is not fully understood due to the difficulties of ASL preservation in vitro. The ASL is estimated to range in depth from 10-30  $\mu\text{m}$  [5], with a volume of approximately 1 $\mu\text{l}$  per  $\text{cm}^2$  of mucosal surface [13]. It has also been suggested that a continuous surfactant-like film is present at the air liquid interface from the central airways to the alveoli [14].

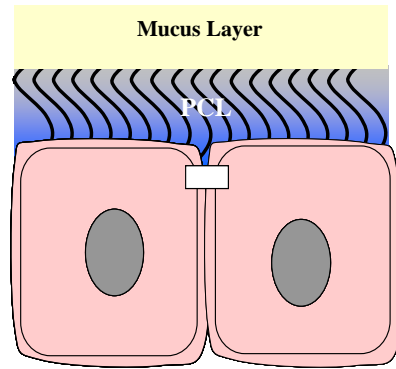


**Figure 1:** Model of two epithelial cells joined by a gap junction with the above airway surface liquid (ASL).

## 2.2 CYSTIC FIBROSIS

### 2.2.1 Pathogenesis

Cystic Fibrosis (CF) is an autosomal recessive disease affecting the pancreaticobiliary, intestinal, and reproductive systems, amongst others. The primary morbidity and mortality in CF is associated with the respiratory system. Over 30,000 Americans suffer from this disease and approximately 10 million are carriers of the defective CF gene. The median survival age is currently 36.8 years [15]. People with CF are born with normally functioning lungs but typically begin to manifest patterns of bacterial colonization and inflammation early in life. Repeated instances of acute and chronic infection and inflammation can lead to permanent lung damage in the form of bronchiectasis, airway dilation, and airway wall thickening. This lung damage is permanent and often fatal.

A key component of the pathogenesis of CF is the abnormal ion transport across the airway epithelium which is believed to be caused by the lack of a functional apical epithelial chloride channel called the Cystic Fibrosis Transmembrane Conductance Regulator (CFTR) protein (blue channel shown in Figure 2). The CFTR gene has >1000 identified mutations that disrupt the ion balance that exists between the ASL and epithelium [5]. The mutant phenotypes expressed may include: lack of CFTR expression at the cell membrane caused by early termination of translation or protein processing errors; CFTR expression at the membrane with

little or no chloride conduction due to either inactivated or altered channels; or reduction in the total number of functional CFTR channels due to improper mRNA splicing [7]. Studies of ion and fluid transport [16, 17] and patch clamp studies of membrane channels [18] in both excised tissue and cultured airway cells have suggested that CFTR functions not only as a chloride ion pathway, but also to regulate the sodium channel, ENaC. A nonfunctional CFTR results in overactivity of these  $\text{Na}^+$  channels yielding sodium hyper-absorption and decreased  $\text{Cl}^-$  secretion, which results in water absorption across the epithelium. This absorption dehydrates and ultimately depletes the volume of the ASL (Figure 2) which is the major source of the problems associated with CF. Some  $\text{Cl}^-$  is still transported via other chloride channel pathways. When the ASL is depleted, normal mucociliary clearance can be greatly reduced as illustrated in Figure 3.

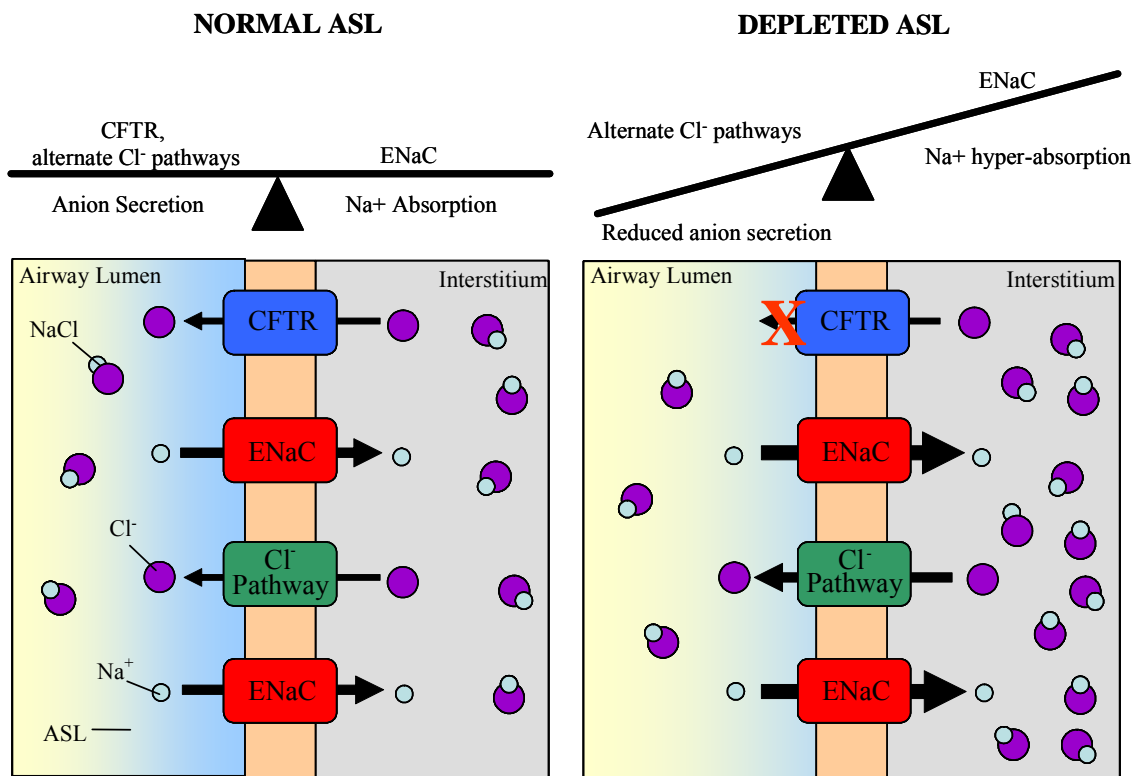


**Figure 2:** The balance of  $\text{Na}^+$  absorption and  $\text{Cl}^-$  secretion is maintained when a functional CFTR is present in normal airway epithelia. The lack of a functional CFTR channel (right) results in  $\text{Na}^+$  hyper-absorption and decreased  $\text{Cl}^-$  secretion via other pathways, resulting in ASL dehydration and volume depletion [7, 19].

### 2.2.2 ASL Volume Regulation

ASL volume regulation is crucial for maintaining normal mucociliary clearance [20]. The regulation of fluid between the mucus and PCL is complex and still poorly understood. It is suggested that there is a system of sensors that monitor the ASL volume and regulate the fluid absorption and secretion [7]. Individuals with fully extended cilia and normal PCL volume are able to maintain normal clearance and therefore little mucus accumulates in the airways (Figure 3, left). The center illustration shows that a depleted PCL volume prevents cilia from fully extending, delaying mucociliary clearance, and resulting in mucus accumulation. The right most illustration has even greater PCL depletion resulting in thickened mucus that is no longer transportable from the airways by cilia. A decrease in mucociliary clearance can lead to the accumulation of infected mucus plugs causing inflammation that may lead to bronchiectasis and peribronchial thickening.

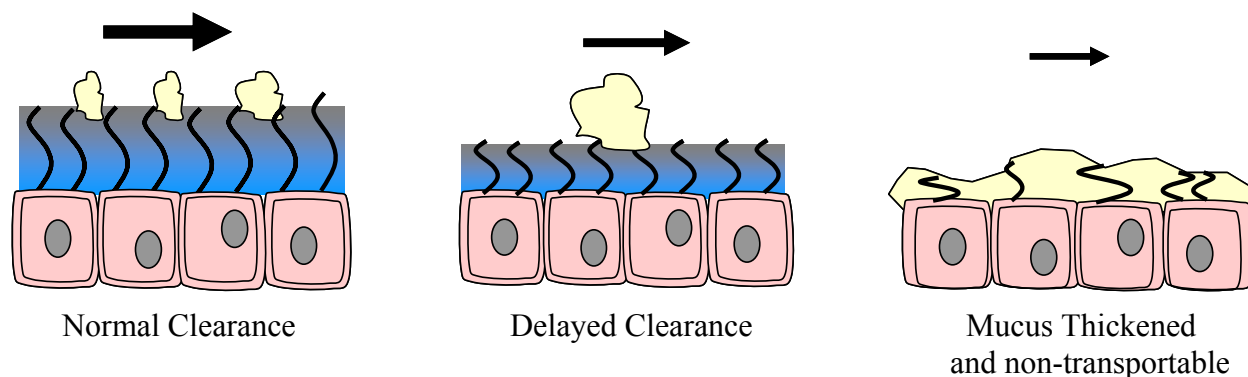


**Figure 3:** ASL depletion leading to delayed mucociliary clearance.

### 2.2.3 In Vitro Study

One of the greatest challenges in studying CF is the lack of a realistic animal or cellular model. The CF mouse, which over expresses the sodium absorbing channel ENaC, may provide a means to test interventions, but provides little use in evaluating the consequences of CFTR mutations

[21]. Human bronchial epithelial (HBE) cells cultured from excised lung specimens are currently the best in vitro model available. When properly cultured at an air-liquid interface, these cells differentiate and develop cilia, mimicking most aspects of the airways epithelium including membrane electrophysiology. Mucus transport rates similar to in vivo conditions have been demonstrated with these cultures [5]. Some difficulties associated with the HBE cultures are the limited number of lung specimens available and maintaining a consistent level of hydration during experimentation. Another cell culture often used for in vitro studies of the epithelium is an adenocarcinoma cell line known as Calu3. Calu3's form a monolayer of cells connected via gap junctions and exhibit high CFTR expression. However, no cilia nor ASL is present, and these cells more closely resemble serous cells [22].

### **2.3 AEROSOL DELIVERY**

Aerosols are defined as suspensions of liquid or solid particles dispersed in a gas [23]. Inhaled aerosol medications are a favorable choice for the treatment of lung disease. Through this route substantial drug dose can be delivered directly to the lung providing rapid drug dosing with minimized systemic effects in many cases. Liquid aerosols are generated using a nebulizer, a device that uses compressed air or another source of atomization energy to produce a mist, or metered dose inhalers (pMDIs), which use pressurized propellants to create an aerosol. Dry power inhalers (DPIs) use different methods to disperse powder aerosols for inhalation. The quick access to the bloodstream available through the lungs also provides an attractive route for systemic drug delivery, which is targeted to the alveoli based on the large total available surface area available in the respiratory zones. Recent research has been conducted on inhaled insulin for diabetes [24] and opiates for pain control [25].

Three specific mechanisms usually result in aerosol deposition in the lungs: inertial impaction, sedimentation, and diffusion. The involvement of each mechanism depends on several factors such as physical aerosol characteristics, ventilation patterns, and the airway anatomy. Aerosol size is a major factor in determining the location of aerosol deposition within the respiratory tract. This size is usually expressed as an aerodynamic diameter ( $D_{ac}$ ), defined as the spherical diameter of a particle of unit density ( $1 \text{ g/cm}^3$ ) having the same terminal velocity as

the particle of interest [26]. Most nebulizers are designed to generate aerosols in the respirable range of  $D_{ac}=1-5\mu\text{m}$  [2]. Inertial impaction occurs when a particle follows a straight-line path instead of the streamlines of the bulk air flow (Figure 4). A particle or droplet may continue along this inertial path if its momentum exceeds the drag force of the conducting air, resulting in deposition. Large aerosols usually deposit by this mechanism in the upper airways, often where flows rapidly change direction or speed and at airway bifurcations. This mechanism is especially important in obstructive lung diseases such as CF, asthma, and chronic obstructive pulmonary disease (COPD), where obstructive disease elements will contribute to increased impaction.

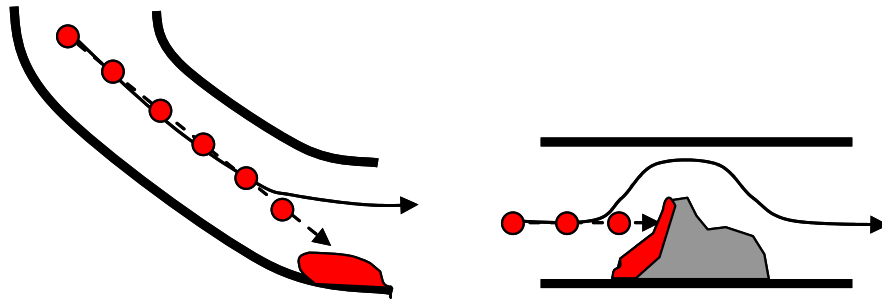


**Figure 4:** Inertial impaction of an aerosol in a normal airway (left) and obstructed airway (right).

Several investigators have performed deposition experiments using airway casts to model aerosol deposition. Schlesinger and Lippmann [27] modeled inertial impaction using an impaction parameter:

$$\mathbf{impaction} = \rho d^2 Q \quad (1)$$

where  $\rho$  is the particle density,  $d$  is the particle diameter, and  $Q$  is the inhalation flow rate. The Stokes number is a parameter often used to predict the likelihood of deposition due to impaction:

$$\mathbf{Stokes} = \frac{\rho d^2 V}{18 \mu D} \quad (2)$$

where  $V$  is the conducting air velocity,  $\mu$  is the viscosity of air, and  $D$  is a geometric parameter of the airways. An increase in aerosol density or size, or an increase in conducting air velocity will yield a higher Stokes number indicating that the aerosol is more likely to deposit through impaction. The high gas velocities in the upper respiratory tract contribute to increased aerosol impaction in the upper airways, decreasing the total dose of medication that reaches the lung periphery.

Aerosol deposition is governed by gravitational forces in the alveolar portion of the lung due to the decreased flow velocities in this region. This deposition mechanism is typically referred to as sedimentation. A particle with diameter  $d$  descending through air with a viscosity  $\mu$  will reach a terminal velocity  $v$  when the gravitational forces equal the drag forces. Assuming only gravity and a vertical Stokesian drag force acting on the particle, the net forces can be described as follows (assuming the Reynolds (Re) number  $\ll 1$ ):

$$\mathbf{F}_{\text{drag}} = 3\pi d\mu v_{\text{terminal}} \quad (3)$$

Using the force of gravity (equation 4) and the volume of a sphere (Volume =  $4\pi r^3/3$ ), we can equate equations 3 and 4 to obtain a terminal velocity,  $v$ . A faster terminal velocity for the aerosol will increase the likelihood of deposition prior to exhalation.

$$mg = \rho Vg \quad (4)$$

$$v_{\text{terminal}} = \frac{\rho g d^2}{18\mu} \quad (5)$$

Based on the above it can be seen that the probability of sedimentation increases with aerosol size and density [28]. Since these variables are also important to inertial deposition, an aerosol size range accommodating both mechanisms must be found to deliver aerosols to the deep lung. The aerosol must be small enough to avoid the inertial filters of the upper airways and yet still large enough to deposit in the deep lung before being exhaled. The probability of deposition in

the deep lung will also increase with a slower breathing pattern that allows for more time for deposition.

Very small aerosols can deposit in the lungs through a mechanism typically referred to as diffusion. Diffusion applies to extremely small particles, those  $<0.5 \mu\text{m}$  in diameter [29]. Aerosols of this size are affected by the random Brownian motion of gas molecules causing them to deposit. To assess the contribution of diffusion in aerosol deposition, the time interval and breathing patterns must be considered along with the specific size of the aerosol [23]. This mechanism is very efficient for the smallest of aerosols ( $\sim 1\text{nm}$ ) causing them to deposit as soon as they enter the respiratory tract. The formulation of drug aerosols in this size range is not routinely performed based on manufacturing considerations. Aerosol size distribution has the potential to vary during transport in the airways due to a number of mechanisms: particle aggregation, droplet evaporation, hygroscopic growth (a condensation of liquid onto the aerosol), and charge related effects.

### **2.3.1 Aerosol Delivery to the Diseased Lung**

Aerosols naturally follow air flows away from regions of high resistance and obstruction, resulting in non-uniform drug deposition. Lung diseases such as CF, asthma, bronchitis, and chronic obstructive pulmonary disease (COPD) exhibit different degrees of airway obstruction resulting in non-uniform ventilation and correspondingly non-uniform aerosol delivery. As previously mentioned obstructions may also contribute directly to deposition. Studies have found that asthma patients with airway obstructions tend to have greater deposition in the central airways vs. the peripheral regions [30], likely due to increased impaction and altered ventilation. This pattern is illustrated by the gamma images in Figure 5. The image on the left demonstrates the non-uniform deposition radiolabeled drug in a single lung transplant recipient suffering from a respiratory infection. The white and red concentrated areas demonstrate that the drug is deposited mainly in the central airways. The image on the right was taken of the same patient after inhalation of a radioactive gas (Xenon) demonstrating that the peripheral regions of the lung were not completely obstructed. The aerosols were not reaching those same areas, most likely due to increased resistance and increased impaction associated with partial obstruction.

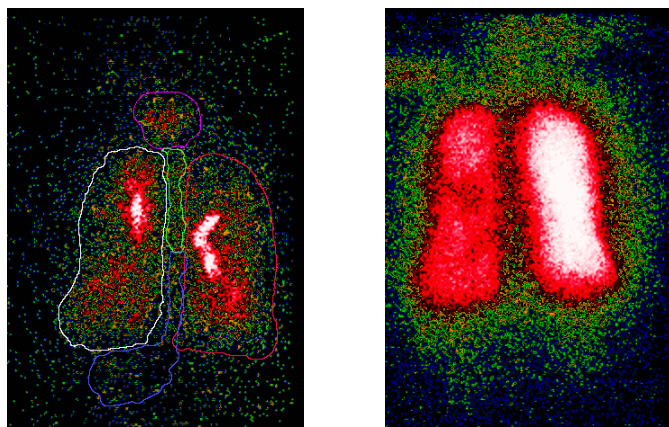


**Figure 5:** Radioscintigraphy images of aerosol drug deposition (left) and xenon gas ventilation (right) in the lungs.

### 2.3.2 Aerosol Antibiotics

Despite the non-uniformities of aerosol administration in diseased lungs, inhalation is still a favorable route for treating lung infections, due to the high drug concentrations that can be achieved in many cases with only minimal associated systemic concentrations and similarly reduced systemic side effects. A convincing example to consider is the inhaled antibiotic, Tobramycin (*TOBI*®, Chiron Corp, Emeryville, CA). TOBI is administered using a jet nebulizer to treat the most common infection seen in CF patients, the gram-negative bacterial pathogen *Pseudomonas aeruginosa* (*PA*). *PA* is found in approximately 70% of CF patients by the age of 17 and found in over 90% of CF patients at some point in their life [31]. The IV form of tobramycin has significant side effects, including potential kidney failure. For the aerosol form however, studies have demonstrated peak sputum concentrations of >25 times the minimum inhibitory concentration (MIC) in approximately 95% of CF subjects tested, with one hour serum concentrations of only 0.95 µg/ml [32], compared to IV serum levels of 4-6 µg/ml [33].

Ramsey et al. conducted a short-term study to evaluate the efficacy of inhaled tobramycin in decreasing the density of *PA* and improving pulmonary function in CF patients [34]. Seventy-one patients received one of two regimens: 28 days of inhaled tobramycin followed by 2, 28-day periods of inhaled saline (placebo) or 28 days of saline first followed by 2, 28-day periods of

tobramycin. The greatest improvement in lung function and largest decrease in PA density was seen during the first 28 days of tobramycin treatment for both groups.

A longer-term study of inhaled tobramycin demonstrated its ability to improve pulmonary function and decrease hospitalization days in a larger sample of the CF population (n=258) [35]. Intermittent TOBI administration was assessed in CF patients with known infections of PA. TOBI or placebo were administered in three on-off cycles, 4 weeks of drug followed by 4 weeks of no drug, for a total of 24 weeks. Patients receiving tobramycin demonstrated improved pulmonary function that was sustained throughout the on-off drug cycle, while the placebo group had a decline in lung function. The group receiving tobramycin was found to be 26% less likely to be hospitalized and 36% less likely to need intravenous antibiotics than the placebo group. TOBI subjects also experienced >100-fold decreases in colony forming units (CFU's) of PA during each 4 week treatment. However, when the drug administration was suspended, the bacterial levels increased within 10 fold of the levels observed at week 0. Collectively, these TOBI trials suggest effective suppression of infection, but not eradication. One potential cause of the resurgence of infection in these subjects is a failure of the aerosol to reach all of the infected regions.

TOBI is the only inhaled antibiotic currently approved for CF or non-CF use. Several antibiotics available in other forms are being developed as aerosols and some others have long histories of off-label inhaled use. Examples include: nebulized colistin [36, 37]; a sustained release liposomal formulation of the antibiotic amikacin (SLIT™ Amikacin) [38, 39]; nebulized aztreonam [40]; nebulized gentamicin [41]; a dry power formulation of ciprofloxacin [42]; and a dry power formulation of tobramycin [43, 44]. The high pulmonary doses associated with aerosol administration may offer a means of overcoming bacterial resistance.

Aerosol antibiotics also provide an alternative to systemic antibiotics in the intensive care setting. Mechanically ventilated patients have an increased risk of ventilator associated pneumonia (VAP). A reported 350,000 cases occur per year with a mortality risk of 20-70% [45]. As mentioned, the aerosol route may decrease systemic toxic effects by localizing medication in the lungs. One study found that in mechanically ventilated patients with nosocomial pneumonia, ceftazidime (antibiotic) concentration in tracheal aspirates was approximately 100 times higher with aerosol administration than with IV, while peak plasma concentrations were approximately 25 times lower [46]. Aerosol antibiotics have never been

widely applied in this setting, which is likely due to the difficulty of delivering aerosols to intubated patients and a perceived risk of developing bacterial resistance. In vitro models are being developed to address these concerns [45].

Uniform distribution of an antibiotic aerosol is essential to whole-lung eradication of pathogens. Attaining this wide spread distribution is made more difficult by the obstructions that would be expected with profound infection. Currently, most aerosolized medications are dissolved in saline and drug distribution is determined by aerosol transport only. An alternative approach is to dissolve these medications in surfactant or surfactant components to enhance distribution following aerosol deposition. Drug distribution may be enhanced by surface tension gradients generating convective flows that distribute drugs in addition to the aerosol transport mechanisms. The development of a self-spreading carrier liquid would have the potential to improve the efficacy of almost every aerosol drug designed to act within the airways.

## 2.4 DRUG DISTRIBUTION FOLLOWING DEPOSITION

### 2.4.1 Diffusion

Once an aerosol deposits on the luminal airway surface its distribution depends primarily on the diffusion of drug over or through the ASL. The rate of diffusion of several antibiotics has been modeled in both water ( $D_{aq}$ ) and a bacterial biofilm ( $D_e$ ) [47]. A diffusion time scale through these materials can be estimated using a specified length scale and the diffusivity,  $\frac{L^2}{D_{aq}}$  or  $\frac{L^2}{D_e}$ . In

the airways, if the ASL is assumed to be 10  $\mu\text{m}$  thick ( $L$ ), using the diffusivity value for tobramycin [48], the estimated time scale for diffusion through water is  $\sim 0.2\text{s}$ . However, when this is applied to the larger length scale of the airway tree, diffusion along 1mm of airway would be  $\sim 1800\text{s}$ . Therefore, the overall distribution of drug is not significantly affected by diffusion following aerosol deposition. This is also demonstrated by examining images similar to those in Figure 5. Little change in drug distribution is observed immediately following an aerosol dose. This is not observed until mucociliary or cough clearance removes drug from the lungs.

## 2.4.2 Surface Tension Driven Flows

### 2.4.2.1 Surface tension

Surface tension ( $\gamma$ ) is a cohesive force that acts tangentially at an air-liquid interface to minimize the interfacial area [49]. Molecules at the surface of a liquid are not surrounded by all like molecules and therefore experience a force perpendicular to and inward from the surface of the liquid. This force causes the molecules to arrange along the boundary with the fewest number of molecules at the surface, minimizing the interfacial area as shown in Figure 6. The surface tension is the cohesive tangential force between the molecules at the surface, measured in dynes/cm or mN/m, as a force per unit length:

$$\gamma = \frac{F}{2l} \quad (4)$$

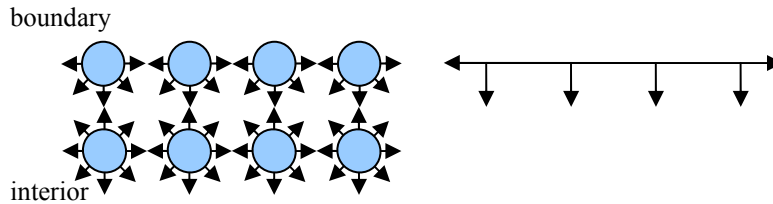


**Figure 6:** Forces experienced by molecules at a boundary surface. The resultant tangential force (right) represents the surface tension force.

### 2.4.2.2 Marangoni flow

Surfactants are wetting agents that lower the surface tension of liquids. Most surfactants are amphiphathic molecules; they contain a hydrophilic polar head group and a non-polar hydrophobic tail. These are surface active molecules that tend to adsorb at surfaces and form a monolayer that minimizes molecule interaction with water [50]. At an air-liquid interface, the surface tension depends on the local concentration of surfactant. If a concentration gradient of surfactant is present, convective flows (Marangoni flows) are generated that drive both the liquid and the surfactant from an area of high to low surfactant concentration [51]. The spreading of

one liquid on the surface of another can be predicted with the spreading coefficient described in equation 8, where  $\gamma_1$  and  $\gamma_2$  are the surface tension values of two liquids,  $\gamma_{12}$  is the interfacial tension between the two liquids, and  $S$  is the spreading coefficient of liquid 2 on liquid 1:

$$S_{1/2} = \gamma_1 - \gamma_2 - \gamma_{12} \quad (5)$$

Spreading will generally occur when a low surface tension liquid is placed on a liquid of higher surface tension, which yields a positive  $S_{1/2}$  [51]. A simple example of this is soap (a surfactant with low surface tension) forming a thin film over a layer of water (liquid with high surface tension). This motion is demonstrated in Figure 7, the “soap boat”. The boat contains a small volume of soap. As the soap is released from the boat, the local surfactant concentration rises, propelling the boat across the water surface visible by the white streak parting the water surface labeled with blue dye.



**Figure 7:** The “soap boat” is a simple example of the surface tension driven Marangoni flows (reprinted with permission, from the Annual Review of Fluid Mechanics, Volume 38 © 2006 by Annual Reviews [www.annualreviews.org](http://www.annualreviews.org))

Figure 8 illustrates this idea applied to the airways. If an aerosol surfactant drug carrier is delivered to the airway surface, Marangoni flows may enhance drug distribution by propelling surfactant and drug over the PCL and/or mucus layers increasing the area over which the drug

will diffuse. Since these flows would be driven by surfactant concentration gradients, the endogenous surfactant present in the lung must be considered.

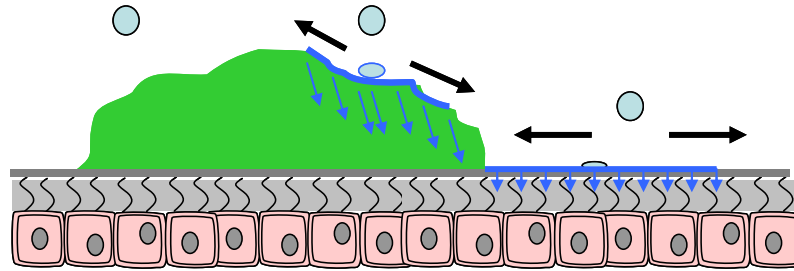


**Figure 8:** Aerosol drug deposition upon the ASL using a surfactant carrier.

### 2.4.3 Pulmonary Surfactant

#### 2.4.3.1 Alveolar

Pulmonary surfactant is largely produced in the alveoli by alveolar Type II cells and is composed of approximately 80% phospholipid, 10% protein, and 10% neutral lipids. The four major surfactant proteins, SP-A, SP-D (hydrophilic) and SP-B, SP-C (hydrophobic) have been found to have host defense and surface tension lowering properties [52]. The presence of surfactant in the alveoli is essential for stabilizing these structures during respiration cycles and maximizing the surface area available for gas exchange. Pulmonary surfactant reduces the surface tension by forming a thin film monolayer at the air-liquid interface (Figure 9). Without it, the surface tension in the alveoli would be similar to that of water (72 mN/m); but in the presence of the surfactant the alveolar surface tension values are  $<5$  mN/m.

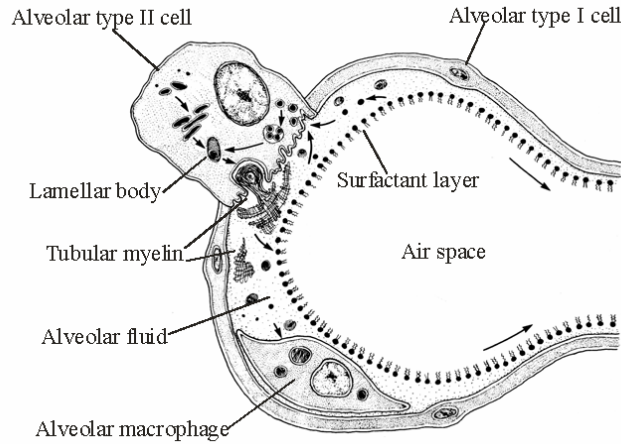


**Figure 9:** Alveolus lined with surfactant monolayer at the air-liquid interface (reprinted with permission from [53]).

### 2.4.3.2 Airway Surfactant

Because most surfactant studies have focused on its presence in the alveoli, the source and function of surfactant in the airways has not been extensively studied. Although there is a lower surfactant concentration in the airways than in the alveoli, the presence of any surfactant components will greatly affect the ASL interaction with exogenous surfactants. It has been established that a surface tension gradient exists from the trachea to the alveoli indicating the presence of surfactants or surfactant components in the central airways (Table 2).

**Table 2:** Approximate surface tension values along the surface of the airway lumen from the trachea to alveoli [54-56].

Location in Lungs	Surface Tension (mN/m)
Trachea	62
Central Airway	32
Alveolus	<5

Gehr and co-workers have performed *in vivo* and *in vitro* measurements of surface tension in the airways of several animals, typically measuring a surface tension of the order of 32 mN/m [55, 57]. In addition, they have noted in cell culture electronmicrographs, an electron-dense line at the air-liquid interface that they claim is a surface tension lowering, surfactant-like layer [58]. Tarran et al also noted this electron dense line in similar cultures and found that the electron dense line remained intact while the surface tension was increased during washings of the mucus from the cultures using a reducing agent. However, they did not conclude that the electron dense line was a surfactant-like layer [59].

Other evidence of surfactants in the airways includes phospholipids found bound to mucins in sputum samples, suggesting the mucus layer as a source for surface active materials [60]. Studies have found local synthesis of surfactant components in the airways. The hydrophobic surfactant proteins SP-B and SP-C were found to have mRNA expression and protein expression in the bronchi and bronchioles [61]. SP-A and SP-D (hydrophilic surfactant proteins) synthesis has been found in Clara cells, but these cells do not produce phospholipids [62]. Local phospholipid synthesis has been found in cells in the trachea as well [63]. Bernhard et al compared the composition and surface tension lowering properties of airway surface material in porcine lungs at the alveolar and tracheal levels. They concluded that a similar phospholipid composition was found in both, but the amount of surfactant proteins and the degree of surface tension lowering properties were diminished in the samples from the trachea, indicating the important role that surfactant proteins are believed to play in lowering surface tension [64].

#### **2.4.3.3 Other Considerations**

Local surfactant concentrations vary with the breathing cycle. The internal surface area of the lungs changes during inhalation and exhalation, causing dynamic changes in local surfactant concentrations. In the alveoli, at small lung volumes, surface tension reaches values as low as 5mN/m. As lung volume increases upon inhalation, the surfactant is spread out over a larger area, decreasing local concentrations, and increasing the alveolar surface tension to values as high as 30mN/m [65]. Airway length and diameter also change during respiration, but to a lesser degree than in the alveoli. The smallest airways experience the largest changes in area during inhalation from 50-100% total lung capacity (small ~50%, medium: ~33%, large: ~19%) [66].

This cycling of local surfactant concentration may cause gradients that further increase the circulation of surfactant-drug mixtures, resulting in better overall distribution.

## **2.5 PREVIOUS WORK**

The spreading of exogenous surfactant along the airway surface has been extensively studied both theoretically and clinically because of its role in Surfactant Replacement Therapy (SRT). SRT is used to treat premature newborns with Respiratory Distress Syndrome (RDS) which is characterized by a lack of adequate surfactant to stabilize alveoli. A bolus of surfactant is instilled at the trachea and reaches the alveoli through a combination of gravity and surface-tension driven flows [67]. Several investigators have speculated that the same forces would apply when using an aerosolized surfactant drug carrier [68, 69]; however, little experimental evidence exists on this topic. Studies that have tested the use of a surfactant drug carrier have been limited to the bolus instillation technique. Other research has been conducted on the use of aerosolized surfactants to treat surfactant deficient lung diseases such as Acute Respiratory Distress Syndrome (ARDS) [70, 71]. Recent studies have noted deficiencies in surfactant protein D in association with cystic fibrosis. Surfactant deficiencies might be associated with depressed clearance and immune function. A pilot study was conducted to determine whether aerosolized surfactant would improve lung function in CF patients [72]. No substantial benefits were demonstrated from the therapy.

### **2.5.1 Surfactant Bolus: Surfactant Replacement Therapy**

In SRT, a bolus of surfactant is administered directly through a catheter placed into an endotracheal tube. Both synthetic and natural surfactants are FDA approved and available for treatment, as listed in Table 3. The natural surfactants are from animal derived products containing phospholipids (usually the majority of which is 1,2-dipalmitoylphosphatidylcholine, DPPC) and some form of the surfactant proteins, SP-A, B, C, and D. The synthetic surfactant, Exosurf®, is a protein-free suspension containing dipalmitoylphosphatidylcholine (DPPC), cetyl

alcohol (DPPC spreading agent), tyloxapol (a non-ionic surfactant) and saline, in the ratio 13.5:1.5:1.0:5.8 [73]. The absence of the surfactant proteins may be the cause of the higher minimum surface tension noted with this preparation.

**Table 3:** Current FDA approved exogenous surfactant formulations for treating RDS and the corresponding measured minimum surface tensions [74-77].

<b>Surfactant</b>	<b>Type</b>	<b>Minimum Surface Tension (mN/m)</b>
Beractant (Survanta®)	Natural - bovine	<8
Calfactant (Infasurf®)	Natural - calf	≤3
Poractant alfa (Curosurf®)	Natural - porcine	≤4
DPPC, Cetyl alcohol, and Tyloxapol (Exosurf Neonatal®)	Synthetic	~22

Extensive theoretical modeling of the spreading of a surfactant bolus has been performed. Espinosa et al. used a model that incorporates the properties of the ASL, such as thickness, viscosity, and endogenous surfactant, as well as airway radius, bolus volume and surfactant content, and gravity. They estimate that a bolus of instilled surfactant travels from the trachea to the lung periphery in ~12 seconds, assuming a 5cm transit distance. They describe gravity and surface tension driven flows as the cause of this transit [78]. Grotberg and co-workers have further investigated this surfactant spreading both theoretically and experimentally. They have tested the effect of instillation technique and ventilation patterns on the propagation distance of the liquid bolus through the airways. Much of their study has focused on the dynamics of bolus propagation and film rupture [79-81].

Anderson et al. recently developed an imaging technique to monitor surfactant transport in the lungs in real-time. They assessed the effect of ventilation rate on the degree of liquid spreading in excised rat lungs. The study revealed that at 20 breaths/min, surfactant was localized to the central airways with the distribution being dominated by gravity forces, while at

60 breaths/min, surfactant coated the airways with a more uniform pattern of deposition, suggesting the contribution of surface tension driven flows [79].

### **2.5.2 Surfactant Bolus: Drug Delivery Vehicle**

Instilled surfactant delivery has been considered as a drug delivery technique based on the success of bolus surfactant instillation in SRT. Kharasch et al. tested beractant or saline mixed with technetium sulfur colloid and pentamidine, delivered to hamster lungs by tracheal instillation. Spontaneous respiration was sustained for 4 hours. The lungs were then excised, inflated, dried, and sliced into 3 mm sections. Using radiosciintigraphy, it was determined that the surfactant drug mixture reached 93% of the slices while the saline drug mixture reached 72% ( $p=0.02$ ). The fraction of the individual lung slices containing radioactivity was also considered. The surfactant drug mixture reached an average of 41% of each slice considered vs. 21% for the saline mixture ( $p=0.02$ ) [82].

A similar study was conducted by Van't Veen et al using a tracheal instillation of tobramycin in mice infected with *Klebsiella pneumonia*. The measured outcome variable was survival. Following the first day of infection, mice received surfactant mixed with tobramycin, surfactant alone or tobramycin alone. The study revealed there was a significant increase in survival when tobramycin was administered with the surfactant carrier, vs. just tobramycin or surfactant alone [83].

Nimmo et al tested in rats, a tracheal instillation of radiolabeled glucocorticoids mixed with beractant. Studies were performed to evaluate the possibility of delivering corticosteroids intratracheally using a surfactant carrier. Following instillation, the trachea and lungs were excised and radioactivity measured in tissue samples taken from the root, middle, peripheral regions of lobe of the lungs. The surfactant vehicle demonstrated more consistent levels of peripheral delivery when compared to saline, which was found deposited more centrally. The addition of the corticosteroids did not appreciably alter the surface tension of the surfactant [84].

Fajardo et al conducted a similar study, however they did not find a significant difference between a surfactant (beractant) and saline vehicle for the instilled delivery of corticosteroids to rabbit lungs [85].  $^3\text{H}$  Budesonide was used to track drug distribution. The study found that both vehicles delivered drug with a similar distribution. This result may have been affected by

methodology. A larger volume of the drug mixture (1.25ml/kg) was administered vs. the study performed by Kharasch et al (0.25ml/kg). The larger volume may have resulted in a more uniform distribution in the lungs.

Beractant has also been tested for the delivery of an adenoviral vector in rat lungs. Gene expression varied with volume and carrier type (beractant or saline). The adenovirus-beractant treated group exhibited more uniform transgenic expression of the virus than the adenovirus-saline treated group. At low volumes (0.5ml, 1.3ml/kg) the beractant group exhibited more pulmonary tissue activity and at high volumes (1.2ml, 4ml/kg) both groups had similar activity [86].

### 3.0 SPECIFIC AIMS

The general aim of these studies was to use a surfactant aerosol carrier in a series of in vitro models to determine whether these carriers could improve the distribution of aerosol drugs in the lungs.

**Aim 1:** To design a testing apparatus for aerosol delivery onto mucus samples and epithelial cell cultures and an imaging method for tracking the delivered material after deposition.

- Select a nebulizer and determine an optimal flow rate and aerosol dose time interval
- Determine aerosol size and ensure that it matches typical values for respiratory aerosols
- Select optimal anionic, cationic, and nonionic surfactants for testing
- Establish imaging protocol to assess spreading using dye and polystyrene spheres

**Aim 2:** To evaluate the potential for surface tension driven flows on a model mucus surface.

- Assess spreading of aerosolized surfactants vs. saline control using three different sized fluorophores

**Aim 3:** To evaluate the potential for surface tension driven flows on model epithelial cell culture surfaces.

- Assess spreading of two selected aerosolized surfactants vs. saline using Calu3, CF-human bronchial epithelial cell cultures (HBE's), and non CF-HBE models, with three different sized fluorophores
- Assess spreading of an aerosolized liposomal drug formulation in surfactant vs. water using both CF and non-CF HBE models

## 4.0 METHODS

### 4.1.1 Aerosol Delivery System

A micropump nebulizer (the Aerogen Pro, Nektar/Aerogen, Sunnyvale, CA) was used to produce a 4-5 micron median diameter aerosol and tubing of decreasing diameter was assembled to deliver aerosol through a 2mm cannula tip (Figure 10). The aerosol was driven through the tubing system using a compressor (Pulmoaide, Sunrise Medical, Somerset, PA). The air was humidified and heated to 37°C using the MR850 Humidification system (Fisher & Paykel Healthcare, Laguna Hills, CA). A flow meter placed upstream of the nebulizer was used to monitor and control the flow rate. The cannula tip was placed through a hole drilled in the cell culture plate lid that fixed its position 1mm above the delivery surface.

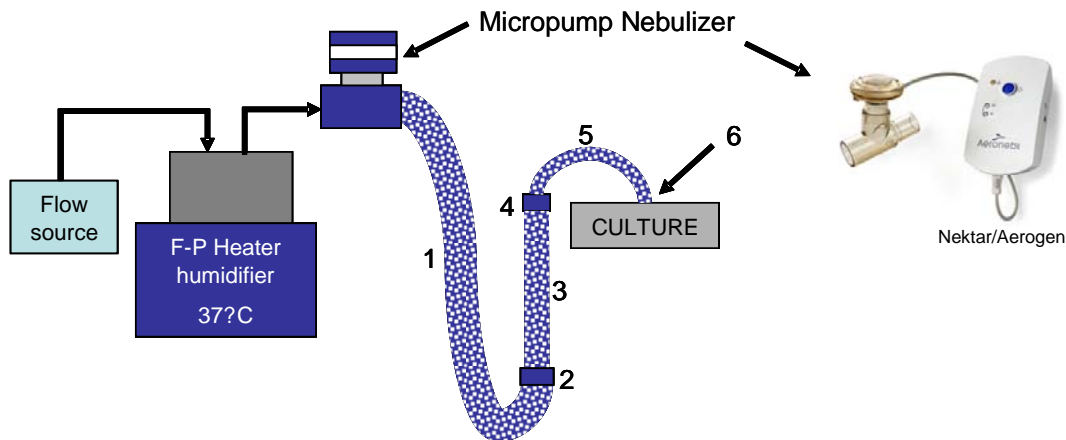


**Figure 10:** Aerosol delivery system. 100% Humidified air at 37°C was used to deliver aerosol to a porcine gastric mucus (PGM) or epithelial cell culture surface. A micropump nebulizer was used to produce an aerosol. The diameters of the tubing and connectors gradually decrease in size: 1- 22mm, 2 - 16, 12mm, 3 - 4mm, 4 - 3.5 mm, 5 - 3mm, 6 - 2mm. The aerosol exiting the end of tubing section 6 ranges from 1-4 microns in median diameter.

Laser diffraction aerosol size measurements were made using a Malvern Mastersizer S (Malvern Instruments, Worcestershire, UK). The aerosol size was measured with a standard mouth piece attached to the cannula tip (#6 in the aerosol system). Measurements for all surfactants, drug, and saline solutions were collected.

#### **4.1.2 Surfactants**

Several surfactants were selected with differing minimum surface tensions and ionic character. The control selected for all experiments was a 0.9% NaCl solution. Calfactant (provided by Dr. Edmund Egan of ONY Inc., Amherst, NY) is a natural lung extract that contains DPPC, fatty acids, and the low-molecular-weight hydrophobic surfactant-associated proteins SP-B and SP-C. Calfactant was selected for these studies due to its low surface tension and approved use for SRT. Tyloxapol (obtained from Sigma-Aldrich, St. Louis, MO) is a nonionic liquid polymer of the alkyl aryl polyether alcohol type and was selected because of its use as a spreading agent in a synthetic surfactant used for SRT, Exosurf® [73]. Its concentration in Exosurf is 1mg/ml in 0.9% NaCl. sodium dodecyl sulfate (SDS), an anionic surfactant and cetyl trimethyl ammonium bromide (CTAB), a cationic surfactant, were both dissolved in distilled water at their critical micelle concentrations (CMC), as shown in Table 4.

**Table 4:** The minimum surface tensions and concentrations used for saline (control) and the surfactants selected for experimentation [73, 74, 77, 87]

<b>Solution</b>	<b>Minimum Surface Tension (mN/m)</b>	<b>Concentration</b>
<b>Saline</b>	72	Isotonic
<b>Calfactant</b>	4	35mg/ml of phospholipid in 0.9% saline
<b>Tyloxapol</b>	22	1 mg/ml (0.22mM = 12 x CMC)
<b>SDS</b>	32	2.39 mg/ml (aq) (8.3mM = 1 x CMC)
<b>CTAB</b>	35	0.364mg/ml (aq) (1mM = 1 x CMC)

### 4.1.3 Microscopy

All imaging was performed at the Center for Biological Imaging, University of Pittsburgh. Images were captured using a Macro zoom fluorescence dissecting microscope (MVX10 MacroView, Olympus, Center Valley, PA) and Coolsnap K4 camera (Photometrics, Tucson, AZ). Images were processed using Metamorph software (Molecular Devices, Sunnyvale, CA). Three fluorescent tags were selected to act as a drug analog when mixed with the surfactant and saline solutions. Texas red dye conjugated to a 10kDa dextran (dextrans are hydrophilic saccharides) was selected due to its neutral charge, high molecular weight, and relative impermeability to the airway epithelium. Texas red dextran (Molecular Probes, Carlsbad, CA) was provided as a pure lyophilized powder and dissolved in phosphate-buffered saline (PBS) to a concentration of 2mg/ml. The other fluorophores selected were polystyrene (PS) fluorescent microspheres (FluoSpheres®, Molecular Probes, Carlsbad, CA) in 0.1 micron (red fluorescence) and 1.0 (green fluorescence) diameters. The spheres are available as a suspension in water plus 2mM sodium azide and have a carboxylate surface group yielding a net negative charge. All surfactant and control solutions were labeled with Texas red (1% by volume) or the microsphere suspensions (0.1% by volume) and vortexed immediately prior to the aerosol delivery.

#### **4.1.4 Mucus Model Surface**

Porcine gastric mucin (PGM) was selected as a preliminary model of airway mucus (Type III mucin, partially purified, ~1% bound sialic acids, Sigma-Aldrich, St. Louis, MO). The lyophilized mucus was reconstituted using 0.9% NaCl at varying concentrations ranging from 90-95% saline. Preliminary experiments were performed to assess spreading of two selected surfactants, Tyloxapol and Tween20. Tween20 is another nonionic surfactant; however it was not used beyond these preliminary experiments. PGM at a concentration of 100 mg/ml (90% saline) with a depth of approximately 5 mm was placed in a transwell culture dish with a diameter of 35 mm. The two surfactants and saline were labeled with blue dye and ~1  $\mu$ l droplets were pipetted onto a PGM surface. Images were captured using a digital camera.

All following experiments with PGM involved solutions delivered to the surface via aerosol. PGM was loaded into 12mm diameter filter inserts (Corning-Costar Transwell Collagen T-cols, Acton, MA), mixed to a concentration of 50 mg/ml (95% saline) and a depth of 4mm. Each filter was placed into a 12-well cell culture dish, and only the surrounding 11 wells were filled with 1ml of PBS, to maintain as close to 100% humidity as possible. The well containing the PGM filter was not filled with PBS. The cannula was placed through a small hole drilled in the cell culture dish lid and it remained approximately 1mm above the PGM surface. Aerosol was delivered at 0.3 LPM for 10 seconds. The five solutions listed in Table 4 were tested for five trials each, using three fluorescent markers: texas red dextran, 0.1 and 1.0 micron polystyrene spheres.

#### **4.1.5 Epithelial Cell Culture Model**

##### **4.1.5.1 Cell culture preparation**

All cell cultures used in this study were provided by Dr. Pilewski's cell culture facility. The first cell line tested was the Calu3 cell line, derived from cancer cells. These cells developed a monolayer and secreted mucins, but no cilia or ASL was present. Calu3 cells were obtained frozen, then thawed and suspended in a 1:1 mixture of Dulbecco's modified Eagle's media (DMEM) and Ham's F-12 medium (F-12) with 10% fetal bovine serum (FBS). The cells were initially seeded onto 75 cm<sup>2</sup> tissue culture flasks. Upon reaching 100% confluence, the cells

were seeded on 12 mm diameter transwell polycarbonate inserts (0.4  $\mu\text{m}$  pore size, Corning-Costar Transwell Collagen T-cols, Acton, MA), pre-coated with human placental collagen at  $10^6$  cells/cm<sup>2</sup>. Figure 11 shows a single filter with both the basolateral and apical surfaces in contact with the media. Upon reaching 100% confluence, the media on the apical surface was removed and the cells were maintained at an air-liquid interface in a 100% humidified incubator. The cells were fed on the basolateral side of the filter twice per week with DMEM/F-12 and 10% FBS and were fully differentiated in approximately 5 days.

The HBEs (CF and non-CF) were prepared from airway specimens excised from fresh explanted or unused donor lung tissue following surgical transplantation. The airway sections were digested in a protease solution overnight to detach the epithelial cells from the tissue. The cells were then resuspended in 1:1 bronchial epithelial growth media/keratinocyte-serum free medium (BEGM/K-SFM) and initially seeded onto sterile tissue culture flasks pre-coated with human placental collagen. After 5-6 days, the cells were seeded onto collagen-coated 12 mm transwell filter inserts at confluence. Similar to the Calu3 cells, the HBEs were maintained at an air-liquid interface and fed twice per week on the basolateral side, but with DMEM/F12 and 2% Ultrosor G (USG), a bovine serum substitute. The cells were fully differentiated after approximately 2-3 weeks and the appearance of cilia occurred anywhere from 4 weeks and beyond, although not all cultures developed cilia. For both the Calu3 and HBE cultures, the apical surface was washed once per week to remove excess mucus and cell debris using 2mM dithiothreitol (DTT), which is a reducing agent. The surface was also washed 24 hours prior to an aerosol experiment.

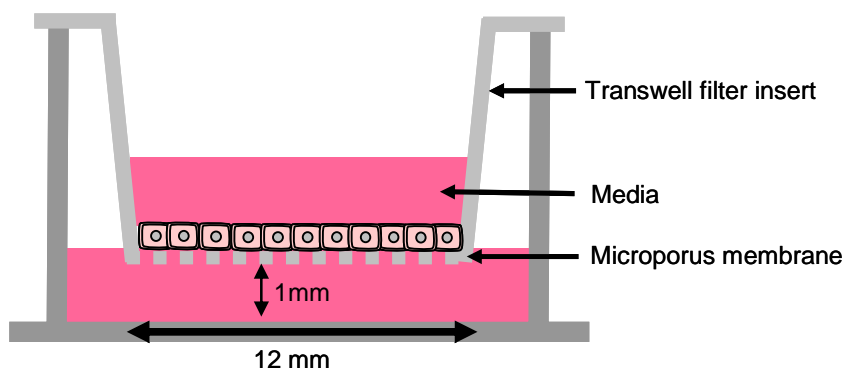


**Figure 11:** A single 12mm transwell filter insert with cells seeded on a microporous membrane. The microporous membrane lies 1mm above the culture dish bottom and contains 0.4 micron pores to allow the passage of media from the lower compartment to the cells. Once confluent, the media on the apical surface is removed and the cells remain at an air-liquid interface with only the basolateral side in contact with media.

#### 4.1.5.2 Calu3 Model

The Calu3 cell line was chosen for initial testing due to its relative availability and shorter time to differentiation when compared to HBE cultures. The Calu3 cultures were used in preliminary experiments for adjusting methodology, such as optimal flow rate, dose-time interval, and dye concentration. Their utility in the model is limited by their lack of a realistic ASL layer. The HBE cell cultures provide the closest available in vivo representation of realistic airway conditions.

For all aerosol experiments, a single filter was placed on a 12-well cell culture plate and 1ml of sterile PBS was placed in the surrounding wells to help maintain 100% humidified conditions. Tyloxapol and calfactant were used with both the Calu3 and HBE cultures. The same three fluorophores used in the PGM experiments were also used for the cell experiments at the same concentrations. The apical surface of both the Calu3 and HBE cells was washed 24 hours prior to the experiment to remove excess mucus and cell debris. All cells were maintained in a 100% humidified incubator until immediately before use. For all cell culture experiments, aerosol was delivered from the cannula tip at approximately 1mm above the cell surface at 0.3 LPM for 5 seconds.

#### 4.1.5.3 HBE Model (CF and non-CF)

Several different HBE cell lines including CF and non CF were used from explanted or unused donor lungs. The HBE cell experiments were divided into two groups based on their preparation prior to aerosol delivery. During our initial studies, the cells were tested using the same methods described for the Calu3 cells. These experiments are reported as Group 1.

A different hydration protocol was utilized for Group 2 based on day to day variability in our initial experiments that we attributed to effects of evaporation. The HBE cultures used here are very similar to those used by Tarran et al. In imaging experiments performed by this group and others, an organic solvent perfluorocarbon (PFC) is added to the mucosal surface to prevent the evaporation of the ASL when taking measurements [59]. This could not be done in the current experiments because of the need for realistic surface conditions and access for aerosol delivery. In the absence of PFC, water from the ASL evaporates quickly when the cultures are taken from the incubator. This is even more of a factor in the CF cultures since the ASL is likely depleted at baseline conditions. We devised a different hydration protocol for group 2 in order to more effectively diminish the effects of evaporation. The group 2 cells were washed 24 hours prior to aerosol delivery similarly to group 1. However, immediately before the aerosol dose, the apical surface of the cells was hydrated with 100uL of PBS that was then suctioned off, providing a more consistent level of hydration. Table 5 shows the cells lines used, their corresponding disease states, and experimental test group(s).

**Table 5:** Cell lines used with corresponding disease state and group number (Group 1 – washed only 24 hours prior to experiment, Group 2 - cells hydrated with PBS immediately prior to experiment).

Cell Line	Disease State	Group
HBE 439	Scleroderma	1
HBE 456	Chronic fibrosing lung disease	1 and 2
HBE 457	Right heart failure	1 and 2
CF 101	Cystic Fibrosis	1
CF 102	Cystic Fibrosis	2
CF 103	Cystic Fibrosis	2
CF 105	Cystic Fibrosis	1 and 2

#### **4.1.5.4 Liposome delivery to HBEs**

Lastly, Ambisome ®, a liposomal formulation of Amphotericin B (Amp B) for injection was mixed with Calfactant and delivered to cell lines HBE 456, 457, and CF 102. Ambisome contains liposomes that are less than 100 nm in diameter. One vial of Ambisome contains 50mg of Amp B [88], which is a potent anti-fungal medication. In the control group, Ambisome was reconstituted with 12mL of distilled water and in the experimental group Ambisome was reconstituted with 6mL of calfactant and 6mL of distilled water. These formulations were both sized and administered to the cell cultures using the same methods used for group 2. The fluorophore selected was the 0.1 micron PS spheres.

#### **4.1.6 Image Analysis**

All images were analyzed using Metamorph software. Using the threshold tool in Metamorph, an image threshold was selected that best optimized the image resolution with the level of image noise. This threshold was applied to all images analyzed for each specific fluorescent tag. Fluorescent regions were selected manually based on sharp gradients in fluorescent light intensity. The Metamorph tracing tool was used to carefully outline these regions and the pixel area within them was determined using the region measurements tools. The pixel area was then scaled to mm<sup>2</sup> using the total area of the filter (113.4mm<sup>2</sup>). Tests of statistical significance were performed to compare the areas reached by all surfactants vs. saline for the three fluorescent tags (student's t-test.).

## 5.0 RESULTS

### 5.1 PRELIMINARY MUCUS EXPERIMENTS

Porcine gastric mucus (PGM) was mixed to 100mg/ml in 0.9% NaCl solution and filled into a 6-well cell culture dish (35mm diameter) to a depth of approximately 5mm. Saline (control), tyloxapol, and tween20 were labeled with blue dye and pipetted onto the PGM (1 $\mu$ l droplets). Figure 12 includes an image taken of the three solutions on the PGM surface. Increased distribution of the tyloxapol and tween20 compared to the saline was noted as the surfactants spread with specific branching patterns within the first second. This image was taken within two minutes of droplet placement. The blue dye did not reach the bottom of the well after five minutes. A phase separation experiment on the PGM was also conducted. At concentrations  $\geq 20$ mg/ml, a dense phase developed at the bottom of the vials after approximately 7-10 days (Figure 13). This concentration is similar to phase separation results found by other groups testing similar PGM [89].



**Figure 12:** PGM with saline (left), tyloxapol (center) and tween20 (right) pipetted on surface, labeled with blue dye.

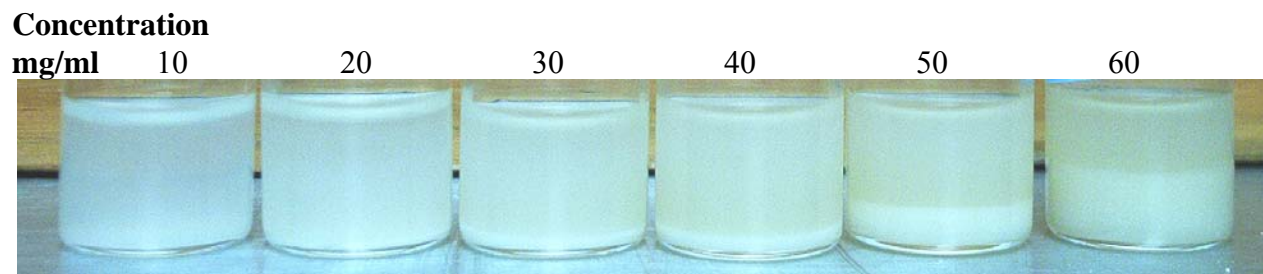


**Figure 13:** PGM phase separation. Phase separation line appears at concentrations of 20 mg/ml and above. No separation occurred for the 10mg/ml.

## 5.2 AEROSOL SIZING

Aerosol size measurements were made at the end of the cannula tip (see Figure 10) and a summary of the average mass median diameters (MMD) is presented in Table 6. By definition, half of the aerosol volume is in sizes larger than the MMD and half is in sizes smaller than the MMD. Saline, several surfactants, and a surfactant drug formulation were tested. Each average includes 5 or 10 size measurements.

Volume histograms for the saline and four surfactants tested, calfactant, tyloxapol, SDS, and CTAB, are presented in Figures 15 and 16. Volume histograms of Ambisome reconstituted with distilled water (control) and Ambisome with calfactant are shown in Figure 17. These histograms represent an average of 10 sizing measurements. The histogram itself depicts the relative aerosol volume in each of a series of aerosol size ranges. In this case a 0.5 micron size interval is utilized.

**Table 6:** Aerosol size measurements taken at the cannula tip of the aerosol delivery system expressed as the average MMD.

<b>Aerosol</b>	<b>Average MMD (microns)</b>
Saline (n=10)	1.4 ± 0.1
Tyloxapol (n=10)	1.9 ± 0.1
Calfactant (n=10)	1.6 ± 0.1
SDS (n=5)	2.8 ± 0.4
CTAB (n=5)	4.0 ± 0.2
Ambisome + dH <sub>2</sub> O (n=10)	2.6 ± 0.2
Ambisome + Calfactant (n=10)	2.6 ± 0.6

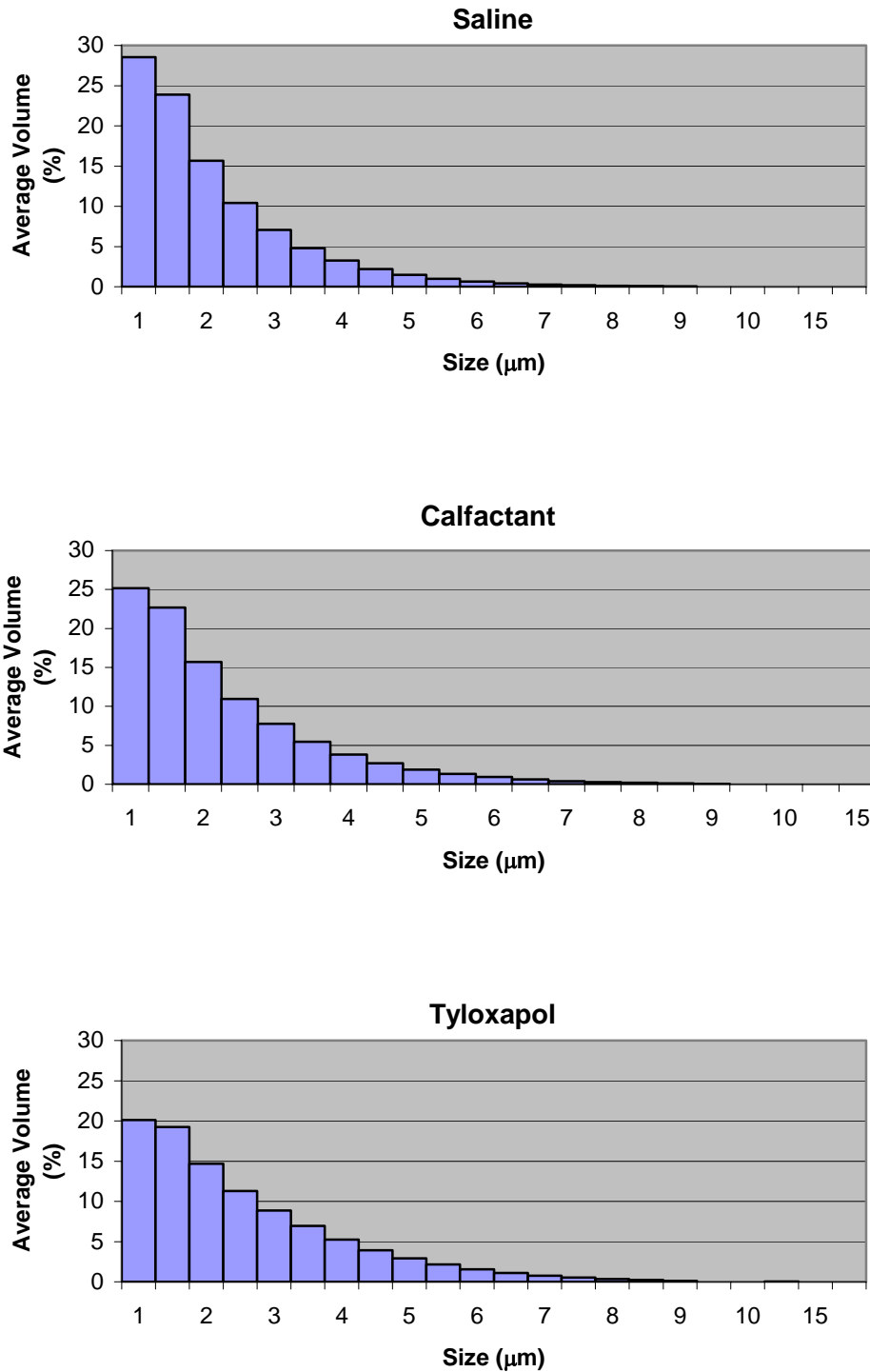


**Figure 14:** Volume histograms for saline (top), calfactant (middle) and tyloxapol (bottom). Measurements were performed using a laser diffraction instrument and the average MMD was calculated from 10 measurements. The histogram represents the relative volume of aerosol with in each size range. Half micron bins were used.

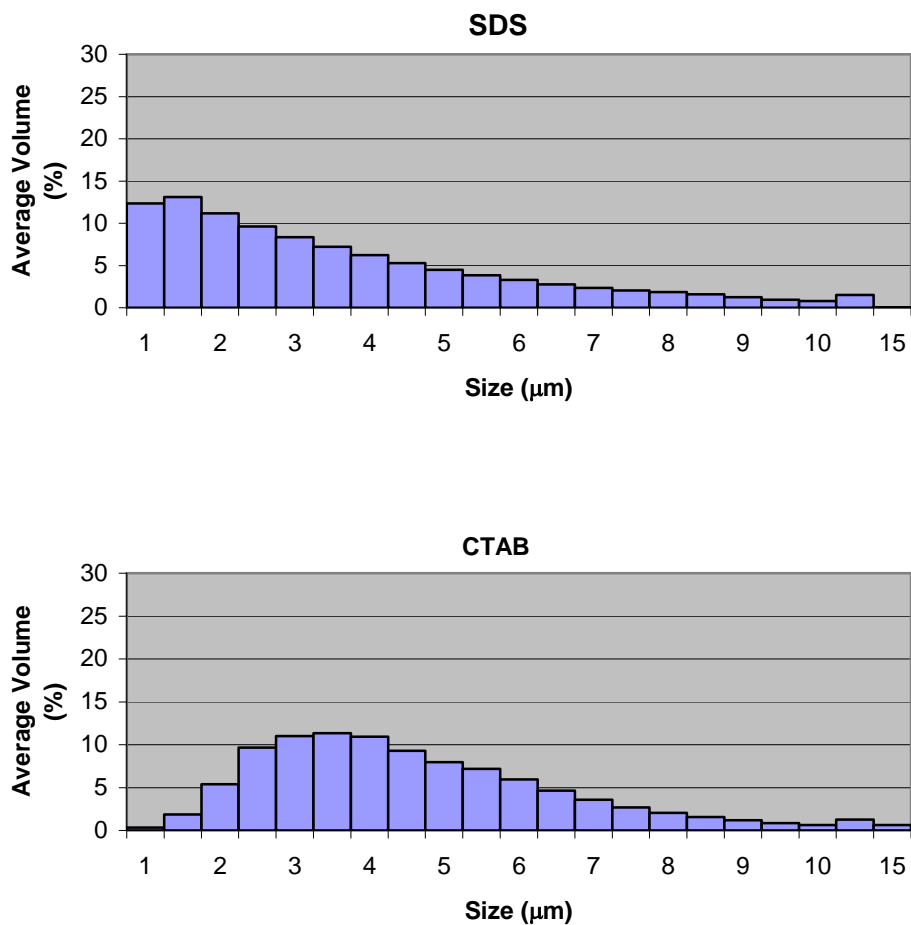


**Figure 15:** Volume histograms (continued) for SDS (top) and CTAB (bottom). Measurements were performed using a laser diffraction instrument and the average MMD was calculated from 5 measurements. The histogram represents the relative volume of aerosol with in each size range. Half micron bins were used.

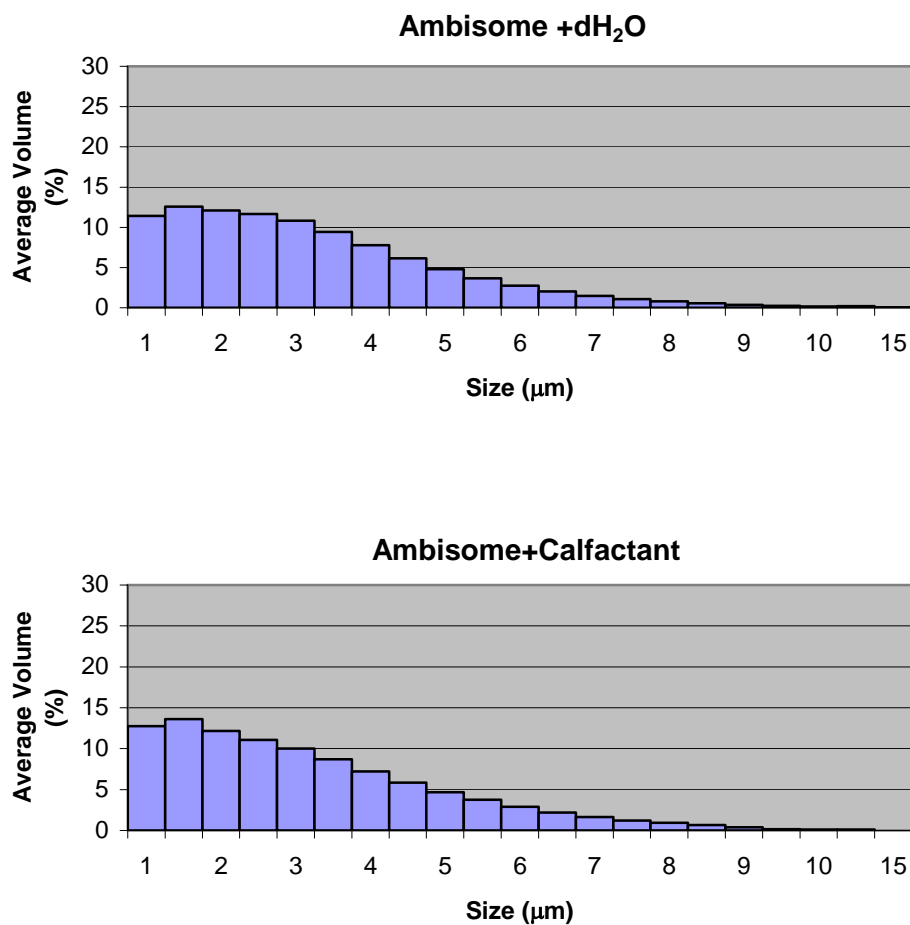


**Figure 16:** Volume histograms for Ambisome dissolved in distilled water only (top) and Ambisome dissolved in Calfactant (bottom). Measurements were performed using a laser diffraction instrument and the average MMD was calculated from 10 measurements. The histogram represents the relative volume of aerosol with in each size range. Half micron bins were used.

The aerosol size of calfactant was also measured in a series of medical nebulizers in order to determine whether it would be respirable if used in future clinical trials. Since aerosol size will affect where these aerosols will deposit in the lungs, a well controlled trial would include an aerosol size that matches closely to that of a saline control. Therefore, saline aerosols were considered in the same devices. Three different nebulizers were used: the Aeroneb Pro the micropump nebulizer (same as in Figure 10), (Nektar/Aerogen, San Carlos, CA), the AeroTech II jet nebulizer (CIS-US, Bedford, MA), and the AeroEclipse breath actuated nebulizer (Monaghan Medical Corp, Plattsburgh, NY). Table 7 contains the MMDs averaged from 5 measurements for each nebulizer and Figure 17 contains the corresponding volume histograms of saline and calfactant for each nebulizer.

**Table 7:** MMD of saline and calfactant measured from three different medical nebulizers.

<b>Nebulizer (n=5)</b>	<b>MMD Saline (<math>\mu\text{m}</math>)</b>	<b>MMD Calfactant (<math>\mu\text{m}</math>)</b>
Aeroneb Pro	$5.2 \pm 0.1$	$5.1 \pm 0.1$
Aerotech II	$4.7 \pm 0.1$	$5.2 \pm 0.1$
AeroEclipse	$3.8 \pm 0.02$	$3.7 \pm 0.2$

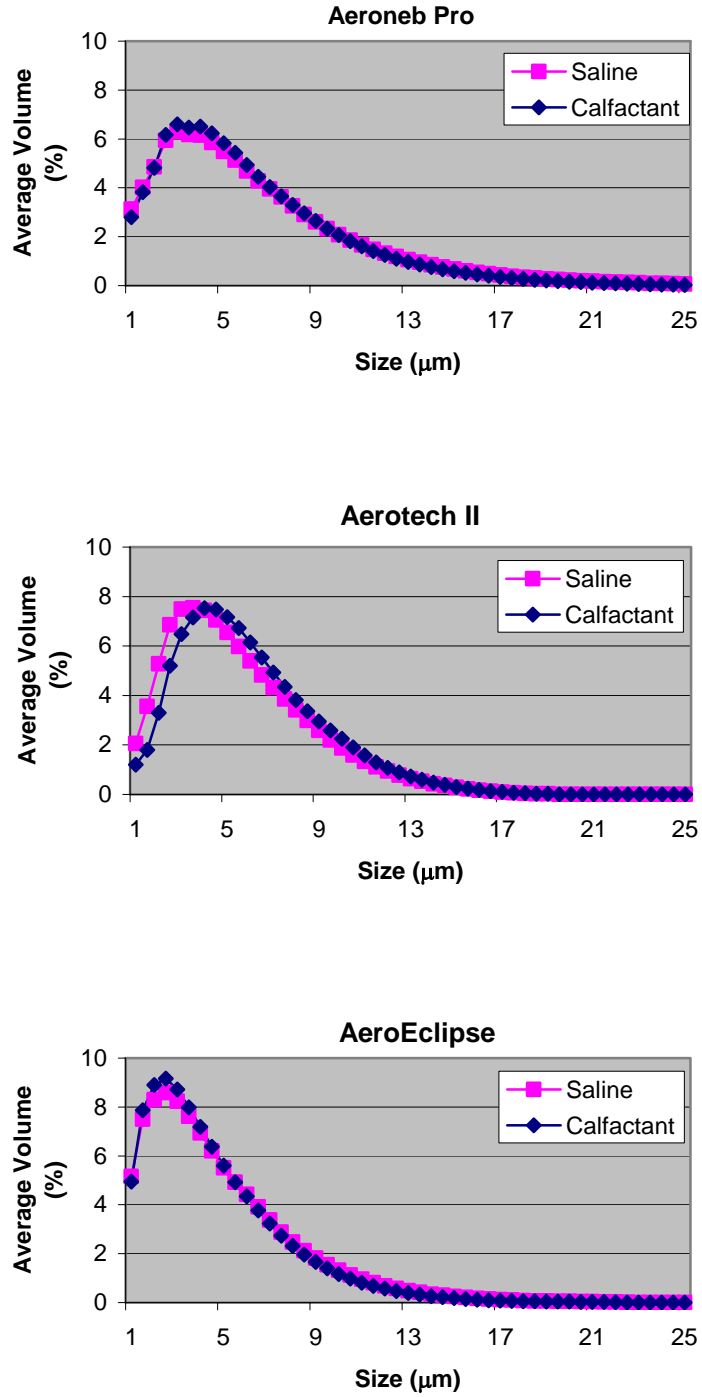


**Figure 17:** Volume histograms of saline (pink) and calfactant (blue) generated by three medical nebulizers: Aerogen Pro (top), AeroTech II (middle), and AeroEclipse (bottom). The histograms represent the relative volume of aerosol within each size range.

## **5.3 AEROSOL DELIVERY**

### **5.3.1 Mucus Model Surface**

Representative images comparing the post aerosol deposition distribution on PGM (50mg/ml, ~95% saline) of four different surfactant carriers vs. saline with three different indicators (texas red dextran, 0.1 and 1.0 micron PS spheres) are included in Figures 18 and 19. A qualitative comparison of the images indicates an improved distribution of all three fluorescent markers with each surfactant.

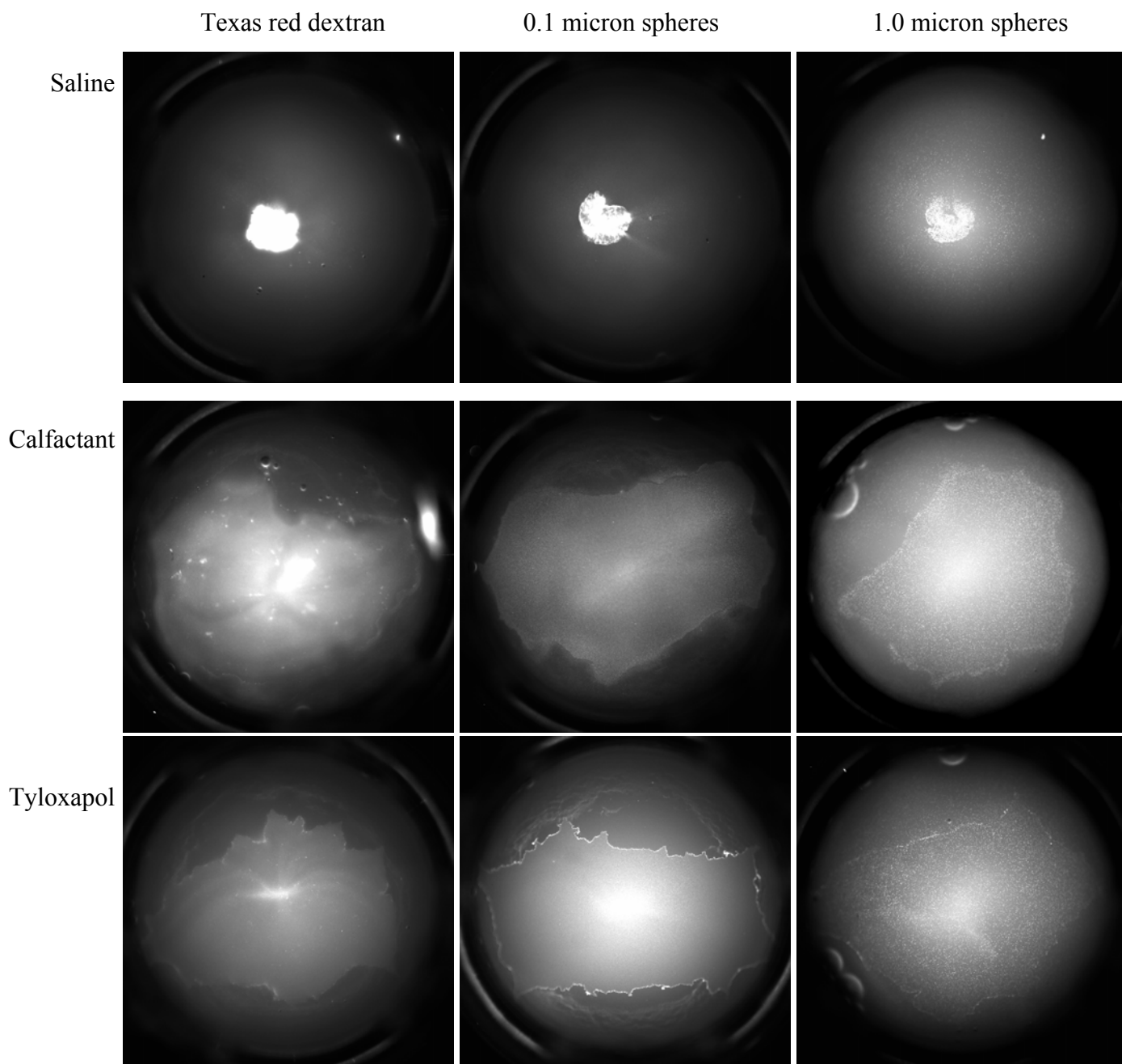


**Figure 18:** Images captured post aerosol deposition on PGM surface. Saline (top row), calfactant (center row), tyloxapol (bottom row) were labeled with texas red dextran (left column), 0.1 (center column) and 1.0 micron PS spheres (right column).

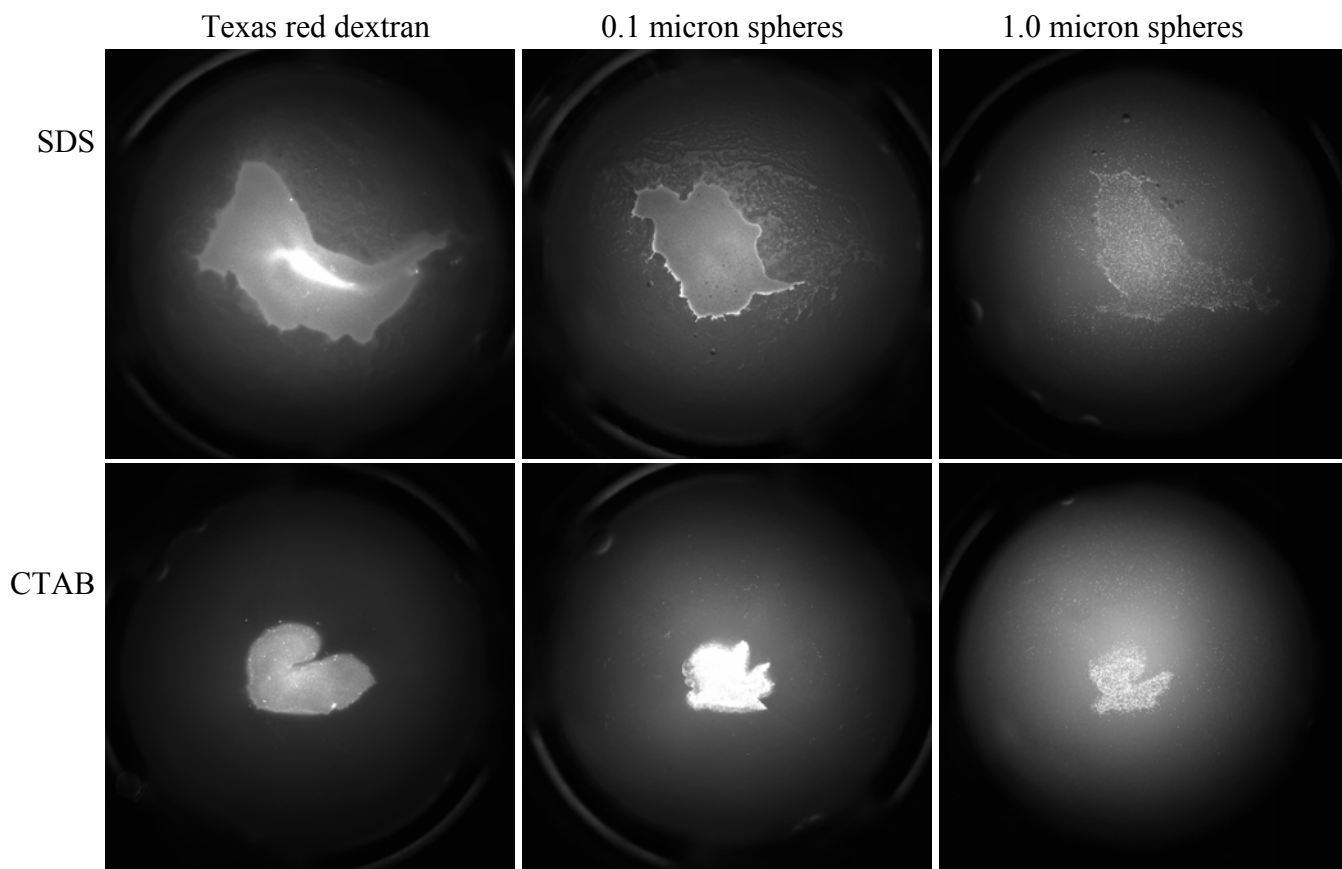


**Figure 19:** Images captured post aerosol deposition on PGM surface. SDS (top row) and CTAB (bottom row) were labeled with texas red dextran (left column), 0.1 (center column) and 1.0 micron PS spheres (right column).

The saline and surfactant areas of distribution were measured and averaged over 5 trials for the three fluorescent tags. The area of distribution was measured using the Metamorph software program and the previously described techniques. Table 8 shows a comparison of the average distribution areas for surfactants vs. saline. The data is expressed as the factor by which the surfactant area exceeded the saline area.

**Table 8:** Factor by which the average surfactant area exceeds the average saline area post aerosol deposition on the PGM.

<b>Surfactant</b>	<b>Texas red dextran</b>	<b>0.1 micron spheres</b>	<b>1.0 micron spheres</b>
<b>Calfactant</b>	17	16	20
<b>Tyloxapol</b>	16	20	20
<b>SDS</b>	6	4	5
<b>CTAB</b>	3	2	2

It was also noted during the PGM studies that the behavior of the cationic and anionic surfactants changed over several minutes following deposition. Saline diffused slightly over time, while CTAB and SDS both retracted in the minutes following deposition. Figure 20 illustrates this retraction of the CTAB and SDS labeled with 0.1 micron PS spheres compared with saline. This retraction behavior did not occur for tyloxapol and calfactant.

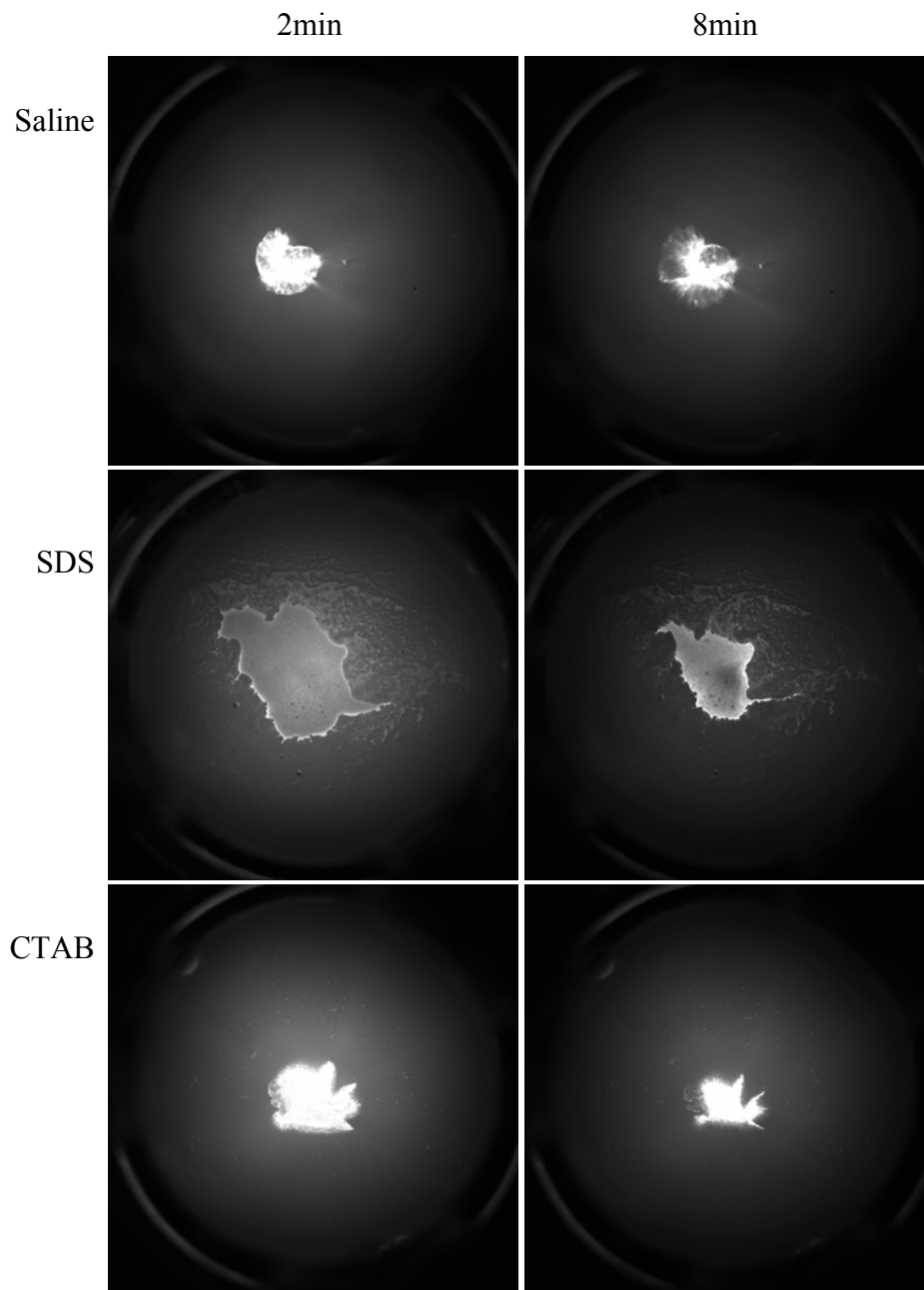


**Figure 20:** Images captured at 2 and 8 minutes post aerosol deposition on the PGM surface demonstrate retraction behavior of ionic surfactants. Saline (top row), SDS (center row) and CTAB (bottom row) are shown labeled with 0.1 micron PS spheres.

### 5.3.2 Calu3 Model

Selected images of saline, calfactant, and tyloxapol distribution (labeled with texas red dextran) following aerosol deposition on the Calu3 cell cultures are shown in Figure 21. It was noted that in each case, a droplet formed on the surface of the culture just below the cannula tip. As demonstrated by the high concentration of dye remaining in the center of cultures and little or no spreading occurred after aerosol deposition for either surfactant. These studies did not include any further hydration steps that were included in only Group 2 experiments.

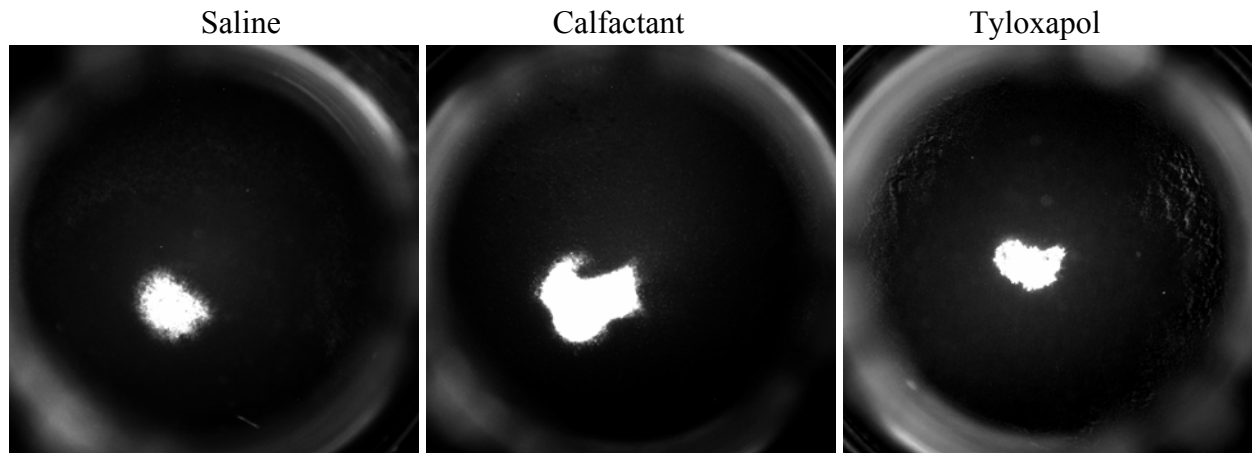


**Figure 21:** Images captured post aerosol deposition on the Calu3 cell cultures. Saline (left), calfactant (center), and tyloxapol (right) were labeled with texas red dextran. A droplet formed on the surface and little to no spreading of surfactants was observed. No further hydration protocol was used.

Figure 22 shows results from the same experiment on another set of calu3 cells. In this case however, tyloxapol had a larger distribution on the culture following aerosol deposition than the saline. As previously described, we believe this variability is associated with hydration level.

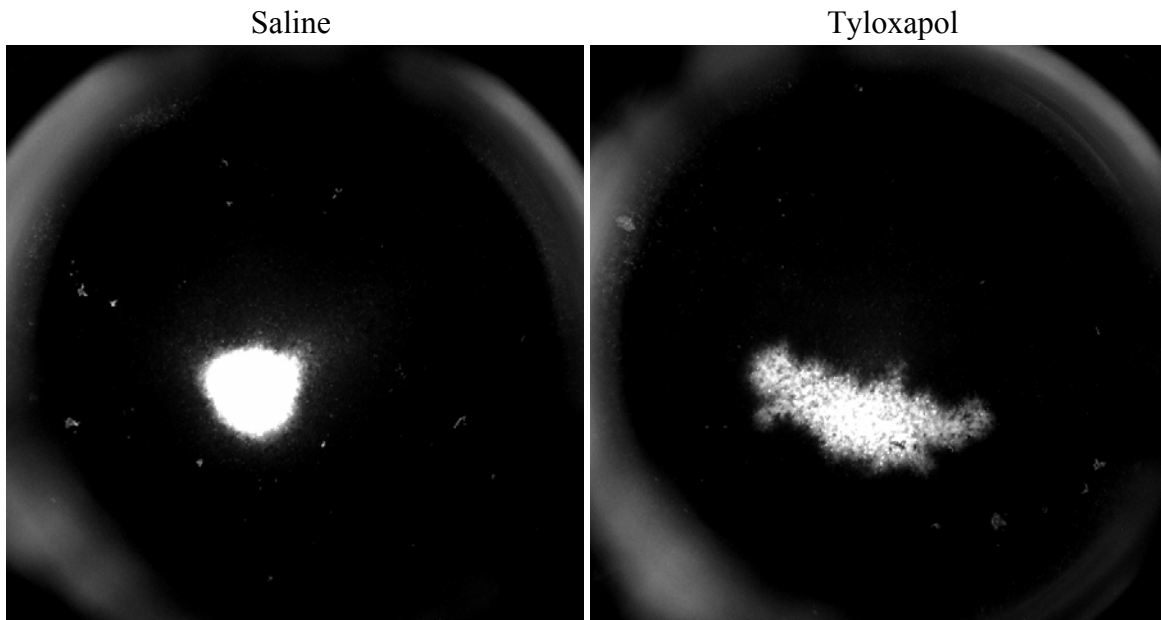


**Figure 22:** Images captured post aerosol deposition on the Calu3 cell cultures. Saline (left) and tyloxapol (right) were labeled with texas red dextran. In this case, a larger degree of spreading occurred when tyloxapol was dosed on the surface of the culture. Because no further hydration protocol was used, we believe this variability is associated with the hydration level.

### 5.3.3 HBE Model – Group 1

Images captured following an aerosol dose on two different cystic fibrosis cell lines (CF 101 and 103) are included in Figure 23. Both the saline and tyloxapol deposited aerosols formed droplets on the surface of the cultures and little to no spreading was observed for tyloxapol during these initial experiments.

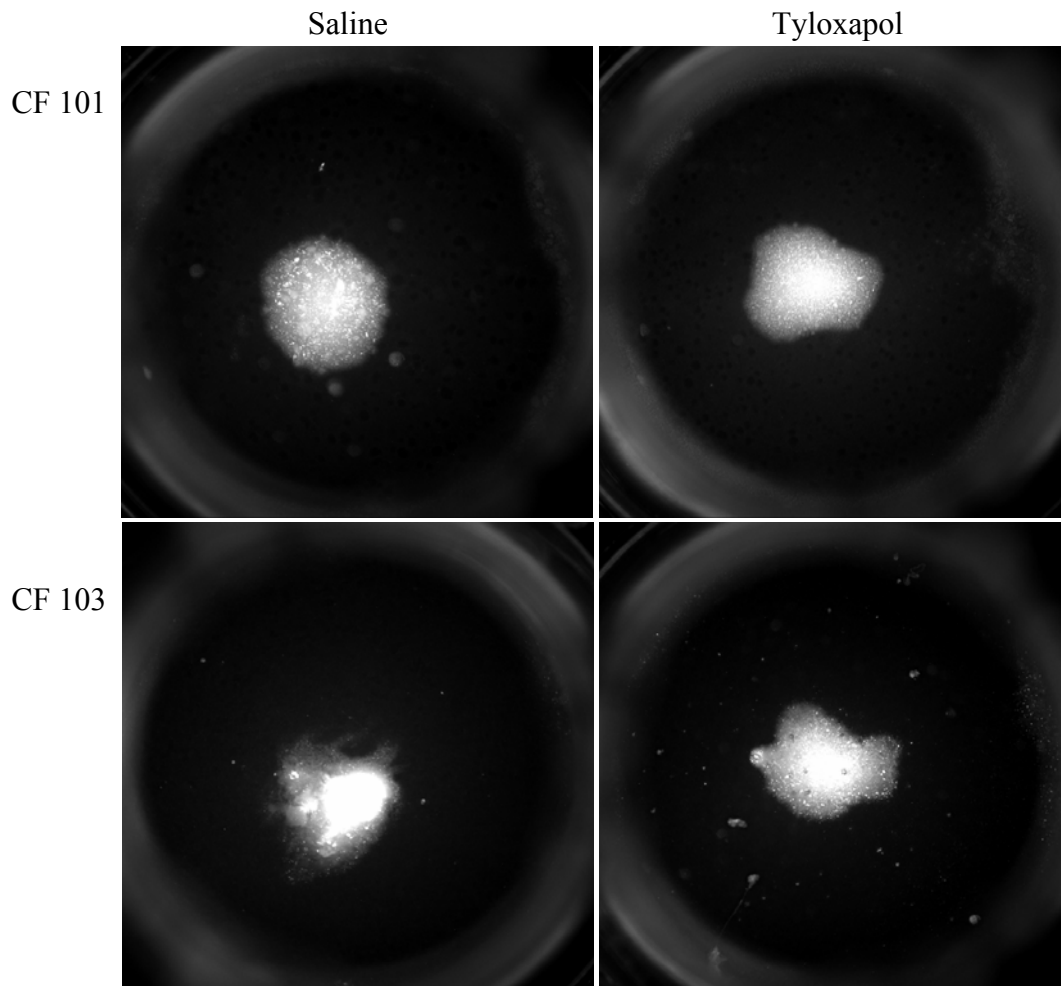


**Figure 23:** Images captured post aerosol deposition on cystic fibrosis cell cultures, CF 101 (top row) and CF 103 (bottom row). Saline (left column) and tyloxapol (right column) were labeled with texas red dextran. A droplet formed on the surface and little to no spreading of surfactant was observed. These group 1 studies did not include the added hydration steps included in group 2 experiments.

The results from a similar experiment using a third CF cell line, CF 105, are shown in Figure 24. Saline, calfactant and tyloxapol were labeled with 0.1 micron PS spheres. As indicated by the high dye concentration localized to the center of the cultures, neither surfactant spread following aerosol deposition and droplets formed on the surface of the cultures.

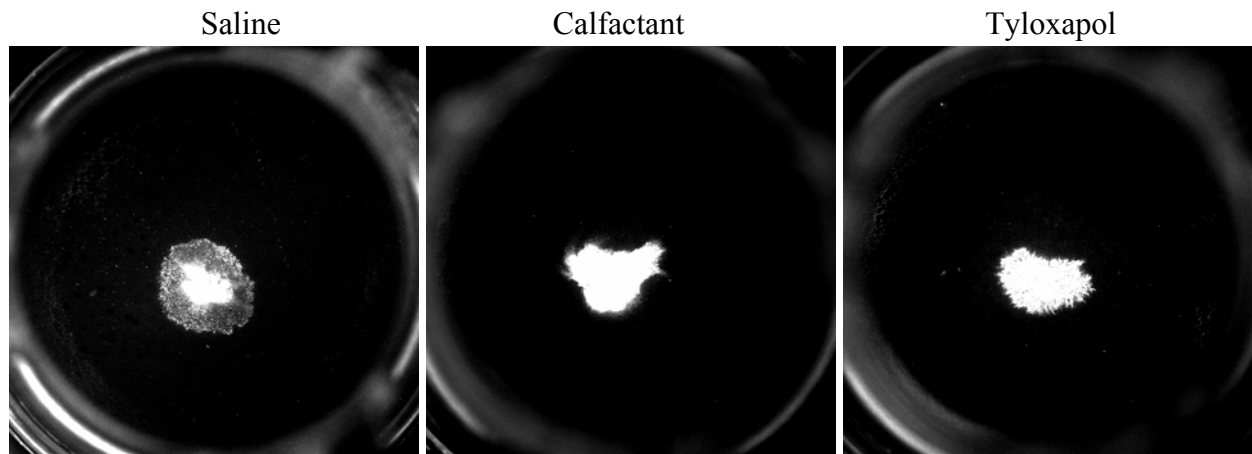


**Figure 24:** Images captured post aerosol deposition on CF 105 cell cultures. Saline (left), calfactant (center), and tyloxapol (right) were labeled 0.1 micron PS spheres. Droplets formed on the surface and little to no spreading of surfactants was observed. These group 1 studies did not include the added hydration steps included in group 2 experiments.

These same methods were used testing HBE, non-CF cultures. Images obtained following aerosol deposition of saline and calfactant onto HBE 439 cultures (donor lung – scleroderma) are included in Figure 25. The high dye concentrations localized to the center of the culture indicating that the surfactant did not distribute following aerosol deposition.

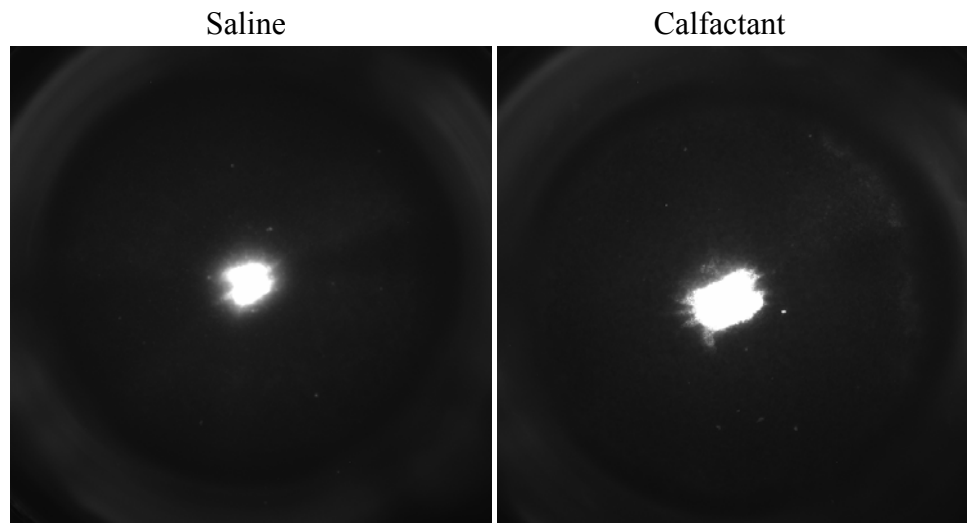


**Figure 25:** Images captured post aerosol deposition onto HBE 439 cell cultures. Saline (left) and calfactant (right) were labeled with texas red dextran. A droplet formed on the surface and little to no spreading of surfactant was observed. These group 1 studies did not include the added hydration steps included in group 2 experiments.

Images obtained following aerosol deposition of saline, calfactant, and tyloxapol labeled with 0.1 micron PS spheres onto HBE 456 (donor lungs - chronic aspiration) cultures are included in Figure 26. The images demonstrate some of the variability noted during group 1 studies, especially in surfactant cases. In general the majority of the fluorescent marker was localized to the center during these studies.

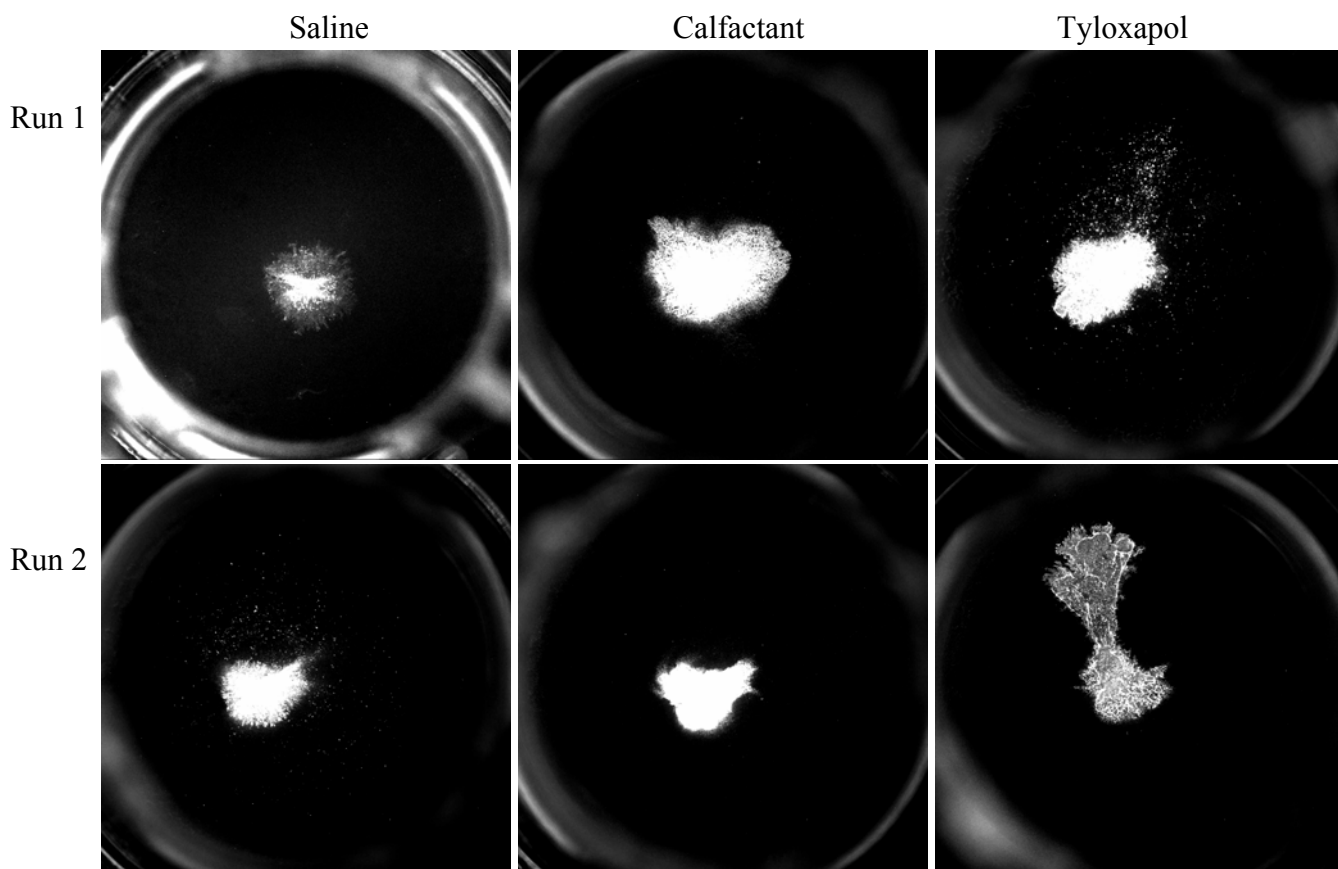


**Figure 26:** Images captured post aerosol deposition on HBE 456 cell cultures. Saline (left column), calfactant (center column), and tyloxapol (right) were labeled with 0.1 micron PS spheres. These group 1 studies did not include the added hydration steps included in group 2 experiments

Figure 27 includes images of saline, calfactant, and tyloxapol distribution (labeled with 0.1 micron PS spheres) post aerosol deposition on HBE 457 cultures (donor lungs – right heart failure). Variability in distribution is again noted with little or no significant spreading demonstrated by the surfactants. Collectively, Figures 21-27, from studies of Calu3's and the cell lines in Group 1 demonstrate the degree of variability in the level of surfactant spreading observed between and among different cell lines when additional hydration steps were not utilized.

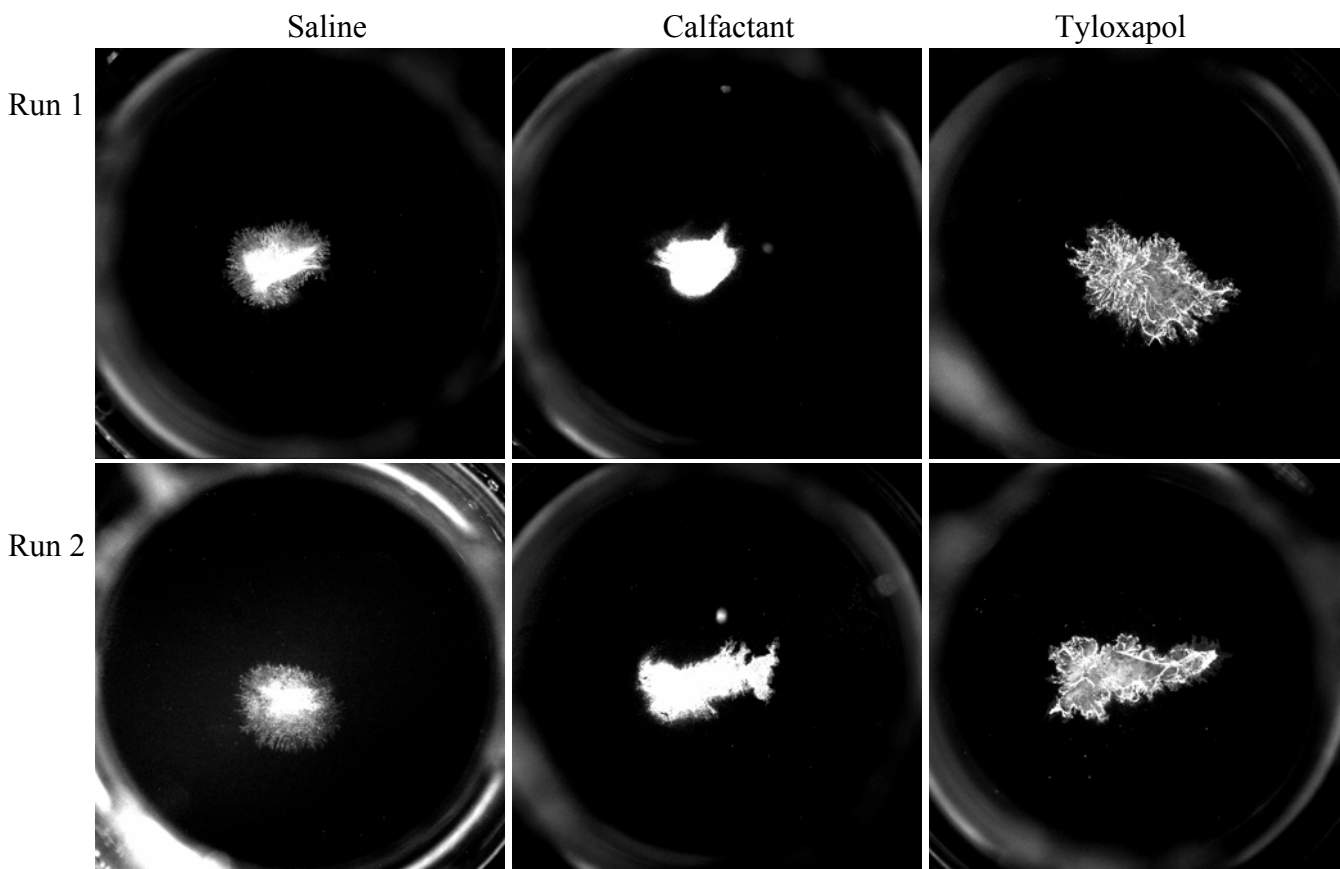


**Figure 27:** Images captured post aerosol deposition on HBE 457 cell cultures. Saline (left column), calfactant (center column), and tyloxapol (right) were labeled with 0.1 micron PS spheres. These group 1 studies did not include the added hydration steps included in group 2 experiments.

### 5.3.4 HBE Model – Group 2

To correct the dehydration that we believed to be occurring in the Calu3 studies and the cell lines in Group 1, 100  $\mu$ l of PBS was added to the apical surface of the cells tested in Group 2 shortly before the experiment and then aspirated off immediately prior to aerosol delivery. Figure 28 shows representative images obtained post aerosol deposition on CF cultured cells (CF 102). Qualitatively, both calfactant and tyloxapol demonstrated substantially higher degrees of spreading for all three fluorescent markers, than the corresponding saline cases. A high dextran/sphere concentration localized to the center of the culture for the saline cases is notable vs. the surfactant cases. Figure 29 shows the aerosol experiment repeated on CF 102 cultures to illustrate the relative repeatability within this CF cell line. Figures 30 and 31 contain images obtained following aerosol deposition on CF 103 and CF 105 cultures, respectively. Only one run for each surfactant and fluorescent maker was performed on these two cell lines due to the limited number of cells available for each line. Similar to the results on CF 102, a high degree of spreading was associated with both calfactant and tyloxapol for all three tags compared to the corresponding saline cases. One difference to note between these three CF cell lines was the degree of cilia present. CF 103 and CF 105 both developed cilia; however, CF 102 did not.

Figures 32-33 and Figures 34-35 contain images of saline and surfactant distribution following aerosol deposition on two non-CF cell lines, HBE 456 and HBE 457, respectively. Both cell lines developed cilia. Similar surfactant and saline distributions were found compared to the CF cells lines tested.

**CF 102 (run 1):**

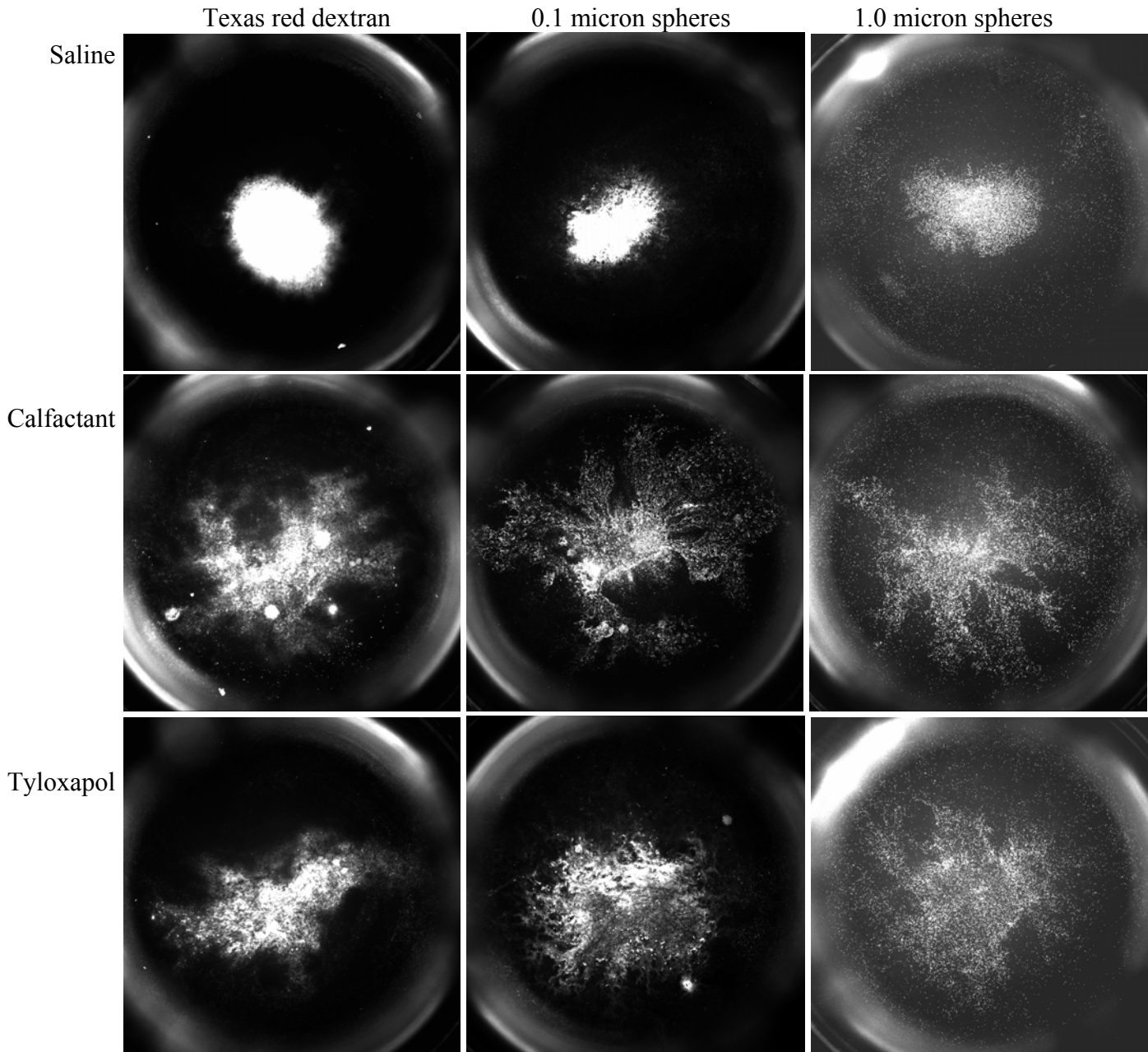


**Figure 28:** Images captured post aerosol deposition onto CF 102 cell cultures (run 1). Saline (top row), calfactant (center row) and tyloxapol (bottom row) were labeled with texas red dextran (left column), 0.1 (center column) and 1.0 micron PS spheres (right column). These group 2 studies included additional hydration steps not performed in group 1.

**CF 102 (run 2):**

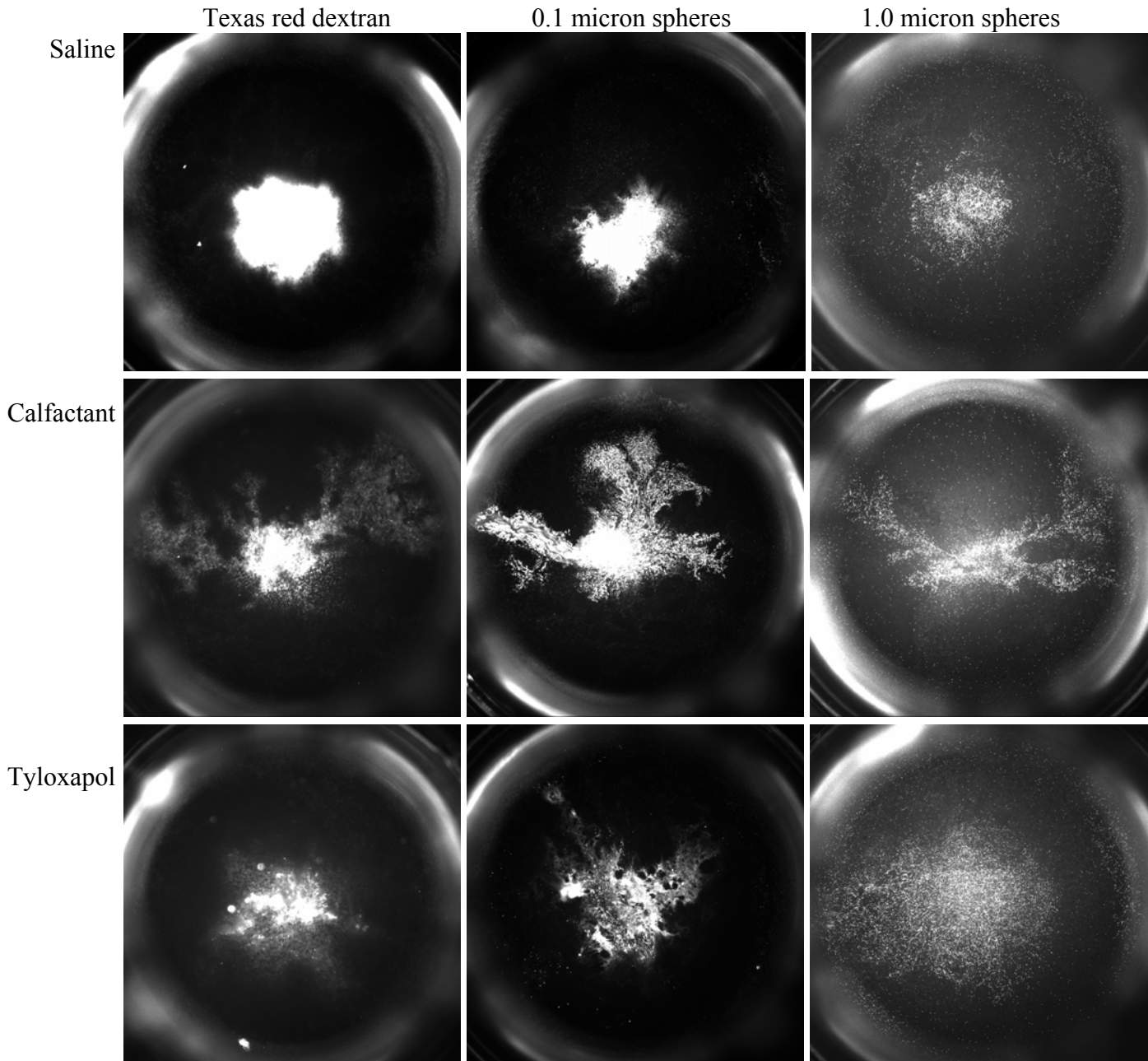


**Figure 29:** Images captured post aerosol deposition onto CF 102 cell cultures (run 2). Saline (top row), calfactant (center row) and tyloxapol (bottom row) were labeled with texas red dextran (left column), 0.1 (center column) and 1.0 micron PS spheres (right column). These group 2 studies included additional hydration steps not performed in group 1.

**CF 103:**

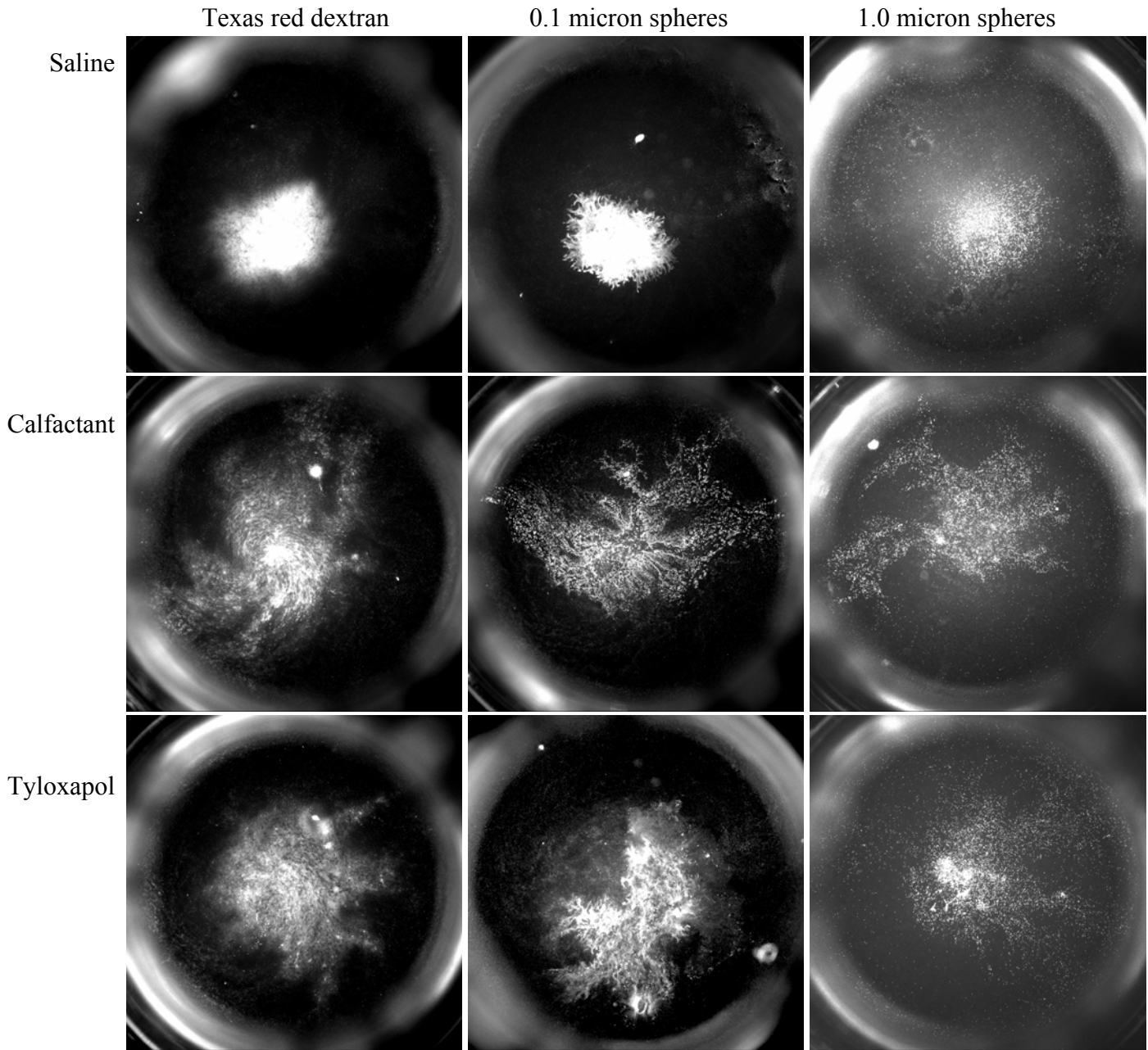


**Figure 30:** Images captured post aerosol deposition onto CF 103 cell cultures. Saline (top row), calfactant (center row) and tyloxapol (bottom row) were labeled with texas red dextran (left column), 0.1 (center column) and 1.0 micron PS spheres (right column). These group 2 studies included additional hydration steps not performed in group 1.

**CF 105:**

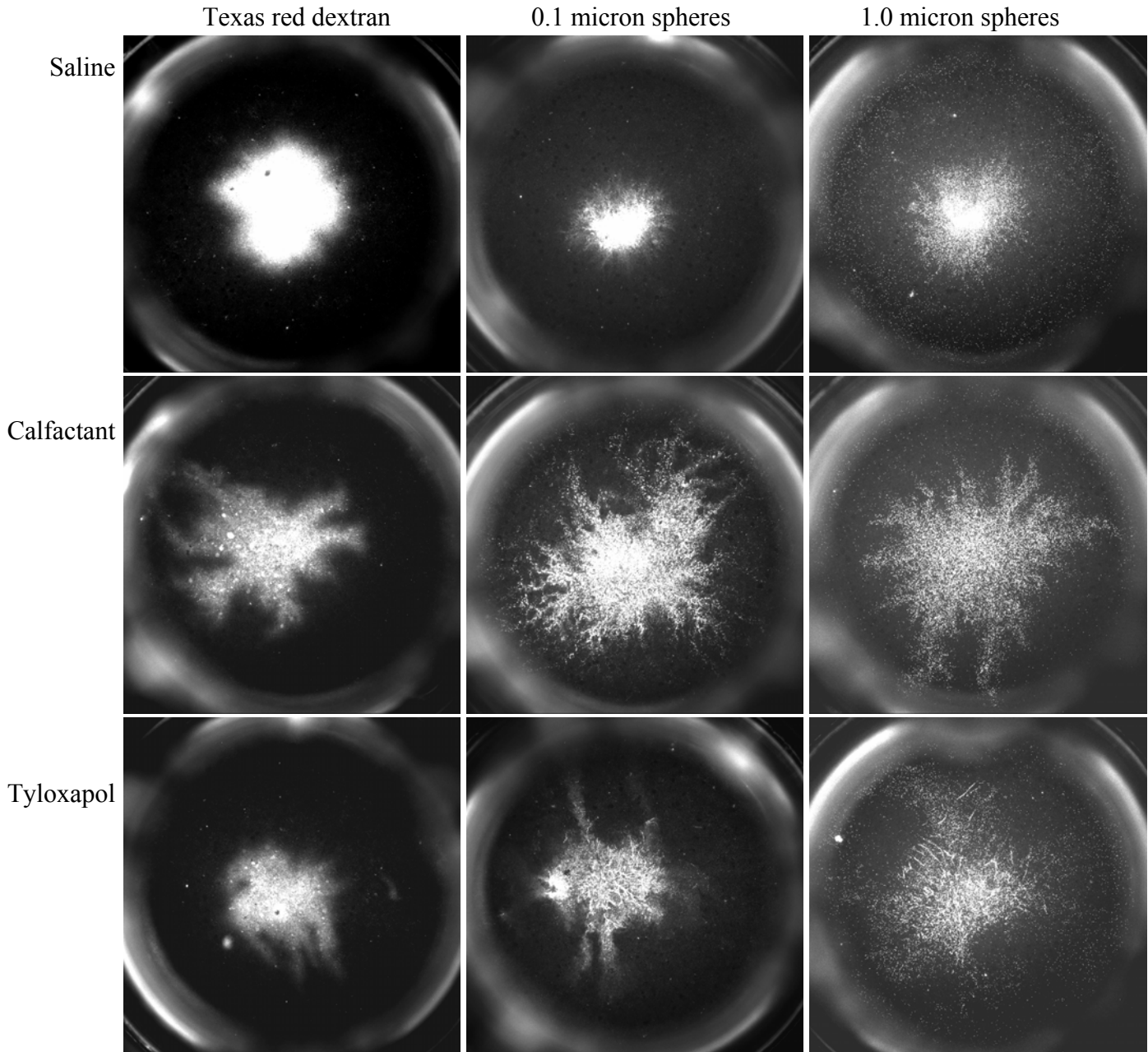


**Figure 31:** Images captured post aerosol deposition onto CF 105 cell cultures. Saline (top row), calfactant (center row) and tyloxapol (bottom row) were labeled with texas red dextran (left column), 0.1 (center column) and 1.0 micron PS spheres (right column). These group 2 studies included additional hydration steps not performed in group 1.

**HBE 456 (run 1):**

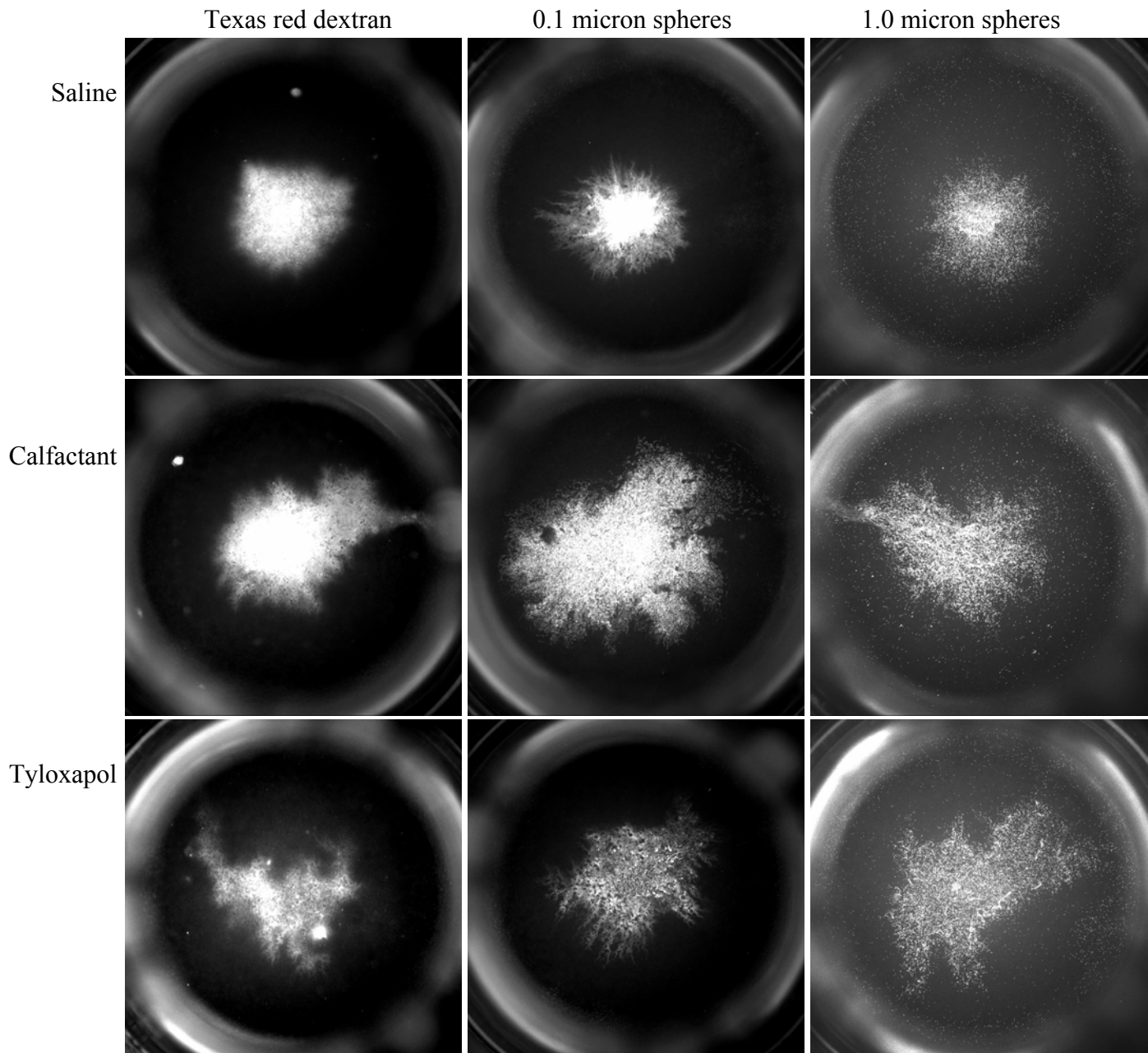


**Figure 32:** Images captured post aerosol deposition onto HBE 456 cell cultures. Saline (top row), calfactant (center row) and tyloxapol (bottom row) were labeled with texas red dextran (left column), 0.1 (center column) and 1.0 micron PS spheres (right column). These group 2 studies included additional hydration steps not performed in group 1.

**HBE 456 (run 2):**

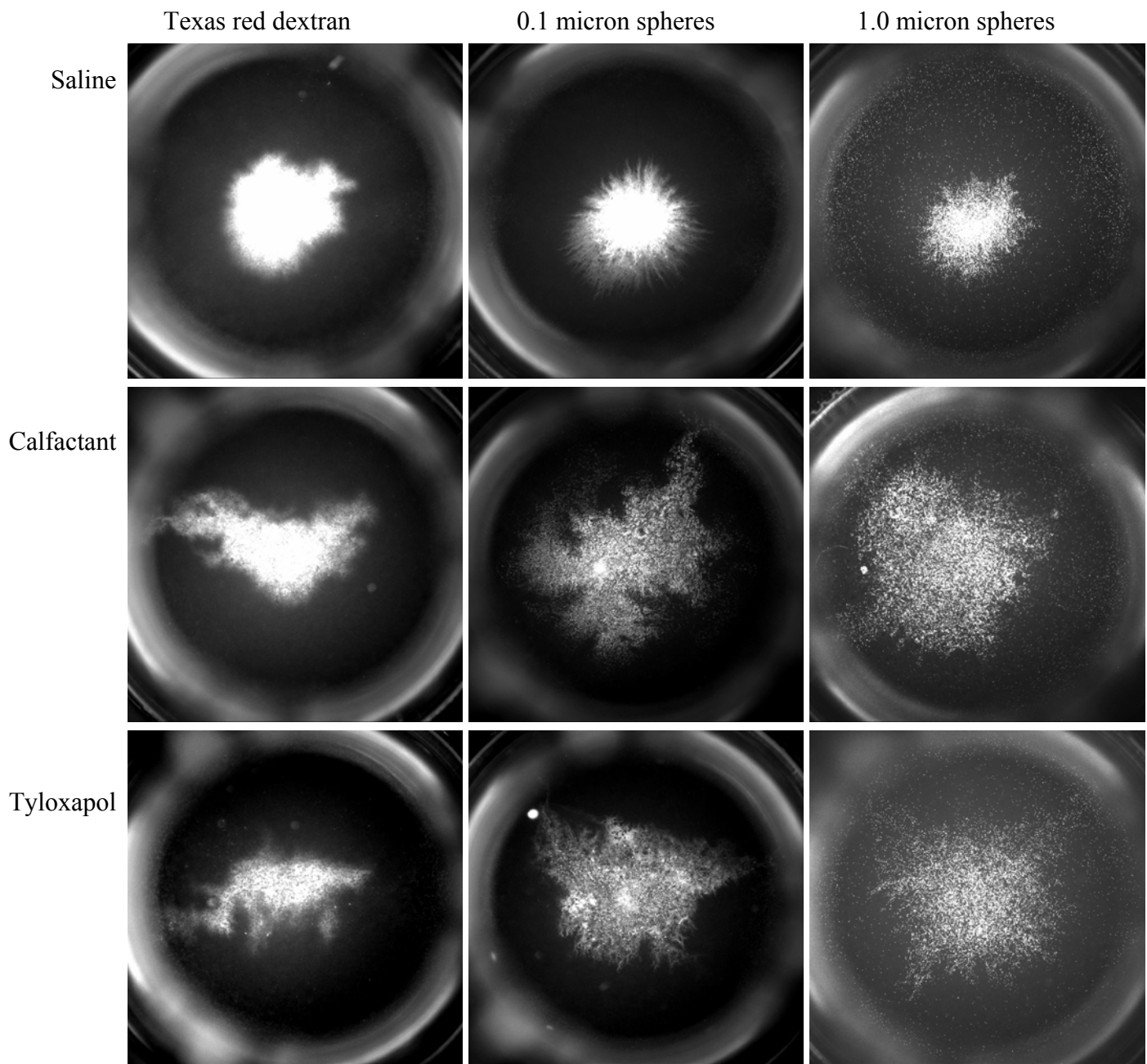


**Figure 33:** Images captured post aerosol deposition onto HBE 456 cell cultures (run 2). Saline (top row), calfactant (center row) and tyloxapol (bottom row) were labeled with texas red dextran (left column), 0.1 (center column) and 1.0 micron PS spheres (right column). These group 2 studies included additional hydration steps not performed in group 1.

**HBE 457 (run 1):**

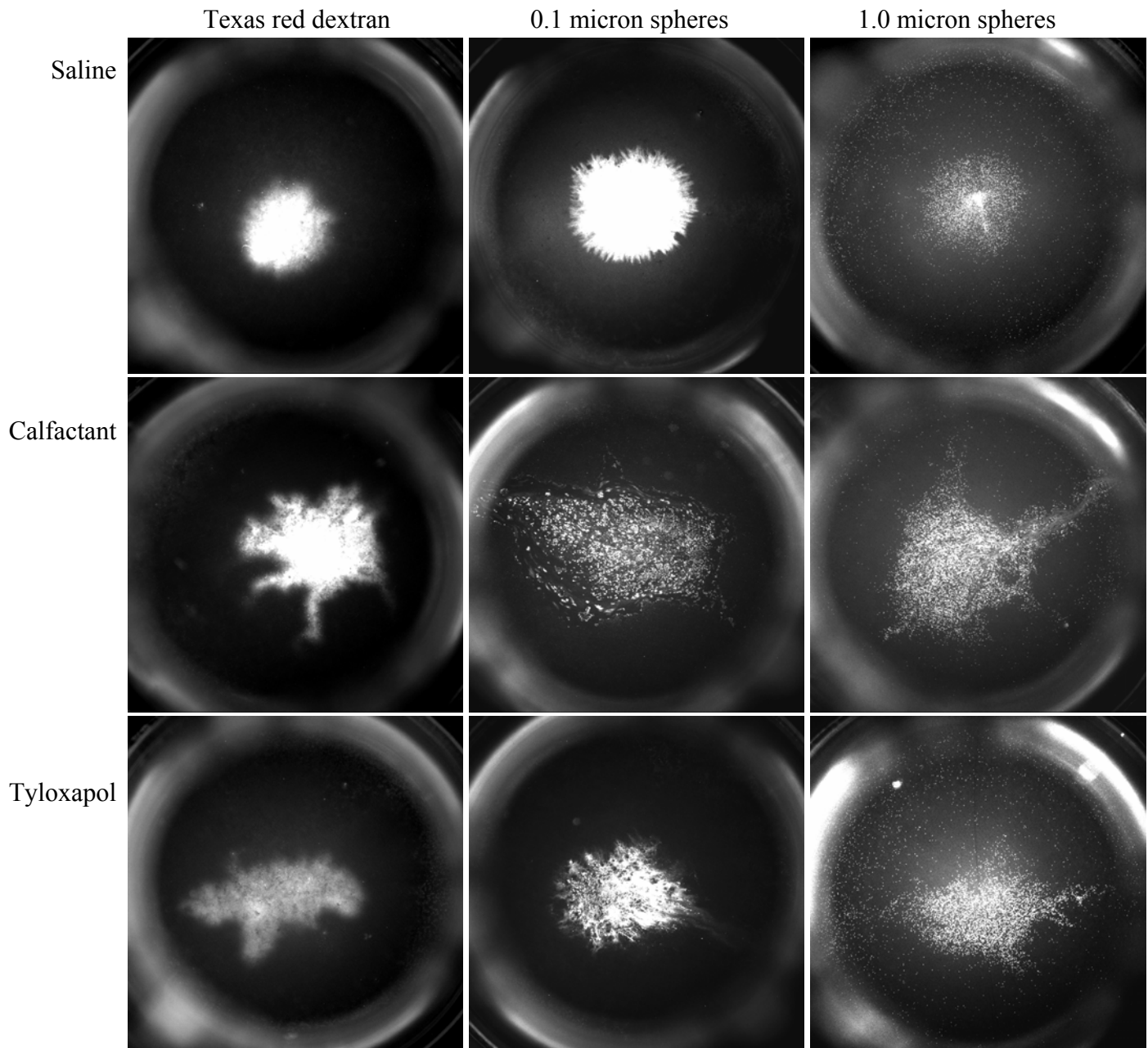


**Figure 34:** Images captured post aerosol deposition onto HBE 457 cell cultures (run 1). Saline (top row), calfactant (center row) and tyloxapol (bottom row) were labeled with texas red dextran (left column), 0.1 (center column) and 1.0 micron PS spheres (right column). These group 2 studies included additional hydration steps not performed in group 1.

**HBE 457 (run 2):**

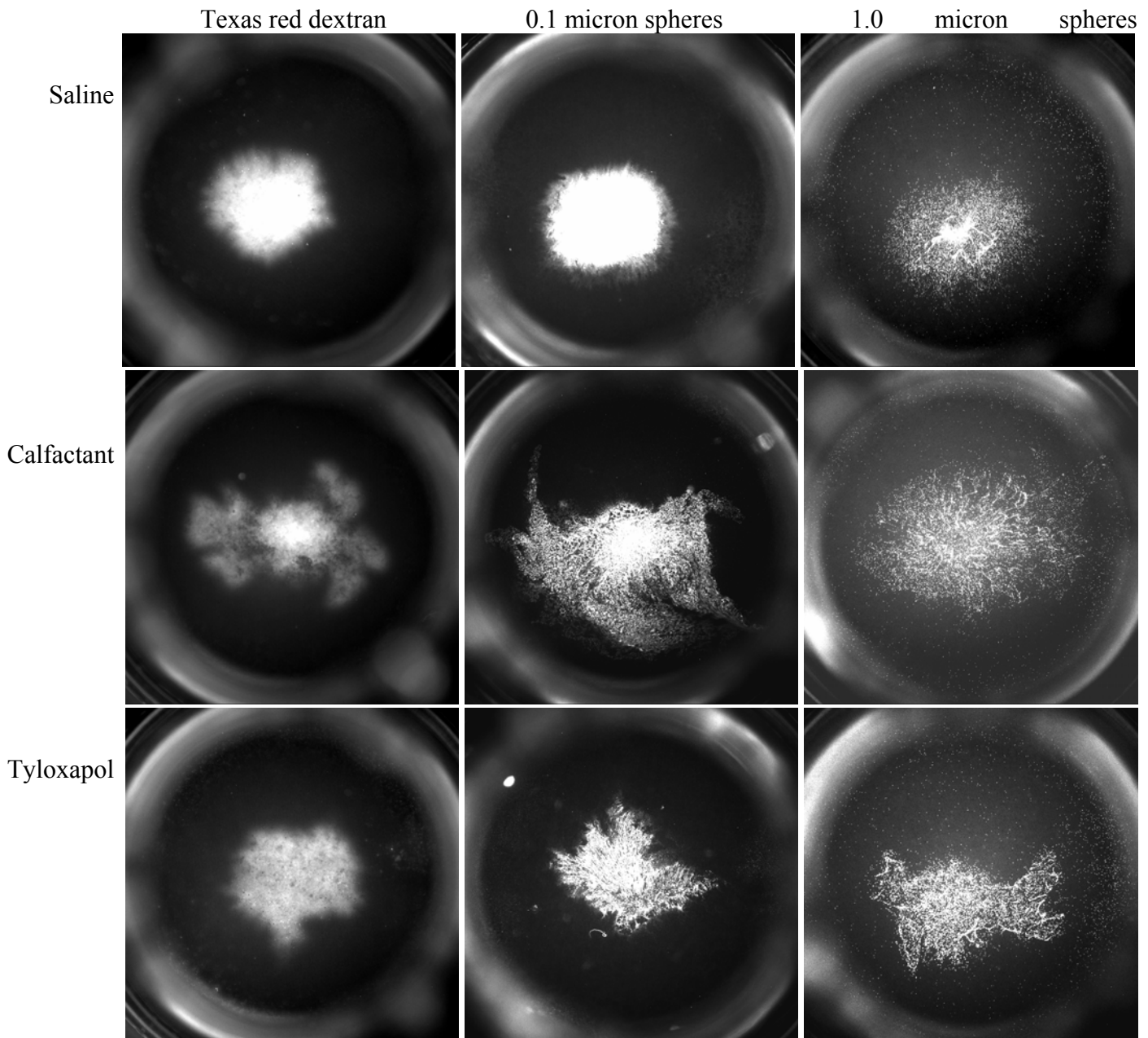


**Figure 35:** Images captured post aerosol deposition onto HBE 457 cell cultures (run 2). Saline (top row), calfactant (center row) and tyloxapol (bottom row) were labeled with texas red dextran (left column), 0.1 (center column) and 1.0 micron PS spheres (right column). These group 2 studies included additional hydration steps not performed in group 1.

Similar to the CF cell lines of Group 2, an increased degree of spreading was associated with the calfactant on the non-CF HBEs for all three tags. However, the degree to which tyloxapol spread on HBE 456 and 457 appeared to be slightly decreased vs. the CF cases, and this pattern was fairly consistent between and among both HBE 456 and 457.

### **5.3.5 Drug Formulation**

The final experimental group tested was the liposomal formulation of Amphotericin-B-Ambisome ®. Ambisome in distilled water (Amb+dH<sub>2</sub>O), the control group, and Ambisome reconstituted with a mixture of 50% calfactant and 50% distilled water (Amb+Calf+dH<sub>2</sub>O), were labeled with 0.1 micron PS spheres and delivered to HBE 456, 457, and CF 102 cell cultures (n=2). The group 2 hydration protocol was used. Figure 36 shows the images obtained post aerosol deposition of Amb + dH<sub>2</sub>O (left column) and Amb+Calf+dH<sub>2</sub>O (right column) on HBE 456. Figures 37 and 38 show the same experiment, delivering aerosol to HBE 457 and CF 102 cell cultures, respectively. By qualitative comparison, an increased degree of spreading and branching was associated with the Ambisome formulation containing calfactant for all three cell lines.

**HBE 456:**

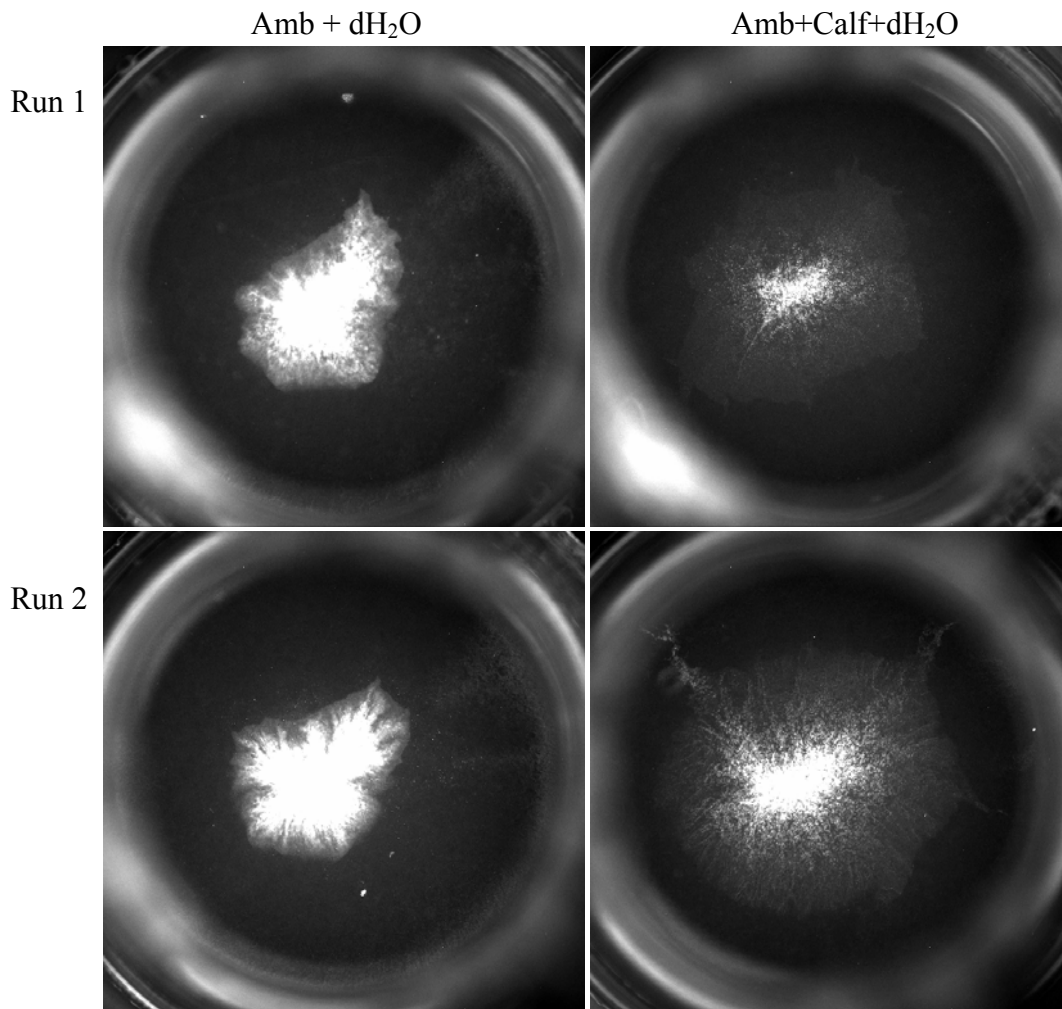


**Figure 36:** Images captured post aerosol deposition onto HBE 456 cell cultures. Ambisome in sterile water (left column) and Ambisome in calfactant/sterile water (right) were labeled with 0.1 micron PS spheres to trace drug movement on the cultures. The Group 2 hydration protocol was utilized.

**HBE 457:**

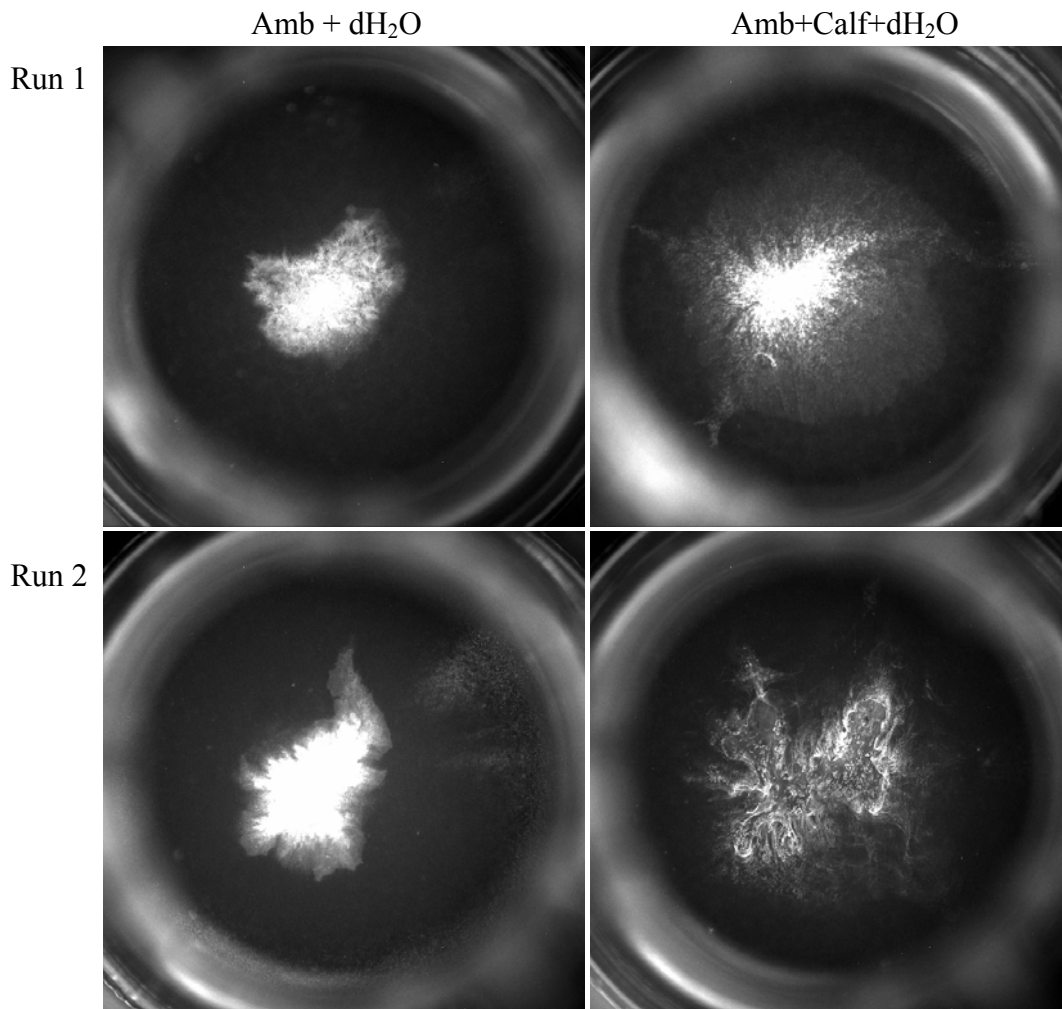


**Figure 37:** Images captured post aerosol deposition onto HBE 457 cell cultures. Ambisome in distilled water (left column) and Ambisome in calfactant/ water (right) were labeled with 0.1 micron PS spheres to trace drug movement on the cultures. The Group 2 hydration protocol was utilized.

**CF 102:**

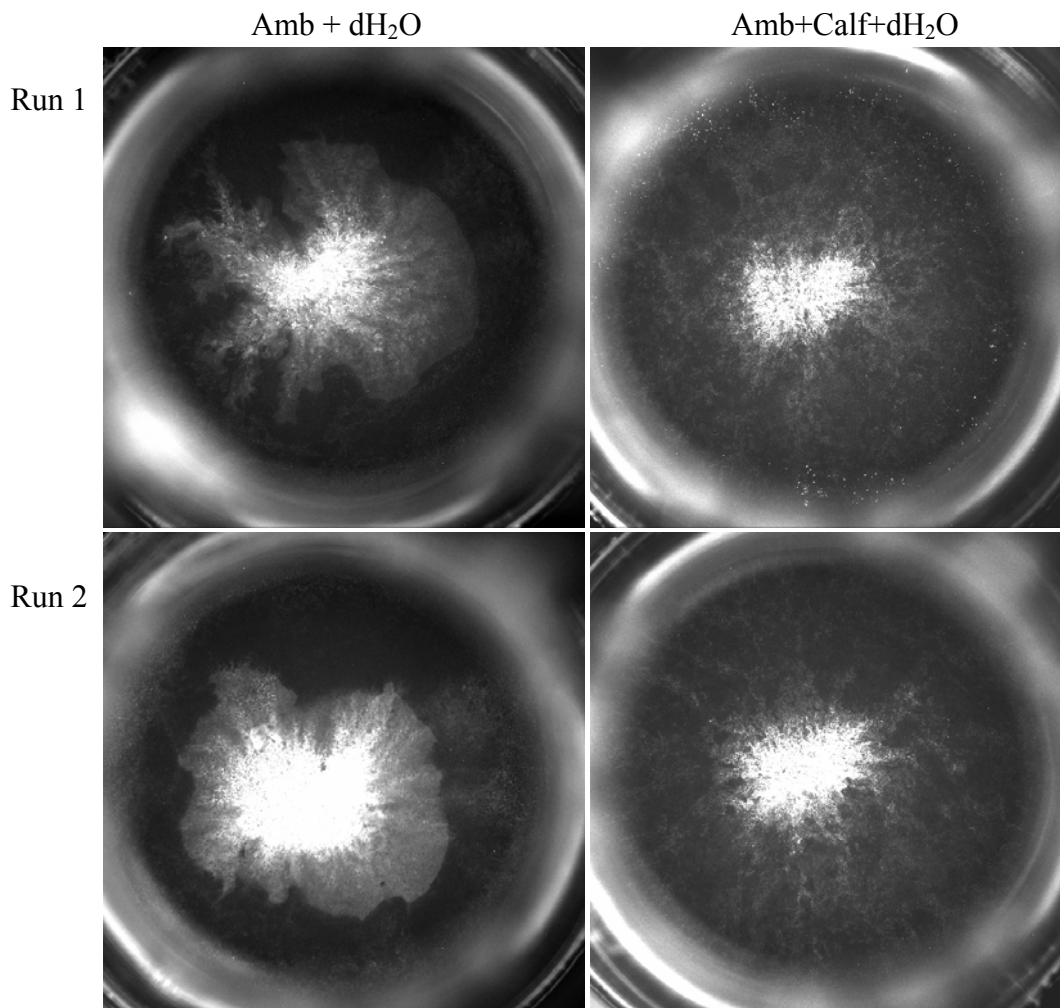


**Figure 38:** Images captured post aerosol deposition onto CF 102 cell cultures. Ambisome in distilled water (left column) and Ambisome in calfactant/ water (right) were labeled with 0.1 micron spheres to trace drug movement on the cultures. The Group 2 hydration protocol was utilized.

## 5.4 QUANTITATIVE ANALYSIS

Quantitative comparisons of saline and the four surfactants delivered to the PGM are summarized in Figure 39. The areas ( $\text{mm}^2$ ) of five trials performed for each surfactant/saline solution is plotted for the three different fluorescent tags, texas red dextran (TR), and PS spheres (0.1 and 1.0 micron). The data is presented as means  $\pm$  the standard deviation. Tests of statistical significance were performed using an unpaired t-test, with  $p < 0.05$  being significant. All four surfactants spread on the PGM post aerosol deposition to a significantly larger area than the saline for all three fluorescent tags. The t-test yielded the following p values for each PGM case:  $p \geq 0.01$ : CTAB (0.1 PS spheres);  $0.001 \leq p < 0.01$ : CTAB (1.0 PS spheres), SDS (1.0 PS spheres); and  $p < 0.001$ : CTAB (TR), SDS (TR, 0.1 PS spheres), tyloxapol (TR, 0.1, 1.0), calfactant (TR, 0.1, 1.0). A single factor ANOVA was also used and yielded a value of  $p < 0.001$ .

Figures 40-46 show similar quantitative comparisons between selected surfactants (calfactant and tyloxapol) and saline tested on each cell line in Group 2: CF 102 (Figure 40), CF 103 (Figure 41), CF 105 (Figure 42), HBE 456 (Figure 43), HBE 457 (Figure 44), all CF cell lines combined (Figure 45), and both HBE non-CF cell lines combined (Figure 46). Tests of statistical significance were performed using an unpaired t-test with  $p < 0.05$  being significant, for the individual cell lines when  $n \geq 2$  and the corresponding p-values are indicated in each figure. An single factor ANOVA was used for each individual cell line and the combined CF and non-CF cell lines. The corresponding p-values are listed in Table 9 and in figures 40-46.

**Table 9:** ANOVA p-values obtained for each individual cell line and the combined CF and non-CF cell lines.

Cell line	p-value
CF 102	0.003
CF 103	0.001
CF 105	0.02
HBE 456	0.08
HBE 457	0.10
CF ALL	0.02
HBE ALL	0.10

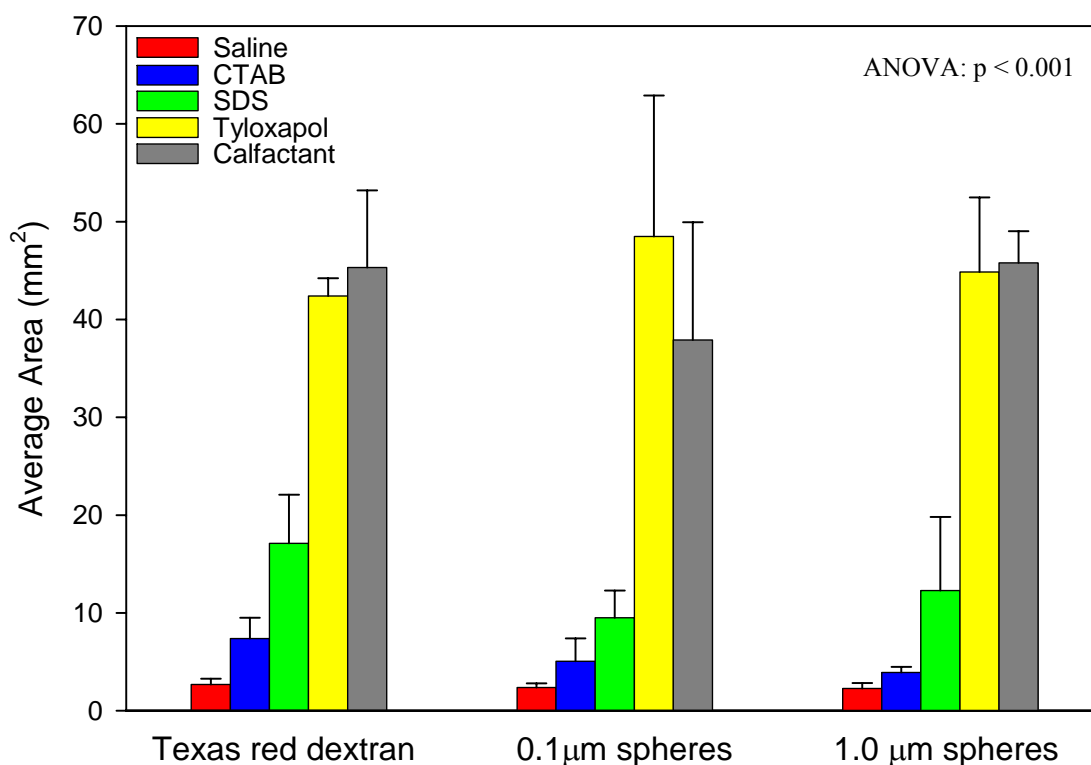


**Figure 39:** Average area of saline (red) or surfactant (CTAB-blue, SDS-green, tyloxapol - yellow, calfactant - gray) distribution on PGM post aerosol deposition (n=5). Each solution was labeled with texas red dextran, 0.1 and 1.0 micron PS spheres. A t-test and ANOVA were performed to obtain the corresponding p-values.

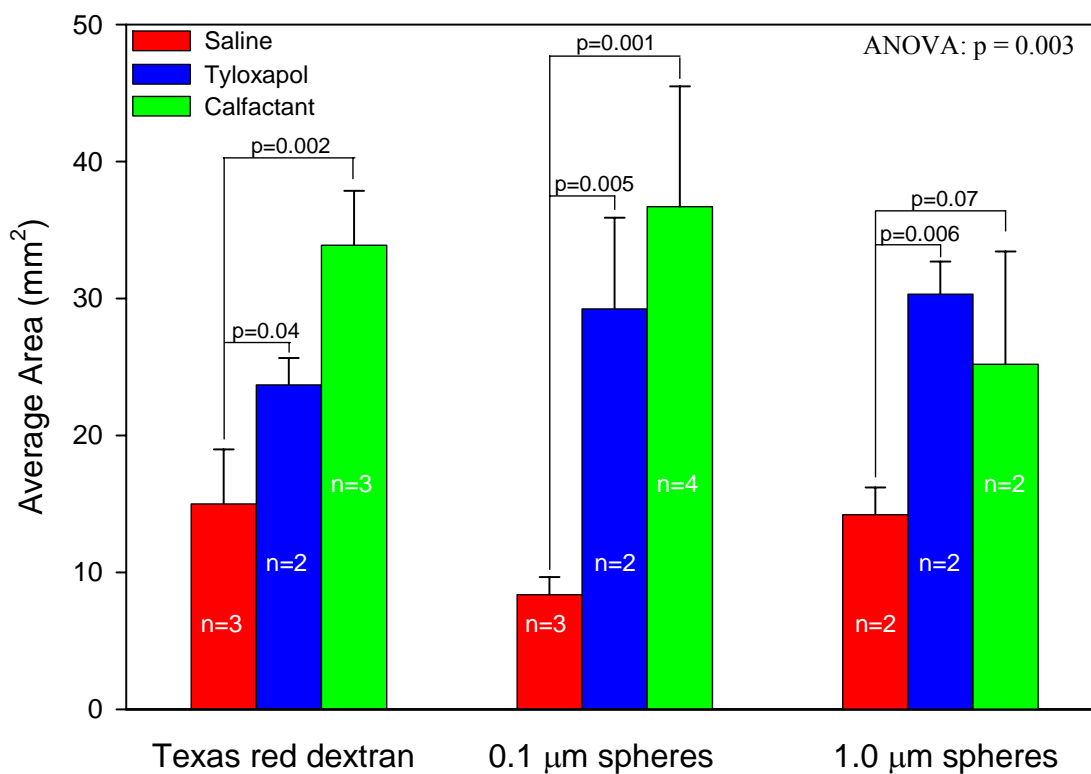


**Figure 40:** Average area of saline/surfactant distribution on CF 102 cell cultures post aerosol deposition. Saline (red), tyloxapol (blue), and calfactant (green) were labeled with texas red dextran, 0.1 and 1.0 micron PS spheres. The Group 2 hydration protocol was used. A t-test and single factor ANOVA were used obtain the corresponding p-values.

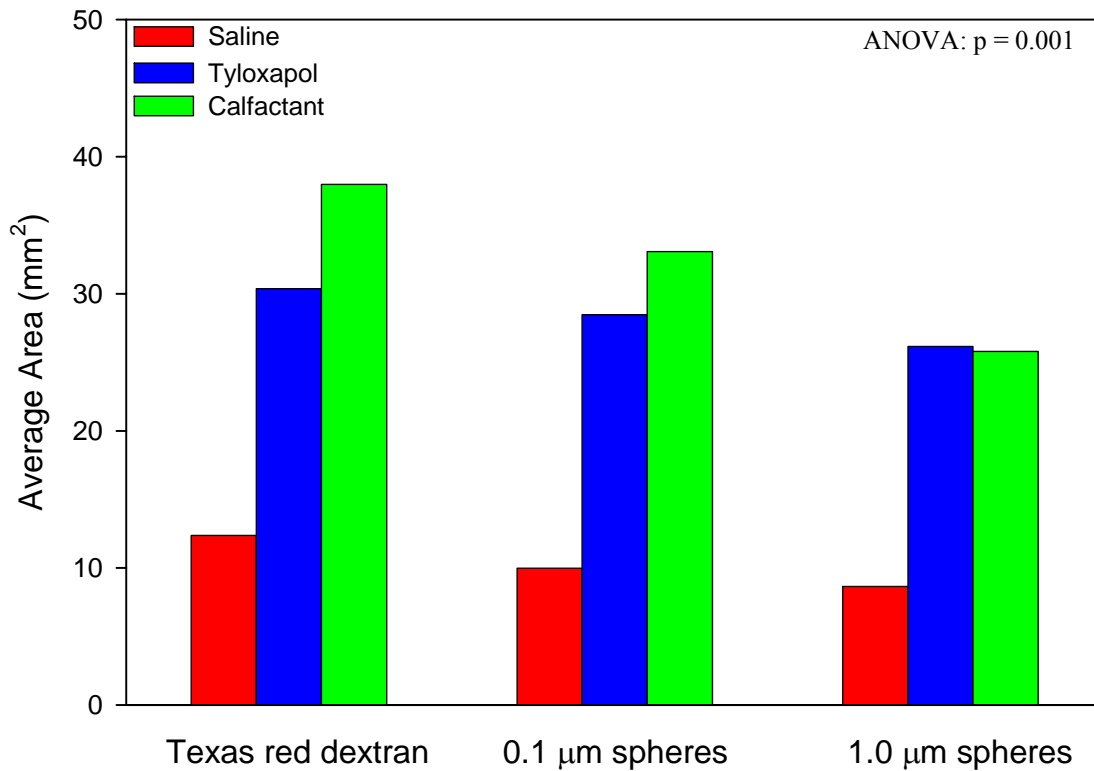


**Figure 41:** Average area of saline/surfactant distribution on CF 103 cell cultures post aerosol deposition. Saline (red), tyloxapol (blue), and calfactant (green) were labeled with texas red dextran, 0.1 and 1.0 micron PS spheres (n=1). The Group 2 hydration protocol was used. A single factor ANOVA was used.

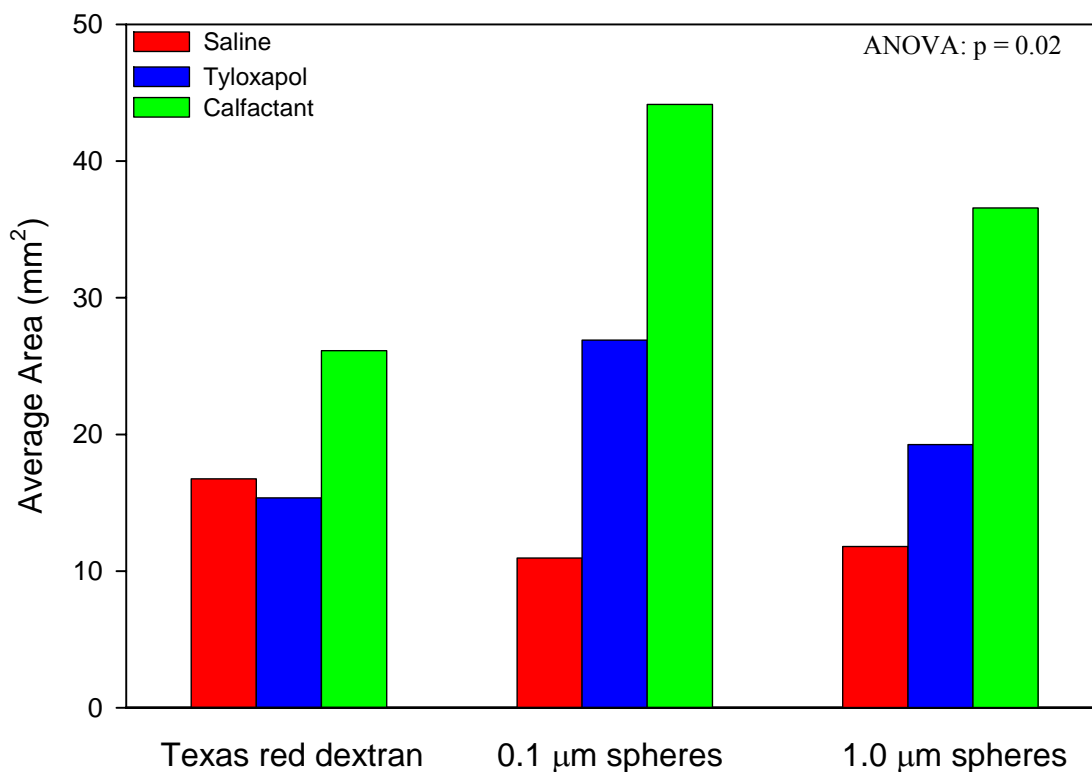


**Figure 42:** Average area of saline/surfactant distribution on CF 105 cell cultures post aerosol deposition. Saline (red), tyloxapol (blue), and calfactant (green) were labeled with texas red dextran, 0.1 and 1.0 micron PS spheres (n=1). The Group 2 hydration protocol was used. A single factor ANOVA was used.

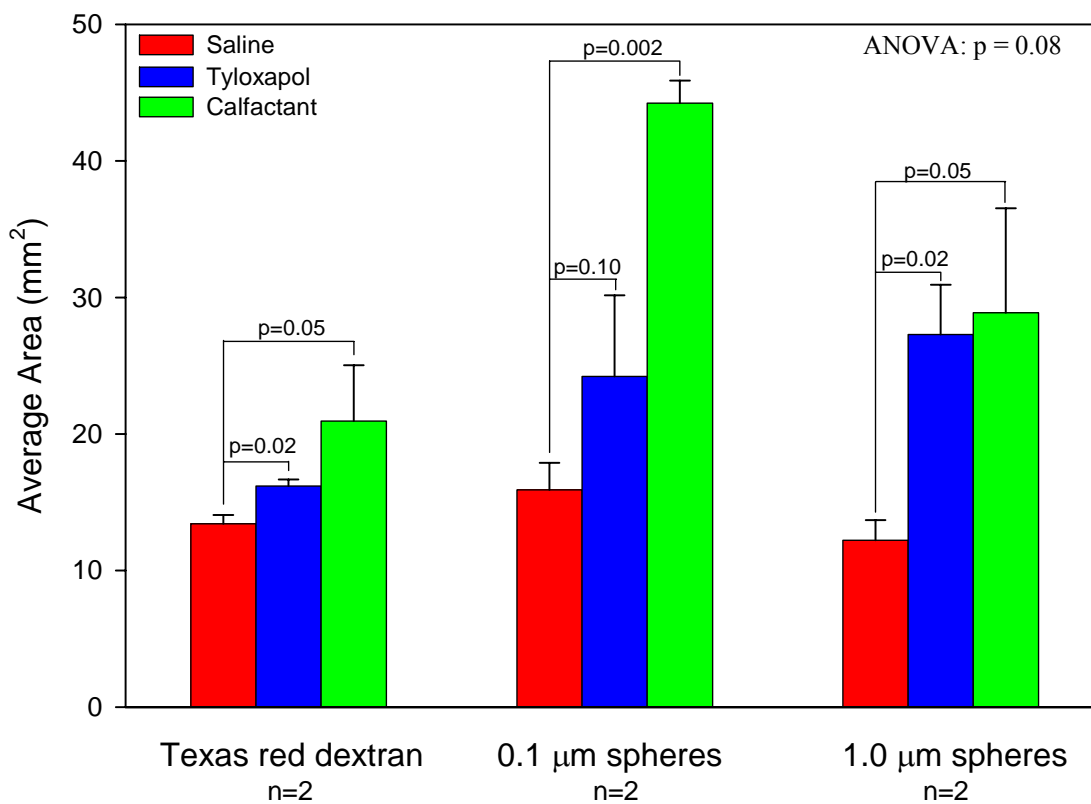


**Figure 43:** Average area of saline/surfactant distribution on HBE 456 cell cultures post aerosol deposition. Saline (red), tyloxapol (blue), and calfactant (green) were labeled with texas red dextran, 0.1 and 1.0 micron PS spheres (n=2). The Group 2 hydration protocol was used. A t-test and single factor ANOVA were used to obtain the corresponding p-values.

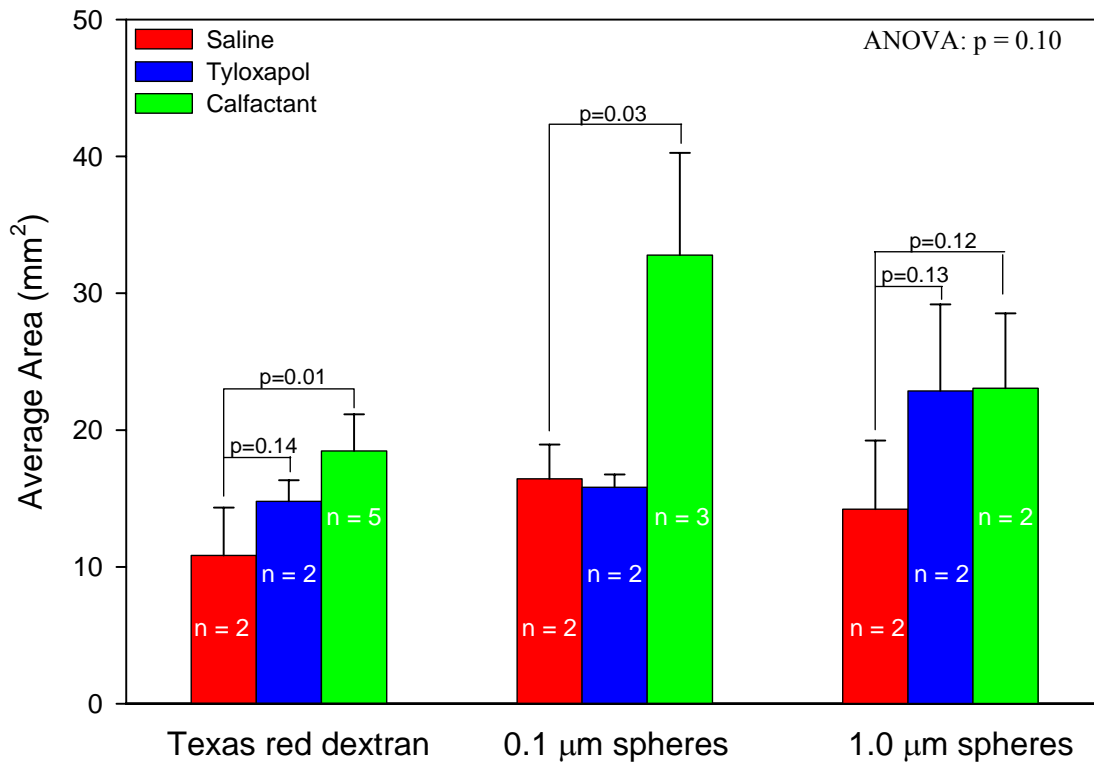


**Figure 44:** Average area of saline/surfactant distribution on HBE 457 cell cultures post aerosol deposition. Saline (red), tyloxapol (blue), and calfactant (green) were labeled with texas red dextran, 0.1 and 1.0 micron PS spheres (n varies for each case). The Group 2 hydration protocol was used. A t-test and single factor ANOVA were used to obtain the corresponding p-values.

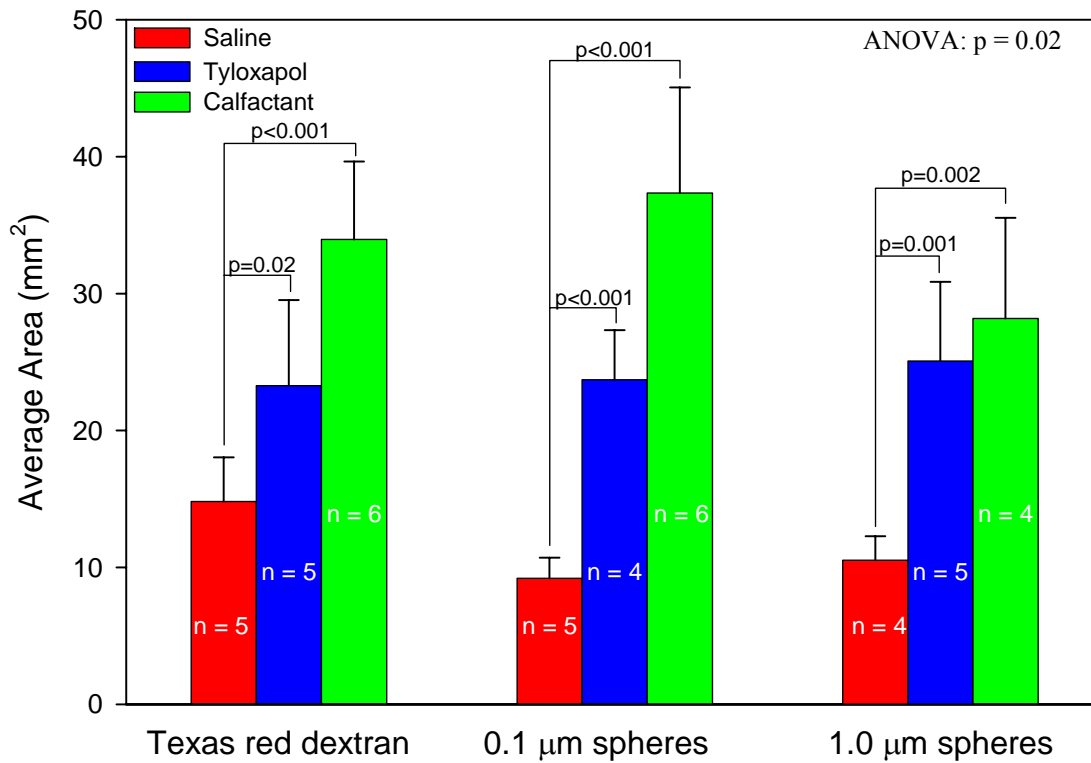


**Figure 45:** Average area of saline/surfactant distribution on all three CF cell lines combined, CF 102, CF 103, CF 105, post aerosol deposition. Saline (red), tyloxapol (blue), and calfactant (green) were labeled with texas red dextran, 0.1 and 1.0 micron PS spheres (n varies for each case). The Group 2 hydration protocol was used. A t-test and single factor ANOVA were used to obtain the corresponding p-values.

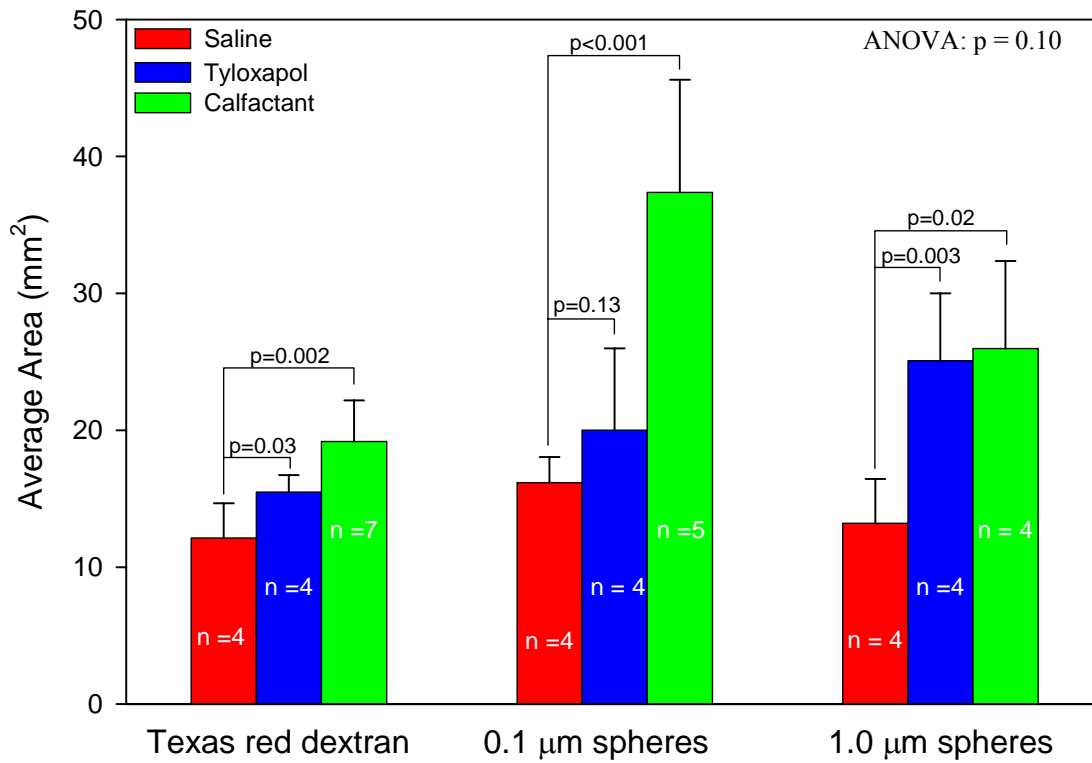


**Figure 46:** Average area of saline/surfactant distribution on HBE 456 and HBE 457 cell cultures combined, post aerosol deposition. Saline (red), tyloxapol (blue), and calfactant (green) were labeled with texas red dextran, 0.1 and 1.0 micron PS spheres (n varies for each case). The Group 2 hydration protocol was used. A t-test and single factor ANOVA were used to obtain the corresponding p-values.

A quantitative comparison of Ambisome in water only and Ambisome in calfactant and water for three different cell lines is included in Figure 47. A t-test was performed for each cell line.

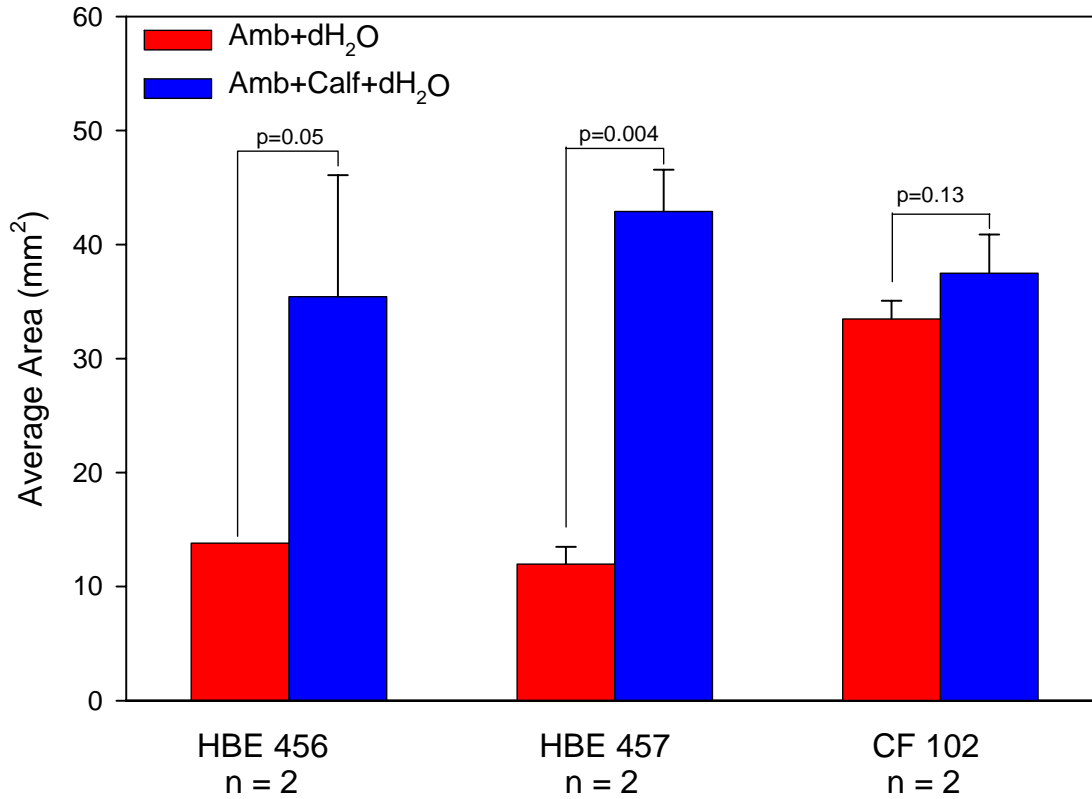


**Figure 47:** Average area of Ambisome+dH<sub>2</sub>O (red) and Ambisome+calfactant+dH<sub>2</sub>O distribution on HBE 456 (left), HBE 457 (center), and CF 102 (right) cultures, post aerosol deposition (n=2). The tag selected was the 0.1 micron PS spheres. The Group 2 hydration protocol was used. A t-test was used to obtain the corresponding p-values.

## **6.0 DISCUSSION**

### **6.1 MUCUS MODEL**

Porcine gastric mucin (PGM) was selected for these studies based on its similarity to pulmonary mucin. It has been reported that PGM and pulmonary bronchial mucins are similar in carbohydrate, amino acid, and sulfate ester composition [90, 91]. In general, mucins are characterized by a large peptide backbone with heavily glycosylated regions, both neutral and acidic, with linear and disulfide-branching [11]. They carry a net negative charge due to the presence of many sialic acid residues. The bare peptide regions tend to be somewhat hydrophobic and make mucins highly surface active [92, 93] and subject to strong interactions with the hydrophobic tails of surfactants [93, 94]. A simple phase separation experiment was performed as a function of concentration and revealed that a separation formed at concentrations ~20mg/ml and above, which agrees with phase behavior results obtained by other investigators using the PGM model [95, 96].

The upper most layer of the airway surface liquid includes mucus in thin layers or in larger plaques. Because of this, and because mucus secretions are typically elevated in diseased states (especially in CF) an understanding of mucin and surfactant interaction and the transport mechanisms associated with them must be considered. The imaging results shown in Figures 18 and 19 indicate that the four aerosolized surfactants significantly enhanced the transport of material in the plane of the mucus surface, up to ~1cm distances, after delivery of a 10 second aerosol dose. The surfactant carriers provided 2-20 fold increases in distributed area vs. saline (Table 8). The spreading patterns observed in the aerosol experiments were similar to the patterns observed in preliminary mucus experiments where single microliter droplets were placed on the PGM (Figure 12). A quantitative comparison indicated statistically significant ( $p < 0.05$ ) increases in distribution area for every surfactant-tag combination, vs. saline (Figure

39). As expected based on their low surface tension values, nonionic tyloxapol and calfactant provided the greatest spreading enhancement of all surfactants tested. The CTAB and SDS did not enhance spreading to the extent of the other surfactants, although they still increased dispersion vs. saline. These mucus studies indicate that the marangoni flows associated with a surfactant carrier can enhance the spreading of a simulated drug on the PGM surface, when the drug-surfactant combination is delivered via aerosol.

Insights on the mechanism of transport (convection vs. diffusion) can be discerned based on the time scale of the spreading. Both experiments indicated that the enhanced spreading was rapid when it occurred, confirming that the transport was convective, as these time scales would correspond to an impossibly large lateral diffusion coefficient on the order of  $10^{-4}$  cm<sup>2</sup>/s. The size of the three fluorescent tags used ranged from the molecular level (texas red dextran) to 0.1 and 1.0 micron diameter polystyrene spheres. All three tags were transported across similar distances and with similar distribution patterns, further supporting the assertion that transport is convective and not diffusive.

Although we believe that surfactant spreading was driven primarily by surface tension gradients on the PGM, several factors such as surfactant chemistry and the yield stress of the mucus might impact spreading. On PGM, saline, CTAB (cationic) and SDS (anionic) were observed over an extended period after deposition as shown in Figure 20. Saline slowly diffused outward during that time period, however both SDS and CTAB slowly retracted, suggesting the role of electrostatic charge in the spreading behavior. This retraction behavior was not observed for the tyloxapol and calfactant cases. Based on studies of the phase transitions of mucus gels, swelling/deswelling is dictated by the balance between attractive (hydrogen bonding, hydrophobic attraction, van der Waals forces) and repulsive (mainly electrostatic) interactions [97-106]. The CTAB may have bound to the negatively charged mucins in response to the electrostatic attraction. At low concentrations, charge neutralization leads to mucin collapse and precipitation of a mucin/surfactant complex and the gel may, or may not, reswell as additional surfactant binding continues beyond the point of charge reversal, depending on the microstructure of the surfactant/mucin complex [107]. This may offer an explanation for the retraction behavior observed for CTAB. In addition, studies on solid oxide surfaces have also demonstrated that cationic surfactants can cause the retraction of a spreading droplet [108-110]. Despite the net electrostatic repulsion, anionic surfactants are known to associate strongly with

mucins above a critical aggregation concentration, primarily by associating their hydrophobic tails with the bare peptide regions of mucins [93, 94]. On solid oxide surfaces, anionic surfactants also enhanced spreading by a marangoni driven flows [111]. This evidence supports the initial spreading of the SDS; however, the electrostatic interaction may have affected the structure post deposition causing the eventual retraction of SDS. There may have been little interaction between the other surfactants and the mucin, and therefore surface tension gradients may have solely affected the transport since no retraction was observed with tyloxapol and calfactant. Studies have indicated that nonionic surfactants interact weakly with mucins [93].

Airway mucus yield stress has been investigated theoretically by Craster et al [112] and its effect on marangoni stresses to induce convective flows. If the surfactant reduces the surface yield stress of the mucus so as to be overcome by the marangoni stress, then flows similar to those discussed in the models of SRT for soluble surfactants on viscoelastic layers may be established [112]. However, if marangoni stresses remain below the surface yield stress of the mucus, the mucus will act like a solid surface with respect to surfactant spreading.

Our experiments demonstrate that surfactant carriers can improve the distribution of a simulated drug over a mucus surface. However, the more complex potential interactions between surfactants and mucus speak to the need for more basic studies that might provide a better understanding of the specific interactions between these molecules. During the preliminary experiments, visual observations on thinner mucus layers (<4mm) indicated that the surfactant solutions actually induced transport of the mucus itself, thinning the layer slightly. The saline solution did not appear to thin the layer. Infections and biofilms within the mucus might be more reachable based on this mode of transport. Studies on mucin-surfactant interaction would allow for the selection of the optimal surfactants for improving drug distribution and might also allow for the exploitation of other effects to improve drug efficacy (such as mucolytic effects).

## 6.2 CELL CULTURE MODEL

The HBE portion of the study revealed that when the apical surface of the culture was sufficiently hydrated, almost all tested surfactants significantly enhanced spreading vs. saline, on both CF and non-CF cells surfaces. Based on the variability found in the Group 1 HBE studies and the calu3 cells, the level of hydration was the key element that affected the degree of spreading that occurred on the epithelial surface in the presence of surfactant. The Group 2 studies, which included a more aggressive protocol for hydration, yielded more consistent results that we believe to be the most physiologically realistic. However, this could not be definitively verified.

The Calu3 cell line was a useful preliminary model, however due to the absence of a native ASL they provided a less physiologically accurate representation of the airway surface. Despite measures to limit evaporation during testing, the hydration level of these cells varied day to day as demonstrated in Figures 21 and 22. When saline, calfactant, and tyloxapol were delivered to the surface of the Calu3s, a droplet formed on the surface for all three indicating there was not a sufficient degree of hydration on the surface to induce a convective marangoni flow (Figure 21). However, the spreading of tyloxapol was found on the calu3s in Figure 22 with a larger branching out area following deposition, indicating the surface was hydrated enough for a surfactant to enhance some spreading. These cell cultures also produce a high level of mucus, which may have also contributed to the varied hydration levels.

In HBE groups 1 and 2, several cell lines were obtained with varying disease states, including both CF and non-CF samples. On the three CF cell lines in HBE Group 1, tyloxapol and calfactant did not enhance spreading (Figures 23 and 24). This was not surprising since the CF cells have a higher probability of exhibiting a depleted ASL, which is a main characteristic of the disease. However, the same variability was found for three HBE (non-CF) cell lines (Figures 25-27) in the which the ASL volume has been established to be approximately  $\sim 7 \mu\text{m}$  [113] at baseline conditions. There is no reason to believe that the disease states of these HBE's (scleroderma, aspiration/infection, and heart failure) would result in specifically depleted ASL. We speculate that the variability in Group 1 was likely caused by different levels of hydration.

Other investigators have acknowledged this same hydration problem and have established a protocol for preventing ASL evaporation. Tarran et al prevent ASL evaporation through the addition of 100  $\mu$ l of PFC to the apical surface of the cultures [59]. However, this PFC protocol could not be used in the current experiments because of the need for realistic surface conditions and immediate access to the surface for aerosol delivery. We instead devised an alternative protocol that included the addition and immediate removal of 100  $\mu$ l of PBS solution for our group 2 studies.

A factor that may have affected the ASL baseline height and the level of hydration in Group1 was the chosen media used to feed the cell cultures. Several groups studying similar cell cultures produce fully differentiated cells using a different range of base medium supplemented with various additives. Specifically, the media used for the cells in this study was DMEM/F-12 base media supplemented with several additives including epidermal growth factor (EPG) and USG, a bovine serum. The cultures used by Tarran and Matsui et al. are grown in base media, laboratory of human carcinogenesis basal medium #9 (LHC-9) and DMEM, with a relatively lower level of EPG and the addition of bovine pituitary extract (BPE), but no USG [113]. Sachs et al. [114] conducted a study in which these two media protocols were compared to quantify the level of differentiation. Although both medium produced fully differentiated cells, the electrophysiological measurements of salt transport varied. The USG cells (similar to ones used in this study) had slightly higher baseline ENaC activity and lower Cl<sup>-</sup> channel activity compared to the media used by Matsui. Elevated sodium movement across the epithelium would also increase the flow of water across the epithelium, depleting the ASL volume, like that of CF cells. Sachs' observations suggest that the differences may have been media dependent and that non-CF HBEs in USG have electrophysiological characteristics similar to CF cell cultures, a depleted PCL and dehydrated mucus layer. We speculate that this idea provides evidence to support the results from Group 1 with the similarities found between the results of the CF and non-CF cell lines and the dehydrated surfaces found. The otherwise “normal” cells may have been ASL volume depleted at baseline conditions, again reinforcing the need for the hydration protocol used in Group 2.

Two aspects of the hydration protocol used in Group 2 should be considered. First, the hydration technique may increase the volume of the native ASL beyond physiological levels. Tarran et al. [59] measured the surface tension of similar cultures before and after an addition of

20 $\mu$ l of PBS to the apical surface and found no significant difference, indicating that the added PBS did not dilute the surfactant components present in the culture. We therefore speculate that small volume additions above physiologic norms would not alter the experimental results.

Also, the possible removal of any surfactant components present on the culture surface when the PBS was removed should be considered. Tarran et al. [59] found that only after vigorous washing of the apical surface of similar cultures with the reducing agent DTT in PBS did the surface tension finally return to the level of water, at  $\sim$ 72 mN/m. This indicates that a large degree of flushing of the cells would be needed to fully remove the surfactant components from the apical surface. Also, we would also have expected less consistency in our Group 2 results if surfactant was being removed during the hydration protocol.

By qualitative comparison of cell lines CF 102, 103, and 105 in Group 2, both tyloxapol and calfactant enhanced spreading of all three tags compared to saline; calfactant to a larger degree than tyloxapol. A quantitative summary of all three cell lines combined in Figure 45 demonstrates that both surfactants exhibited significantly increased dispersion of all three tags compared to saline. Similar results were obtained for HBE 456 and 457 using the hydration protocol and are summarized in Figure 46. The results of Group 2 indicate that in the presence of a sufficient ASL volume on both CF and non-CF cells, surfactants enhance spreading of dye following aerosol deposition vs. saline. The final experiment conducted with the liposomal formulation demonstrated that Ambisome in calfactant consistently enhanced spreading on both CF and non-CF cells lines vs. Ambisome in water. This further supports the notion that surfactant will have a larger distribution on an epithelial surface than a high surface tension fluid such as saline or water.

The degree of spreading of tyloxapol varied somewhat between CF and non CF HBE's. Calfactant spread to a similar distance and with a similar pattern on both of these cultures. However, the difference between the area of tyloxapol and saline distribution was consistently larger on the CF cultures. The average difference between saline and tyloxapol distribution on the CF cultures was  $\sim$ 2 times greater than on the non-CF cultures, while the average difference between the saline and calfactant was between 1-2 times greater on the CF versus non-CF cultures. Potentially this could suggest that the initial level of surfactant present in the non-CF cultures may have been higher than the CF cultures and only the lower surface tension surfactant (calfactant) was able to enhance spreading. Studies of CF sputum samples have found decreased

levels of surfactant components, specifically surfactant protein D, suggesting surfactant depletion to be associated with CF; however, studies have not considered this in the HBE's. Additional studies of a larger number of CF and non-CF HBE's would ultimately be necessary to determine whether these spreading behaviors are actually different. Measurements of surface tension in these HBE's and measurements of the concentration of surfactant components would be necessary to further speculate on this mechanism.

### **6.3 CONCLUSIONS**

In this study, we evaluated the potential for an aerosolized surfactant carrier to enhance spreading on two in vitro airway surfaces. The results demonstrate that a surfactant aerosol delivered to either a hydrated mucus surface or a hydrated epithelial cell culture surface enhances spreading compared to saline. Basic studies of mucus-surfactant interaction would offer a better understanding of the transport mechanisms observed and provide a basis for selecting optimal surfactants. Future experiments are needed to validate the alternative hydration protocol used in Group 2 and to develop similar techniques that provide the most physiologically realistic conditions possible. HBE models are being investigated for many other applications, and will no doubt evolve into even more realistic models in the future. Surface tension measurements of the cultures used in this study and detailed studies of their surfactant components would further validate these models and provide valuable information on the exact mechanism of dispersion. Our results demonstrate the potential for surfactant aerosol carriers to improve the uniformity of drug distribution in the lungs. Further development is needed to demonstrate their efficacy in this capacity and their ultimate clinical efficacy with specific drugs.

## BIBLIOGRAPHY

1. West, J.B., *Respiratory Physiology The Essentials*. 6th ed. 2000, Philadelphia: Lippincott Williams & Wilkins.
2. Hickey, A.J., *Pharmaceutical Inhalation Aerosol Technology*. 2004, New York: Marcel Dekker, Inc.
3. *Pulmonary Biology in Health and Disease*, ed. E.E. Bittar. 2002, New York: Springer-Verlag Inc.
4. *The Airway Epithelium: physiology, pathophysiology, and pharmacology*, ed. S.G. Farmer and D.W.P. Hay. 1991, New York: Marcel Dekker.
5. Boucher, R.C. New concepts of the pathogenesis of cystic fibrosis lung disease. *Eur Respir J*. 2004. 23(1): p. 146-58.
6. Samet, J.M. and P.W. Cheng. The role of airway mucus in pulmonary toxicology. *Environ Health Perspect*. 1994. 102 Suppl 2: p. 89-103.
7. Pilewski, J.M. and R.A. Frizzell. Role of CFTR in airway disease. *Physiol Rev*. 1999. 79(1 Suppl): p. S215-55.
8. Carlstedt, I. Sheehan, J.K., Corfield, A. P., and J.T. Gallagher. Mucous glycoproteins: a gel of a problem. *Essays in Biochemistry*. 1985. 20: p. 40-76.
9. Allen, A. *Physiology of the Gastrointestinal Tract*. . 1981, New York: Raven Press.
10. Strous, G.J. and J. Dekker. Mucin-type glycoproteins. *Crit Rev Biochem Mol Biol*. 1992. 27(1-2): p. 57-92.
11. Carlson, D.M. Structures and immunochemical properties of oligosaccharides isolated from pig submaxillary mucins. *J Biol Chem*. 1968. 243: p. 616-626.
12. Shi, L.S., Ardehali, R., Caldwell, K.D., and P. Valint. Mucin coating on polymeric material surfaces to suppress bacterial adhesion. *Colloids and Surfaces B: Biointerfaces* 2000. 17: p. 229-39.

13. Widdicombe, J.H. Regulation of the depth and composition of airway surface liquid. *J Anat.* 2002. 201(4): p. 313-8.
14. Geiser, M., Schurch, S., and P. Gehr. Influence of surface chemistry and topography of particles on their immersion into the lung's surface-lining layer. *J App Physiol.* 2003. 94(5): p. 1793-801.
15. C.F. Foundation. 2004. <http://www.cff.org>.
16. Hirsch, A.J. and R.C. Boucher. Absorption of Na<sup>+</sup> channel inhibitors by cystic fibrosis airway epithelium. *Pediatr Pulmonol Suppl.* 2000. 20: p. 248.
17. Blouquit, S., et al. Ion and Fluid Transport Properties of Small Airways in Cystic Fibrosis. *Am J Respir Crit Care Med.* 2006.
18. Chinet, T.C., et al. Mechanism of sodium hyperabsorption in cultured cystic fibrosis nasal epithelium: a patch-clamp study. *Am J Physiol.* 1994. 266(4 Pt 1): p. C1061-8.
19. Rowe, S.M., Miller, S., and E.J. Sorscher. Cystic fibrosis. *N Engl J Med.* 2005. 352(19): p. 1992-2001.
20. Eliezer, N., et al. The role of mucus in transport by cilia. *Am Rev Respir Dis.* 1970. 102(1): p. 48-52.
21. Frizzell, R.A. and J.M. Pilewski. Finally, mice with CF lung disease. *Nat Med.* 2004. 10(5): p. 452-4.
22. Shen, B.Q., et al. Calu-3: a human airway epithelial cell line that shows cAMP-dependent Cl<sup>-</sup> secretion. *Am J Physiol.* 1994. 266(5 Pt 1): p. L493-501.
23. Finlay, W.H. *The Mechanics of Pharmaceutical Aerosols.* 2001, San Diego: Academic Press.
24. Patton, J.S., Bukar J., and S. Nagarajan. Inhaled insulin. *Adv Drug Deliv Rev.* 1999. 35(2-3): p. 235-247.
25. Mather, L.E., et al. Pulmonary administration of aerosolised fentanyl: pharmacokinetic analysis of systemic delivery. *Br J Clin Pharmacol.* 1998. 46(1): p. 37-43.
26. Schlesinger, R.B. Comparative deposition of inhaled aerosols in experimental animals and humans: a review. *J Toxicol Environ Health.* 1985. 15(2): p. 197-214.
27. Schlesinger, R.B. and M. Lippmann. Particle deposition in casts of the human upper tracheobronchial tree. *Am Ind Hyg Assoc J.* 1972. 33(4): p. 237-51.

28. Suarez, S. and A.J. Hickey. Drug properties affecting aerosol behavior. *Respir Care*. 2000. 45(6): p. 652-66.
29. Lippmann, M. *Regional deposition of particles in the human respiratory tract handbook of physiology*. 1977: American Physiological Society.
30. Laube, B.L., et al. The effect of bronchial obstruction on central airway deposition of a saline aerosol in patients with asthma. *Am Rev Respir Dis*. 1986. 133(5): p. 740-3.
31. Foundation., C.F., *Patient Registry 1998 annual data report*. 1999, Bethesda, MD: The Foundation.
32. Geller, D.E., et al. Pharmacokinetics and bioavailability of aerosolized tobramycin in cystic fibrosis. *Chest*. 2002. 122(1): p. 219-26.
33. Label for Nebcin ®. 2004. <http://www.rxlist.com/cgi/generic3/tobramycin.htm>.
34. Ramsey, B.W., et al. Efficacy of aerosolized tobramycin in patients with cystic fibrosis. *N Engl J Med*. 1993. 328(24): p. 1740-6.
35. Ramsey, B.W., et al. Intermittent administration of inhaled tobramycin in patients with cystic fibrosis. Cystic Fibrosis Inhaled Tobramycin Study Group. *N Engl J Med*. 1999. 340(1): p. 23-30.
36. Katz, S.L., Ho, S.L., and A.L. Coates. Nebulizer choice for inhaled colistin treatment in cystic fibrosis. *Chest*. 2001. 119(1): p. 250-5.
37. Diot, P., et al. Nebulization and anti-*Pseudomonas aeruginosa* activity of colistin. *Eur Respir J*. 1997. 10(9): p. 1995-8.
38. Schaad, U.B., et al. Efficacy of inhaled amikacin as adjunct to intravenous combination therapy (ceftazidime and amikacin) in cystic fibrosis. *J Pediatr*. 1987. 111(4): p. 599-605.
39. Nicholson, S.C. Development and Studies of Nebulized SLIT Amikacin for the Treatment of *Pseudomonas Aeruginosa* Airway Infection in CF (S12.3-Session Summary). *Pediatr Pulmonol*. 2005. 40(S12.3): p. 144.
40. Gibson, R.L., et al. Microbiology, safety, and pharmacokinetics of aztreonam lysinate for inhalation in patients with cystic fibrosis. *Pediatr Pulmonol*. 2006.
41. Heinzl, B., et al. Effects of inhaled gentamicin prophylaxis on acquisition of *Pseudomonas aeruginosa* in children with cystic fibrosis: a pilot study. *Pediatr Pulmonol*. 2002. 33(1): p. 32-7.

42. Nektar ® Press Release. Jan 2005.  
[http://www.nektar.com/wt/page/pr\\_1106667344/?ref=Archived\\_Press\\_Releases](http://www.nektar.com/wt/page/pr_1106667344/?ref=Archived_Press_Releases).
43. Pilcer, G., Sebti, T., and K. Amighi. Formulation and Characterization of Lipid-Coated Tobramycin Particles for Dry Powder Inhalation. *Pharm Res*. 2006.
44. Newhouse, M.T., et al. Inhalation of a dry powder tobramycin PulmoSphere formulation in healthy volunteers. *Chest*. 2003. 124(1): p. 360-6.
45. Smaldone, G.C. Aerosolized antibiotics in mechanically ventilated patients. *Respir Care*. 2004. 49(6): p. 635-9.
46. Bressolle, F., et al. Endotracheal and aerosol administrations of ceftazidime in patients with nosocomial pneumonia: pharmacokinetics and absolute bioavailability. *Antimicrob Agents Chemother*. 1992. 36(7): p. 1404-11.
47. Stewart, P.S. Theoretical aspects of antibiotic diffusion into microbial biofilms. *Antimicrob Agents Chemother*. 1996. 40(11): p. 2517-22.
48. Anderl, J.N., M.J. Franklin, and P.S. Stewart. Role of antibiotic penetration limitation in *Klebsiella pneumoniae* biofilm resistance to ampicillin and ciprofloxacin. *Antimicrob Agents Chemother*. 2000. 44(7): p. 1818-24.
49. Hiemenz, P.C. *Principles of Colloid and Surface Chemistry, 3rd ed.* 1997, New York: Marcel Dekker.
50. Malmsten, M., *Surfactants and Polymers in Drug Delivery, Drugs and the Pharmaceutical Sciences*. 2002, New York: Marcel Dekker, Inc.
51. Adamson, A.W. *Physical Chemistry of Surfaces*. 1976, New York: John Wiley & Sons, Inc.
52. Devendra, G. and R.G. Spragg. Lung surfactant in subacute pulmonary disease. *Respir Res*. 2002. 3(1): p. 19.
53. Hawgood, S. and J.A. Clements. Pulmonary surfactant and its apoproteins. *J Clin Invest*. 1990. 86(1): p. 1-6.
54. Kirkness, J.P., et al. Effect of surface tension of mucosal lining liquid on upper airway mechanics in anesthetized humans. *J Appl Physiol*. 2003. 95(1): p. 357-63.
55. Gehr, P., Schurch, S., Berthiaume, Y., Im Hof, V., and M. Geiser. Particle retention in airways by surfactant. *J Aero Med*. 1990. 3(27-43).
56. Schurch, S. Surface tension at low lung volumes: dependence on time and alveolar size. *Respir Physiol*. 1982. 48(3): p. 339-55.

57. Im Hof, V., et al. In vivo determination of surface tension in the horse trachea and in vitro model studies. *Respir Physiol.* 1997. 109(1): p. 81-93.
58. Sims, D.E. and M.M. Horne. Heterogeneity of the composition and thickness of tracheal mucus in rats. *Am J Physiol.* 1997. 273(5 Pt 1): p. L1036-41.
59. Tarran, R., et al. The relative roles of passive surface forces and active ion transport in the modulation of airway surface liquid volume and composition. *J Gen Physiol.* 2001. 118(2): p. 223-36.
60. Zahm, J.M., et al. Improvement of cystic fibrosis airway mucus transportability by recombinant human DNase is related to changes in phospholipid profile. *Am J Respir Crit Care Med.* 1998. 157(6 Pt 1): p. 1779-84.
61. Khor, A., et al. Temporal-spatial distribution of SP-B and SP-C proteins and mRNAs in developing respiratory epithelium of human lung. *J Histochem Cytochem.* 1994. 42(9): p. 1187-99.
62. Voorhout, W.F., et al. Immunocytochemical localization of surfactant protein D (SP-D) in type II cells, Clara cells, and alveolar macrophages of rat lung. *J Histochem Cytochem.* 1992. 40(10): p. 1589-97.
63. Barrow, R.E. Chemical structure of phospholipids in the lungs and airways of sheep. *Respir Physiol.* 1990. 79(1): p. 1-8.
64. Bernhard, W., et al. Conductive airway surfactant: surface-tension function, biochemical composition, and possible alveolar origin. *Am J Respir Cell Mol Biol.* 1997. 17(1): p. 41-50.
65. Bachofen, H., et al. Relations among alveolar surface tension, surface area, volume, and recoil pressure. *J Appl Physiol.* 1987. 62(5): p. 1878-87.
66. Escolar, J.D., Escolar, M.A., Guzman J., and M. Roques. Morphological hysteresis of the small airways. *Histol Histopathol* 2003. 18(1): p. 19-26.
67. Grotberg, J.B., Halpern D., and O.E. Jensen. Interaction of exogenous and endogenous surfactant: spreading-rate effects. *J Appl Physiol.* 1995. 78(2): p. 750-6.
68. Haitzma, J.J., Lachmann U., and B. Lachmann. Exogenous surfactant as a drug delivery agent. *Adv Drug Deliv Rev.* 2001. 47(2-3): p. 197-207.
69. Dhand, R. New frontiers in aerosol delivery during mechanical ventilation. *Respir Care.* 2004. 49(6): p. 666-77.
70. Bahlmann, H., et al. Aerosolized surfactant in lung-lavaged adult rats: factors influencing the therapeutic response. *Acta Anaesthesiol Scand.* 2000. 44(5): p. 612-22.

71. Anzueto, A., et al. Aerosolized surfactant in adults with sepsis-induced acute respiratory distress syndrome. Exosurf Acute Respiratory Distress Syndrome Sepsis Study Group. *N Engl J Med.* 1996. 334(22): p. 1417-21.
72. Griese, M., et al. Nebulization of a bovine surfactant in cystic fibrosis: a pilot study. *Eur Respir J.* 1997. 10(9): p. 1989-94.
73. Label for Exosurf. 2004. <http://www.rxlist.com/cgi/generic3/exosurf.htm>.
74. Label for Survanta. 2004. <http://www.rxlist.com/cgi/rxlist.cgi?drug=survanta>.
75. Label for Infasurf. 2004. <http://www.rxlist.com/cgi/generic/calfactant.htm>.
76. Label for Curosurf. 2004. <http://rxlist.com/cgi/generic2/curosurf.htm>.
77. Park, S.Y., Chang, C.H., Ahn, D.J., Franses, E.I. Dynamic Surface Tension Behavior of Hexadeconal Spread and Absorbed Monolayers. *Langmuir.* 1993. 9(12): p. 3640-3648.
78. Espinosa, F.F., et al. Spreading of exogenous surfactant in an airway. *J Appl Physiol.* 1993. 75(5): p. 2028-39.
79. Anderson, J.C., et al. Effect of ventilation rate on instilled surfactant distribution in the pulmonary airways of rats. *J Appl Physiol.* 2004. 97(1): p. 45-56.
80. Cassidy, K.J., et al. A rat lung model of instilled liquid transport in the pulmonary airways. *J Appl Physiol.* 2001. 90(5): p. 1955-67.
81. Halpern, D., Jensen, O.E., and J.B. Grotberg. A theoretical study of surfactant and liquid delivery into the lung. *J Appl Physiol.* 1998. 85(1): p. 333-52.
82. Kharasch, V.S., et al. Pulmonary surfactant as a vehicle for intratracheal delivery of technetium sulfur colloid and pentamidine in hamster lungs. *Am Rev Respir Dis.* 1991. 144(4): p. 909-13.
83. Van't Veen, A., et al. Pulmonary surfactant as vehicle for intratracheally instilled tobramycin in mice infected with *Klebsiella pneumoniae*. *Br J Pharmacol.* 1996. 119(6): p. 1145-8.
84. Nimmo, A.J., et al. Intratracheal administration of glucocorticoids using surfactant as a vehicle. *Clin Exp Pharmacol Physiol.* 2002. 29(8): p. 661-5.
85. Fajardo, C., et al. Surfactant versus saline as a vehicle for corticosteroid delivery to the lungs of ventilated rabbits. *Pediatr Res.* 1998. 43(4 Pt 1): p. 542-7.
86. Katkin, J.P., et al. Exogenous surfactant enhances the delivery of recombinant adenoviral vectors to the lung. *Hum Gene Ther.* 1997. 8(2): p. 171-6.

87. ZHANG Zhi-guo, and Y. Hong. Interaction of nonionic surfactant AEO9 with ionic surfactants. *Journal of Zhejiang University SCIENCE*. 2005. 6B(6): p. 597-601.
88. Label for Ambisome®. 2004. <http://rxlist.com/cgi/generic2/ambisome.htm>.
89. Dedinaite, A.B. Interactions between mucin and surfactants at solid-liquid interfaces. *Langmuir*. 2002. 18: p. 9383-92.
90. Boat, T.F., Cheng, P.W., and Wood, R.E. Tracheobronchial mucus secretion in vivo and in vitro by epithelial tissues from cystic fibrosis and control subjects. *Mod Probl Paediatr*. 1977. 19: p. 141-52.
91. Scawen, M. and A. Allen. The action of proteolytic enzymes on glycoproteins from pig gastric mucin. *Biochem J*. 1977. 163: p. 363-68.
92. Shi, L.S., Ardehali, R., Caldwell, K.D., Valint, P. Mucin coating on polymeric material surfaces to suppress bacterial adhesion. *Colloids and Surfaces B: Biointerfaces* 2000. 17: p. 229-239.
93. Dedinaite, A.B. Interactions between mucin and surfactants at solid-liquid interfaces. *Langmuir*. 2002. 18: p. 9383-9392.
94. Bastardo, L., Claesson, P., and W. Brown. Interactions between mucin and alkyl sodium sulfates in solution. *Langmuir*. 2002. 18: p. 3848-3853.
95. Waigh, T.A., et al. Entanglement Coupling in Porcine Stomach Mucin. *Langmuir*. 2002. 18: p. 7188-95.
96. Davies, J.M., and C. Viney. Water–mucin phases: conditions for mucus liquid crystallinity. *Thermochim Acta*. 1998. 315(1): p. 39-49.
97. Kokufuta, E. Polyelectrolyte gel transitions: experimental aspects of charge inhomogeneity in the swelling and segmental attractions in the shrinking. *Langmuir*. 2005. 21: p. 10004-10015.
98. Nichifor, M., Zhu, X.X., Cristea, D., and A. Carpov. Interaction of hydrophobically modified cationic dextran hydrogels with biological surfactants. *J Physical Chem B*. 2001. 105: p. 2314-2321.
99. Lynch, I., Sjöström, J., and L. Picullel. Reswelling of polyelectrolyte hydrogels by oppositely charged surfactants,” *J Physical Chem B*. 2005. 109: p. 4258-4262.
100. Lynch, I. and L. Picullel. Presence or absence of counterion specificity in the interaction of alkylammonium surfactants with alkylacrylamide gels. *J Physical Chem B*. 2006. 110: p. 864-870.

101. Nilsson, P., and P. Hansson. Ion-exchange controls the kinetics of deswelling of polyelectrolyte microgels in solutions of oppositely charged surfactant. *J Physical Chem B*. 2005. 109: p. 23843-23856.
102. Sjöström, J. Simple gel swelling experiments distinguish between associating and nonassociating polymer-surfactant pairs. *Langmuir*. 2001. 17: p. 3836-3843.
103. Abed, M.A.B., H.B. Surfactant induced softening in gelatin hydrogels. *Eur Polymer J*. 2005. 41: p. 2395-2405.
104. Ogawa, K., Ogawa, Y., and E. Kokufuta. Effect of charge inhomogeneity of polyelectrolyte gels on their swelling behavior. *Colloids and Surfaces A: Physicochemical and Engineering Aspects*. 2002. 209: p. 267-279.
105. Picullel, L., Sjöström, J., and I. Lynch. Swelling isotherms of surfactant-responsive polymer gels *Langmuir*. 2001. 122: p. 103-112.
106. Costa, D., et al. Interaction between covalent gels and a cationic surfactant. *Biomacromolecules (in press)*. 2006.
107. Lafitte, G., Thuresson, K., and O. Söderman. Mixtures of mucin and oppositely charged surfactants aggregates with varying charge density. Phase behavior, association and dynamics. *Langmuir*. 2005. 21: p. 7097-7104.
108. Frank, B. and S. Garoff. Surfactant Self-Assemblies Near Contact Lines: Control of Advancing Surfactant Solutions. *Colloids and Surfaces A*. 1996. 116: p. 31.
109. Frank, B. and S. Garoff. Temporal and Spatial Development of Surfactant Self-Assemblies Controlling Spreading of Surfactant Solutions. *Langmuir*. 1995. 11: p. 4333.
110. Frank, B and S. Garoff. Origins of the Complex Motion of Advancing Surfactant Solutions. *Langmuir*. 1995. 11: p. 87.
111. Espinosa, F.F. and R.D. Kamm. Bolus dispersal through the lungs in surfactant replacement therapy. *J Appl Physiol*. 1999. 86(1): p. 391-410.
112. Craster, R.V. and K. Matar. Surfactant transport on mucus films. *J. Fluid Mech*. 2000. 425: p. 235-58.
113. Tarran, R., et al. Soluble mediators, not cilia, determine airway surface liquid volume in normal and cystic fibrosis superficial airway epithelia. *J Gen Physiol*. 2006. 127(5): p. 591-604.
114. Matsui, H., et al. Coordinated clearance of periciliary liquid and mucus from airway surfaces. *J Clin Invest*. 1998. 102(6): p. 1125-31.

